ADSORPTION BEHAVIOUR OF SE(-II) AND TC(IV)

ADSORPTION BEHAVIOUR OF SE(-II) AND TC(IV) ONTO GRANITE, SHALE, LIMESTONE, ILLITE, AND MX-80 BENTONITE IN CA-NA-CL AND NA-CA-CL SOLUTIONS

By JOSHUA RACETTE, B.ENG

A Thesis Submitted to the School of Graduate Studies in Partial Fulfillment of the Requirements for the

Degree Doctor of Philosophy

McMaster University © Copyright by Joshua Racette, August 2023

McMaster University DOCTOR OF PHILOSOPHY (2023) Hamilton, Ontario (Engineering Physics)

TITLE: Adsorption Behaviour of Se(-II) and Tc(IV) onto Granite, Shale, Limestone, Illite, and MX-80 Bentonite in Ca-Na-Cl and Na-Ca-Cl Solutions

AUTHOR: Joshua Racette, B. ENG (McMaster University)

SUPERVISOR: Dr. S. Nagasaki

PAGES: xiii, 99

Lay Abstract

Determining the adsorption of Se(-II) and Tc(IV) onto granite, shale, limestone, illite, and MX-80 bentonite is beneficial to choosing a location within Canada to locate a used nuclear fuel repository. This thesis aims to quantify the adsorption behaviour of Se(-II) and Tc(IV) in Ca-Na-Cl and Na-Ca-Cl solutions with respect to a varying solution ionic strength and pH. Quantification of the adsorption was accomplished with adsorption experiments used in conjunction with geochemical simulations. New simulated surfaces specific to granite, shale, and MX-80 bentonite have been developed to complete these simulations. A final achievement was quantifying the adsorption of Se(-II) and Tc(IV) in groundwater representative solutions specific to locations considered for the used nuclear fuel repository.

Abstract

Canada is in the process of implementing a Deep Geologic Repository (DGR) to dispose of used nuclear waste. Adsorption behaviour of both Se(-II) and Tc(IV) onto granite, shale, limestone, illite, and MX-80 bentonite has been elucidated. Se(-II) adsorption onto granite and MX-80 bentonite displays a decrease in R_d with an increase in solution pH. Se(-II) adsorption onto granite decreases with an increase in solution ionic strength. Se(-II) adsorption onto MX-80 bentonite does not return evidence which supports an apparent effect due to the ionic strength. Tc(IV) adsorption onto shale, limestone, illite, and MX-80 bentonite remains constant as the solution pH increases. Ionic strength does not affect the magnitude of Tc(IV) adsorption across the adsorbents, however an increase in ionic strength accelerates Tc(IV) adsorption. Se(-II) surface complexation models are best simulated with the following surface complexes: ≡Feldspar_sSe$^-$, ≡Biotite_sOH$_2$HSe, ≡Albite_sSe$^-$, ≡Montmorillonite_sSe$^-$, and ≡Montmorillonite_sOH$_2$HSe. Tc(IV) adsorption is best simulated with: ≡Biotite_sOTcO(OH), ≡Quartz_sOTcO(OH), (≡Feldspar_sOH)$_2$TcO(OH)$^-$, ≡Montmorillonite_sOTcO(OH), (≡Albite_sOH)$_2$TcO(OH)$^-$, ≡Illite_sOTcO(OH), and ≡Chlorite_sOTcO(OH). Se(-II) adsorption onto granite and MX-80 bentonite in CR-10 solution returns R_d values of (1.80 ± 0.10) m^3·kg^{-1} and (0.47 ± 0.38) m^3·kg^{-1}, respectively. Tc(IV) adsorption onto granite and MX-80 bentonite in CR-10 solution returned R_d values of (1.47 ± 0.25) m^3·kg^{-1} and (2.19 ± 0.33) m^3·kg^{-1}, respectively. Tc(IV) adsorption onto shale, limestone, illite, and MX-80 bentonite in SR-270-PW solution returned R_d values of (0.16 ± 0.10) m^3·kg^{-1}, (0.44 ± 0.21) m^3·kg^{-1}, (1.86 ± 0.44) m^3·kg^{-1}, and (0.23 ± 0.10) m^3·kg^{-1}, respectively. This thesis will further deepen the understanding of Se(-II) and Tc(IV) adsorption.

Acknowledgments

Boundless appreciation for Dr. Nagasaki, as I am grateful to have had the opportunity to pursue a PhD under his supervision. I have learned much from him, and hope to continue to learn more.

Table of Contents

List of Figures and Tables

Figures

Tables

List of all Abbreviations and Symbols

Abbreviations

NWMO - Nuclear Waste Management Organization
DGR - Deep Geologic Repository
ORP - Oxidation Reduction Potential
TDS - Total Dissolved Solids
CR-10 - Crystalline Rock Porewater with TDS of approximately 10.0 $g \cdot L^{-1}$
SR-270-PW - Sedimentary Rock Porewater with TDS of approximately 270.0 $g \cdot L^{-1}$
WE - Working Electrode
CE - Counter Electrode
RE - Reference Electrode
OCP - Open Circuit Potential
CV - Cyclic Voltammetry
ICP-MS - Inductively Coupled Mass Spectrometer
SCM - Surface Complexation Model
2SPNE SC/CE - 2 Site Protolysis Non-Electrostatic Surface Complexation/Cation Exchange
CA - Component Additive
PHREEQC - pH Redox Equilibrium in C (A computer program for speciation, batch-reaction, one-dimensional transport, and inverse geochemical calculations)
UV-VIS - Ultra Violet - Visible Spectroscopy
BET - Brünauer - Emmett - Teller Theory
XRD - X-Ray Diffraction
AFM - Atomic Force Microscopy
RPM - Rotations Per Minute
RCF - Relative Centrifugal Force
SSA - Specific Surface Area
$SSA_{adsorbent}$ - Specific surface area associated with either granite, shale, illite, or MX-80 bentonite
SSA_i - Specific Surface Area associated with mineral assemblage *I*
LFER - Linear Free Energy Relationship
DFT - Density Functional Theory
MD - Molecular Dynamics

Symbols

E_{max} - Maximum energy associated with an irradiative decay product
β^- - Beta particle
R_d - Adsorption distribution ratio $[m^3 \cdot kg^{-1}]$
$C_{initial}$ - Initial concentration of either Se(-II) or Tc(IV) in solution prior to adsorption experiments [mol]
C_{final} - Final concentration of either Se(-II) or Tc(IV) in solution following adsorption experiments [mol]
L - Volumetric liquid amount used in adsorption experiments $[m^3]$
M - Solid adsorbent mass used in adsorbent experiments [kg]
z_j - Charge of ion j,
D - Debye-Hückel term,
m_k - Molality of ion k, which is oppositely charged to ion j
$\varepsilon(j, k)$ - Specific ion interaction parameter

Declaration of Academic Achievement

This work presents the results of both Se(-II) and Tc(IV) adsorption experiments, and the associated Se(-II) and Tc(IV) surface complexation modelling. Numerous adsorption experimental results have been achieved and these include the following: First, R_d values for Se(-II) adsorption onto granite and MX-80 bentonite in 0.05, 0.10, 0.24, and 1.00 mol·kgw^{-1} Ca-Na-Cl solutions at pH_m = 5.0, 6.0, 8.0, and 9.0. Secondly, R_d values specific to Tc(IV) adsorption onto granite and MX-80 bentonite at pH_m = 4.0, 5.0, 8.0, and 9.0 were determined in identical Ca-Na-Cl solutions. Thirdly, R_d values related to Tc(IV) adsorption onto shale, limestone, illite, and MX-80 bentonite in 0.1, 1.0, 3.0, and 6.0 mol·kgw^{-1} Na-Ca-Cl solutions at pH_m = 4.0, 5.0, 8.0, and 9.0 were measured. Finally, R_d values for both Se(-II) and Tc(IV) adsorption onto granite and MX-80 bentonite in CR-10 solution and Tc(IV) adsorption onto shale, limestone, illite, and MX-80 bentonite in SR-270-PW solution are presented.

Achievements regarding the geochemical surface complexation models include the following: First, surfaces which simulate granite, shale, and MX-80 bentonite, based on mineral assemblage components have been created. Second, there are successful simulations of both Se(-II) and Tc(IV) adsorption onto granite and MX-80 bentonite in all Ca-Na-Cl solutions. Third, there are successful simulations of Tc(IV) adsorption onto shale, illite, and MX-80 bentonite in 0.1, 1.0, and 3.0 mol·kgw^{-1} Na-Ca-Cl solutions. Finally, the presentation of all Se(-II) and Tc(IV) surface complexation reactions with their respectively optimized surface complexation constants.

Chapter 1 - Introduction

As of 2023, two locations remain in the candidate repository site selection process which are relevant to Canada's implementation of a Deep Geologic Repository (DGR). These candidate repository sites are The Revell Site and The South Bruce Site. These are located in North-western Ontario and Southern Ontario, respectively [1, 2]. At the Revell Site, the bedrock is characterized by a crystalline granite bedrock formation with a saline, reducing, Ca-Na-Cl dominant electrolyte groundwater [1]. Whereas, the South Bruce Site is characterized with sedimentary shale and limestone bedrock formation, and an Na-Ca-Cl dominant electrolyte groundwater that is a brine and under reducing conditions [2]. The DGR concept presently considered consists of placing the used nuclear fuel into used fuel canisters which are then entombed within an MX-80 bentonite buffer box before being buried within the bedrock for disposal [1 - 4]. The bedrock will act as a natural barrier in conjunction with the MX-80 bentonite which acts as an engineered barrier to radionuclide migration [3, 4]. These barriers are utilized to ensure that the near-field conditions associated with the DGR are hydraulically maintained. This will ensure that migration of radionuclides, in the event of a release, is diffusion controlled. Determination of a radionuclides adsorption behaviour onto one of the barrier adsorbents assists with quantifying that radionuclides migration rate. This adsorption behaviour can be elucidated when a combined approach of batch adsorption experiments and surface complexation models are employed.

In post-closure safety assessments associated with a used nuclear fuel repository in either crystalline and sedimentary rock, ^{79}Se and ^{99}Tc have been identified as radionuclides of interest given their existence in used nuclear fuel [3, 4]. These two radionuclides exhibit safety concerns from both a radiological and chemical perspective [3, 4]. Radiologically, ^{79}Se is a long-lived radionuclide with a half-life of 3.27×10^5 years, an instant release fraction of 0.6%, and is characterized with a β^- emission which has an E_{max} = 150.9 keV that results in ^{79}Br as the decay product [5 - 10]. Similarly, ^{99}Tc is also a long-lived radionuclide with a half-life of 2.11×10^5 years that accounts for 6.0% of all fission product yield within used nuclear fuel, and decays through a β^- emission which has an E_{max} = 290.0 keV that results in ^{99}Ru as the decay product [11 - 43]. The amount of ^{79}Se or ^{99}Tc is dependant upon the burn up

associated with the used nuclear fuel upon its removal from the reactor. When the burn up is 220.0 $MWh \cdot kgU^{-1}$, the ^{79}Se inventory is $1.76x10^{-5}$ $mol \cdot kgU^{-1}$ and the ^{99}Tc inventory is $2.41x10^{-3}$ $mol \cdot kgU^{-1}$ [3, 4]. However, when the burn up of the fuel increases to 280.0 $MWh \cdot kgU^{-1}$, the ^{79}Se and ^{99}Tc inventories increase to $2.20x10^{-5}$ $mol \cdot kgU^{-1}$ and $3.02x10^{-3}$ $mol \cdot kgU^{-1}$, respectively [3, 4]. Specifically, there is a serious chemical concern associated with ^{79}Se as a radionuclide as it behaves similar to sulphur chemically. As such, it is able to be up taken into the biosphere with ease [44 - 51]. Furthermore, Se and Tc are redox sensitive elements and exhibit different migration behaviours when present in either a reduced or oxidized form. Under aerobic and oxidizing conditions, Se will exist in either the Se(IV) or Se(VI) valence state, which will speciate as selenite (SeO_3^{2-}) and selenate (SeO_4^{2-}), respectively. Whereas, under anaerobic and reducing conditions Se will exist in the Se(-II) valence state and speciate as hydroselenide (HSe^-). Tc will exist as Tc(VII) or Tc(IV) when exposed to oxidizing or reducing conditions. This will influence Tc speciation, as Tc(VII) speciates as pertechnetate (TcO_4^-), while Tc(IV) speciates as an oxo-ion of the form, $TcO(OH)_2$.

At the present, the adsorption behaviour of Se(-II) and Tc(IV) onto granite and MX-80 bentonite in Ca-Na-Cl solutions and the adsorption behaviour of Tc(IV) onto shale, limestone, illite, and MX-80 bentonite in Na-Ca-Cl solutions has been elucidated. This behaviour has been quantified with relation to the two physicochemical solution properties, pH and ionic strength. Se adsorption experiments investigate pH_m = 5.0, 6.0, 8.0, and 9.0 whereas Tc adsorption experiments investigate a pH_m = 4.0, 5.0, 8.0, and 9.0. Adsorption experiments in the Ca-Na-Cl solutions investigate an ionic strength range of 0.05 to 1.0 $mol \cdot kgw^{-1}$, while in Na-Ca-Cl solutions the ionic strength ranges from 0.1 to 6.0 $mol \cdot kgw^{-1}$. An important comment is that units of concentration used within this study are reported in molal units [$mol \cdot kgw^{-1}$ ($mol \cdot (kilogram\ water)^{-1}$)] as opposed to molar units [$mol \cdot L^{-1}$]. To support these adsorption experiments, non-electrostatic surface complexation models have been created, and simulations have been optimized using the experimental data. Before surface complexation constants are compared with Linear Free Energy Relationships (LFER). Finally, the adsorption of Se(-II) and Tc(IV) onto granite and MX-80 bentonite in CR-10 solution and the adsorption of Tc(IV) onto shale, limestone, illite, and MX-80 bentonite in SR-270-PW solution has been completed. CR-10 and SR-270-PW solutions are

representative of the groundwater that is anticipated to exist at the depths associated with DGR emplacement in either the crystalline or sedimentary bedrock, respectively. Presently, the combination of batch adsorption experiments and surface complexation modelling will be beneficial to furthering the understanding of Se(-II) and Tc(IV) adsorption within Canadian bedrock. With an increased understanding of Se(-II) and Tc(IV) adsorption, confidence in a DGR concept can be increased in Canada and globally. At the moment, it is considered that this is the first adsorption study of the radionuclides Se(-II) and Tc(IV) in high ionic strength solutions which are supported with geochemical surface complexation modelling.

Chapter 2 - Materials and Experimental Methodology

All chemicals used throughout the experiments were reagent grade, and supplied by Fisher Scientific unless explicitly stated. The solid masses of all chemicals and adsorbent materials were measured using a Sartorius Quintix 213-1S scale. Deionized water was prepared using a Milli-Q Direct 8 system which guarantees that the volumetric resistivity of the deionized water is 18.2 MΩ·cm. To ensure anoxic conditions were present for the duration of the experiments, a precise controlled atmospheric glovebox supplied by Labconco was utilized. This glovebox was filled with N_2 gas (>99.999%), which was constantly flowing through the glovebox for the duration of the experiments to continuously vent the glovebox preserving O_2 levels below 2.0 ppm, and to ensure that contaminant CO_2 is removed. A Fisherbrand accumet AB200 Benchtop pH meter was used with a Fisherbrand accumet pH combination electrode (#13-620-297) and a platinum tipped Fisherbrand accumet Metallic ORP electrode (#13-620-115), to determine the pH and Eh, respectively. Calibration of the pH meter was completed using pH 4.0, 7.0, and 10.0 pH buffer solutions.

A topic of discussion is that the adsorption kinetic and batch adsorption experiments investigate ionic strengths > 0.1 mol·kgw^{-1}. This requires that the measured pH value (pH_{obs}) be designated as an observed operational apparent value. Any one pH_{obs} value is related to any one molal H^+ concentration ($pH_m = -\log m_{H+}$), and a molar H^+ concentration ($pH_c = -\log c_{H+}$) through a linear relationship that is of the form, $pH_{(m\ or\ c)} = pH_{obs} + A_{(m\ or\ c)}$. In this relationship, $A_{(m\ or\ c)}$ is an empirical correction factor that accounts for variation in liquid junction potential between measuring in dilute and saline solutions, and the individual H^+ activity coefficient [52 - 54]. This study used the molal pH_m conversion opposed to the molar pH_c conversions. Linear relationships were derived for all Ca-Na-Cl and Na-Ca-Cl solutions with a Metrohm Ti-Touch 916. Table 1 presents the derived $pH_m = pH_{obs} + A_m$ conversion relationships for the 0.05, 0.1, 0.24, and 1.0 mol·kgw^{-1} Ca-Na-Cl solutions. Table 2 presents the derived $pH_m = pH_{obs} + A_m$ conversion relationships for the 0.1, 1.0, 3.0, and 6.0 mol·kgw^{-1} Na-Ca-Cl solutions.

Table 1 - $pH_m = pH_{obs} + A_m$ conversion relationships for Ca-Na-Cl solutions with ionic strengths of 0.05, 0.1, 0.24, and 1.0 mol·kgw^{-1}.

Ionic Strength [mol·kgw^{-1}]	$pH_m = pH_{obs} + A_m$ Conversion Relationships
0.05	$pH_m = 1.0570 \cdot pH_{obs} - 0.2838$
0.10	$pH_m = 1.0470 \cdot pH_{obs} - 0.2682$
0.24	$pH_m = 1.0507 \cdot pH_{obs} - 0.1593$
1.00	$pH_m = 1.0671 \cdot pH_{obs} - 0.0227$

Table 2 - $pH_m = pH_{obs} + A_m$ conversion relationships for Na-Ca-Cl solutions with ionic strengths of 0.1, 1.0, 3.0, and 6.0 mol·kgw^{-1}.

Ionic Strength [mol·kgw^{-1}]	$pH_m = pH_{obs} + A_m$ Conversion Relationships
0.1	$pH_m = 0.9898 \cdot pH_{obs} - 0.1130$
1.0	$pH_m = 1.0526 \cdot pH_{obs} - 0.8562$
3.0	$pH_m = 0.9756 \cdot pH_{obs} - 0.6629$
6.0	$pH_m = 1.0010 \cdot pH_{obs} - 1.0825$

2.1 - Production of Se(-II)

The chemical reduction methodology utilized is well known to be successful with respect to the reduction of either Se(IV) or Se(VI) to the required Se(-II) [55 - 63]. Preparation of all Se(-II) containing solutions were completed within the glovebox to prevent O_2 or CO_2 contamination throughout the reduction procedure. All Se used in adsorption kinetic and batch adsorption experiments is derived from a 1000 ± 1 µg·mL^{-1} Se standard solution within a 1.0% nitric acid matrix that was supplied by Agilent Technologies. No confirmation of the exact Se redox state in the standard solution was completed. As such, the standard solution was presumed to contain a mixture of both Se(IV) and Se(VI). Subsequently, an aliquot of the standard solution was mixed with deionized water so that the resultant Se concentration was approximately 1.0 µmol·L^{-}. Preliminary experiments were performed to ensure that

this concentration was below the solubility limit of Se(cr) to prevent precipitation from occurring. Following these experiments, an amount of 0.2 mol·L^{-1} hydrazine monohydrate ($N_2H_4 \cdot H_2O$) was added to the Se solution to ensure reducing conditions were present within the solution. Finally, the Se solution was allowed to mature for a minimum of five days while contained within the glovebox to ensure that Se(-II) was the dominant oxidation state present within the solution. Figure A1 provides the Pourbaix diagram for the Se - O - H system, and associated pH vs Eh measurements [64].

Additionally, UV-VIS absorbance measurements were taken to confirm that the Se(-II) redox state exists in solution stably for a minimum of a month thus providing confidence that the Se reduction was successful. UV-VIS measurements were completed with the blank solution being [CR-10 + $N_2H_4 \cdot H_2O$], and [CR-10 + Se(-II) + $N_2H_4 \cdot H_2O$] being the solution of interest. For reference, the pH of the solution during the UV-VIS measurements was 6.4. The absorbance spectra associated with HSe^- is 247.0 nm [55 - 60]. Figure A2 presents the UV-VIS spectrum associated with the successful production of Se(-II). There is no discernible absorbance peak however, which can be identified with certainty at 247.0 nm in Figure A2. From previous publications however, the absorbance of Se(-II) has been shown to be effected by not only the concentration of Se(-II) in solution, but also the pH of the solution [55 - 60].

Currently, it is being considered that since the concentration of Se utilized in the reduction methodology was approximately 1.0 µmol·L^{-1}, and the pH of the solution throughout the UV-VIS measurements was 6.4, these conditions could allude to the absence of an observable absorbance peak at 247.0 nm. Previously Iida et al., remarked that absorption spectra peaks were assigned to Se(-II) species from solubility experiments in the undersaturation direction, but not the oversaturation direction due to a Se(-II) concentration that was considered too low [60]. The concentration of Se(-II) from oversaturation experiments is approximately on par with the concentration of Se(-II) used in this study [60]. Further, Iida et al. reported that the pH of the solution in oversaturation experiments are of similar circumneutral pH values to the measured solution in this study. This evidence is considered as justification for the lack of an observable spectra peak [60]. Undersaturation experiments carried out by Iida et al. did return an observable Se(-II) spectra at 247.0 nm which was assigned to HSe^- [60]. In contrast, the concentration of Se(-II) in the undersaturation experiments were on the order of 10.0 to

100.0 $\mu mol \cdot L^{-1}$ with solution pH > 9.0 [60]. The reduction methodology utilized by Walker et al., with success is identical to the reduction methodology utilized within this study, further providing confidence that this methodology is successful [61].

2.2 - Production of Tc(IV)

The production of Tc(IV) utilized an electro-chemical reduction methodology. The original Tc(VII) solution with which all Tc(IV) was produced from was supplied by the Health Physics department at McMaster University. This solution contained a concentration of 36.5 $mgTc \cdot mL^{-1}$ ammonium pertechnetate in a 0.75 $mol \cdot L^{-1}$ nitric acid matrix. The method adopted is based upon previously published materials which do employ similar electro-chemical reduction methodologies [11, 12, 16, 22, 25, 33, 38, 41]. All equipment necessary to reduce Tc(VII) to Tc(IV) has been supplied by EC Frontier Co., Ltd. The electrolytic cell is a 50.0 mL glass vial with an O-ring sealed lid. There are five openings in the lid to allow for a Pt mesh working electrode (WE), a Pt wire counter electrode (CE), an Ag/AgCl reference electrode (RE), an incoming N_2 gas line, and a vent to release pressure within the electrolytic cell. Figure A3 provides an image of the electrolytic cell with all electrodes.

Initially, a 40.0 mL solution containing 0.2 $mol \cdot L^{-1}$ $N_2H_4 \cdot H_2O$, 0.2 $mol \cdot L^{-1}$ sodium dithionite ($Na_2S_2O_4$), and Tc(VII) with an approximate concentration of 10.0 $\mu mol \cdot L^{-1}$ was prepared. The initial concentration of Tc(VII) used is known to be below the solubility limit of 4.40×10^{-8} $mol \cdot kg^{-1}$ associated with Tc(IV) [65]. This is to ensure that during the reduction process, there will not be enough Tc(IV) produced that would allow for Tc(IV) precipitation to occur. The combined usage of $Na_2S_2O_4$ and $N_2H_4 \cdot H_2O$ as chemical reducing agents is to promote the reduction of Tc(VII) to Tc(IV), and to ensure reducing conditions are preserved in solution thus preserving Tc(IV) as the dominant redox state. This solution is then pH adjusted to pH = 5.0, using either HCl of NaOH to provide conditions which ensure that Tc(IV) speciates as $TcO(OH)_2(aq)$. Figures A4 and A5 present provides the Pourbaix diagram for the Tc - O - H system, and associated pH vs Eh measurements in both Ca-Na-Cl solutions and Na-Ca-Cl solutions, respectively [25, 65].

The 40.0 mL Tc(VII) solution is added into the glass vial and then a magnetic stir bar is added into the electrolytic cell. Magnetic stirring is achieved through usage of a Fisher Scientific magnetic stirrer (#11676263) which will increase the efficiency of the reduction procedure [66]. The CE is then filled with 1.0 N HCl, and the RE is filled with 3.0 mol·L^{-1} KCl before emplacement into the electrolytic cell through openings in the cell lid along with the WE. Finally, the N_2 gas line is placed into the electrolytic cell with the exit of the gas line near to the magnetic stir bar. It is presumed that with increased mixing of the N_2 gas with the magnetic stirrer in the solution during the reduction procedure will facilitate an increase in reduction efficiency, and remove contaminant O_2, preventing oxidation of Tc(VII) to Tc(IV).

Initially, an open circuit potential (OCP) measurement is recorded with the resultant value being recorded as 750.0 mV, which coincides with the known potential associated with the Tc(VII)/Tc(IV) redox couple [67 - 69]. Subsequently, a cyclic voltammatry (CV) measurement was carried out to confirm that the Tc(VII)/Tc(IV) redox couple was the only redox couple present in the solution. Previous studies presented that only one peak exists in both the anodized branch, and the cathodic branch [70, 71]. These two peaks were observed from the CV measurements carried out within this study which is considered to provide confidence in preparation of the Tc(VII) reduction solution. The reduction procedure is completed through usage of an amperometric reduction procedure. A constant current of 10.0 mA is transferred from the cathodic WE to the anodic CE. Throughout the reduction procedure, reduced Tc(IV) in the form of a $TcO{\cdot}1.6H_2O(am)$ will electrodeposit onto the surface of the WE [67, 70, 71]. This reduction procedure is utilized for a period of 1.0 hour. This amount of time was determined from preliminary experiments that found the RE potential to become approximately constant at the current stated. One important aspect of utilizing this reduction methodology is that the Tc(VII)/Tc(IV) redox couple appears irreversible when a Pt electrode is used [72, 73]. The reduction of Tc(VII) to Tc(IV) occurs via intermediately adsorbed H^+ ions with the overall process being described with the following reactions [73].

$$3H^+ + 3e^- \leftrightarrow 3H_{ads} \quad (1)$$

$$TcO_4^- + 3H_{ads} + H^+ \leftrightarrow TcO_2{\cdot}1.6H_2O(am) + 0.4H_2O \quad (2)$$

The Pt mesh WE is gently removed from the electrolytic cell after the reduction is completed. The WE is then immersed into a second glass vial which contains 40.0 mL of a 0.2 mol·L^{-1} $Na_2S_2O_4$ and 0.2 mol·L^{-1} $N_2H_4 \cdot H_2O$ solution which was pH adjusted to pH = 5.0. Prior to the WE being immersed in the solution, the Eh is measured to confirm reducing conditions are present within the solution. This is considered an essential measurement as it provides confidence that when Tc(IV) desorbs off the WE, Tc(IV) will speciate as $TcO(OH)_2(aq)$. The WE is then placed into the solution and allowed to remain in solution for a minimum of three days. Previous solubility study results indicated that three days was adequate to dissolve Tc [13]. After the desorption period, the WE is removed from the solution, the solution is transferred from the glass vial into a polycarbonate reaction vessel that has been given a batch number, and subsequently moved into the N_2 glovebox for storage of the Tc(IV) solution batch. A second measurement of the redox conditions was performed within the glovebox to confirm reducing conditions were present and were maintained for the duration of the 3-day desorption period.

Following the successful production of a Tc(IV) batch, a 1.0 mL aliquot of the Tc(IV) solution is removed and added into a polycarbonate reaction vessel that contains 9.0 mL of deionized water. This diluted solution is subsequently measured using an Agilent 8800 Inductively Coupled Mass Spectrometer (ICP-MS) to determine the concentration of Tc(IV) present within the solution batch. An important comment is that the concentration of Tc(IV) within any given solution batch is unknown until measurement is performed with the ICP-MS. Initial dilution by a factor of 10 with deionized water is required as the solution salinity must to be below 0.75 mol·L^{-1} for accurate measurements with the ICP-MS [61, 74]. In the event it is necessary to produce more Tc(IV) for an adsorption experiment, the reduction method is repeated to produce consecutive batches. After a proper amount of Tc(IV) has been prepared for usage in any of the adsorption kinetic or batch adsorption experiments, the appropriate volumetric amount from the batch solutions is added to any one of the prepared Ca-Na-Cl solutions, Na-Ca-Cl solutions, CR-10 solution, or SR-270-PW solution, so that the concentration of Tc(IV) within that solution is approximately 1.0 nanomol·L^{-1}.

2.3 - Preparation of the Ca-Na-Cl and Na-Ca-Cl Solutions

Four different Ca-Na-Cl solutions were prepared with ionic strengths of 0.05, 0.1, 0.24, and 1.0 mol·kgw^{-1}. All four Ca-Na-Cl solutions have a constant molar Na/Ca ratio of 1.60, which is approximately the same molar Na/Ca ratio as the CR-10 solution. Four different Na-Ca-Cl solutions were prepared that had ionic strengths of 0.1, 1.0, 3.0, and 6.0 mol·kgw^{-1}. All four Na-Ca-Cl solutions have a constant molar Na/Ca molar ratio of 2.70, which is the same molar Na/Ca ratio as the SR-270-PW solution. Table 3 presents masses required of the NaCl and $CaCl_2 \cdot 2H_2O$ salts used to prepare the Ca-Na-Cl solutions, while Table 4 presents masses required to produce the Na-Ca-Cl solutions.

Table 3 – Masses required of NaCl and $CaCl_2 \cdot 2H_2O$ salts that were used to prepare 1.0 L of 0.05, 0.1, 0.24, or 1.0 mol·kgw^{-1} Ca-Na-Cl solutions.

Ionic Strength [mol·kgw^{-1}]	NaCl Mass [g]	$CaCl_2 \cdot 2H_2O$ Mass [g]
0.05	1.019 ± 0.0001	1.598 ± 0.0001
0.10	2.038 ± 0.0001	3.196 ± 0.0001
0.24	4.891 ± 0.0001	7.67 ± 0.0001
1.00	20.38 ± 0.0001	31.96 ± 0.0001

Table 4 – Masses required of NaCl and $CaCl_2 \cdot 2H_2O$ salts that were used to prepare 1.0 L of 0.1, 1.0, 3.0, and 6.0 mol·kgw^{-1} Na-Ca-Cl solutions.

Ionic Strength [mol·kgw^{-1}]	NaCl Mass [g]	$CaCl_2 \cdot 2H_2O$ Mass [g]
0.1	2.765 ± 0.0001	2.579 ± 0.0001
1.0	27.683 ± 0.0001	25.792 ± 0.0001
3.0	83.651 ± 0.0001	77.376 ± 0.0001
6.0	166.1 ± 0.0001	154.75 ± 0.0001

2.4 - Preparation of the CR-10 and SR-270-PW Solutions

CR-10 reference saline groundwater solution has a known pH of 7.1, an Eh of -194.0 mV (vs. SHE), and a total dissolved solids (TDS) content of 11.625 $g \cdot L^{-1}$ [3]. Table 5 presents the mass of compounds required to produce CR-10, and they are presented in order of addition required to properly prepare the CR-10 solution [75]. SR-270-PW reference brine solution is known to have a pH = 5.8, an Eh = -200 mV (vs. SHE), and a TDS content of 276.2 $g \cdot L^{-1}$ [4]. Table 6 presents the necessary mass of compounds needed and are listed in the order of addition to prepare the SR-270-PW solution. When either of the CR-10 or SR-270-PW solutions are prepared for usage in Se(-II) adsorption experiments, only 0.2 $mol \cdot L^{-1}$ $N_2H_4 \cdot H_2O$ is added to solution. When either of the CR-10 or SR-270-PW solutions are prepared for usage in Tc(IV) adsorption experiments, both 0.2 $mol \cdot L^{-1}$ $N_2H_4 \cdot H_2O$ and 0.2 $mol \cdot L^{-1}$ $Na_2S_2O_4$ are added to solution. A small comment is that $N_2H_4 \cdot H_2O$ acts as a chemical buffer and will increase the pH of the CR-10 and SR-270-PW solution. This required the addition of 0.1 N HCl to adjust the pH back to the required pH_m initial value.

Table 5 – Masses required, and molal concentrations of all compounds used to prepare 1.0 L CR-10 saline solution. Ionic strength of the CR-10 solution is approximately 0.24 $mol \cdot kgw^{-1}$ for reference.

Compound	Mass [g]	Molal Concentration [$mol \cdot kgw^{-1}$]
NaCl	4.83 ± 0.0001	0.0823
KCl	0.029 ± 0.0001	0.0004
$CaCl_2 \cdot 2H_2O$	6.28 ± 0.0001	0.0429
$MgCl_2 \cdot 6H_2O$	0.502 ± 0.0001	0.0025
$SrCl_2 \cdot 6H_2O$	0.076 ± 0.0001	0.0003
$CaSO_4 \cdot 2H_2O$	1.61 ± 0.0001	0.0094

Table 6 – Masses required, and molal concentrations of all compounds used to prepare 1.0 L SR-270-PW brine solution. Ionic strength of the SR-270-PW solution is approximately 6.0 mol·kgw^{-1} for reference.

Compound	Mass [g]	Molal Concentration [mol·kgw^{-1}]
KCl	22.2485 ± 0.0001	0.2575
KBr	2.5318 ± 0.0001	0.0184
$NaHCO_3$	0.1514 ± 0.0001	0.0016
$SrCl_2{\cdot}6H_2O$	3.6515 ± 0.0001	0.1188
Na_2SO_4	0.3253 ± 0.0001	0.0020
$MgCl_2{\cdot}6H_2O$	68.5901 ± 0.0001	0.3113
$CaCl_2{\cdot}2H_2O$	117.3828 ± 0.0001	0.8265
NaCl	126.7194 ± 0.0001	2.583
$Na_2S{\cdot}9H_2O$	0.55 ± 0.0001	0.0027

2.5 - Rock and Mineral Adsorbents

Granite originates from the Lac du Bonnet batholith in Manitoba, Canada. Shale, and limestone samples originate from the South Bruce repository candidate site. Illite has been supplied by The Clay Mineral Society and originates from Silver Hill, Montana, USA. MX-80 bentonite has been passed through an 80-mesh sieve and is supplied by the American Colloid Company after being sourced from Wyoming, USA. Granite, shale, limestone, and illite were crushed with a tungsten carbide cylinder that was supplied by Nichika. Particles that ranged between 150 μm to 300 μm were collected with a range of stainless-steel sieves and used in all subsequent adsorption kinetic and batch adsorption experiments. MX-80 bentonite was used as received in all subsequent adsorption kinetic and batch adsorption experiments.

Prior to usage in any experiment, all adsorbents underwent a preconditioning period. Preconditioning was completed using any one of the prepared CR-10, SR-270-PW, Ca-Na-Cl, and Na-Ca-Cl solutions which do no contain either Se(-II) or Tc(IV). The pH_m of the precondition solution is then

pH adjusted to the necessary pH_m based upon the adsorption experiment to be performed. Each sample being preconditioned contains (20.0 ± 1.0) mg of the solid adsorbent, and (5.0 ± 0.05) mL of precondition solution. Upon completion of the preconditioning period, the samples were centrifuged for 6.0 minutes at 5860.0 RPM or approximately 3000.0 RCF using a Beckman Coulter Allegra X-30R bench-top centrifuge equipped with a F0630 rotor. This was performed to separate the liquid and solid components. Precondition solution was subsequently removed using a pipette to minimize any potential agitation of the centrifuged solids. Adsorption kinetic or batch adsorption experiments then began upon spiking the preconditioned solids with the required experimental solution which contained either Se(-II) or Tc(IV).

2.6 - Adsorption Kinetics Experimental Methods

All adsorption experiments have been performed in triplicate at room temperature inside of the N_2 atmospheric glovebox. Adsorption was quantified with the adsorption distribution ratio R_d [$m^3 \cdot kg^{-1}$], and is calculated following Equation (3). Where: $C_{initial}$ is the initial concentration in solution [mol], C_{final} is the concentration remaining in solution [mol], L is the volumetric liquid amount [m^3], and M is the solid adsorbent mass [kg].

$$R_d = \frac{C_{initial} - C_{final}}{C_{final}} \cdot \frac{L}{M} \tag{3}$$

2.6.1 - Adsorption Kinetics of Se(-II) in Ca-Na-Cl Solutions

The Se(-II) adsorption kinetic steady-state periods with granite and MX-80 bentonite in Ca-Na-Cl solutions were necessary to be determined. There was (20.0 ± 1.0) mg of preconditioned adsorbent, with (10.0 ± 0.5) mL of liquid used, for a resultant liquid/solid ratio of (0.50 ± 0.03) $m^3 \cdot kg^{-1}$. Two experiments were performed with the 0.05 $mol \cdot kgw^{-1}$ and 1.0 $mol \cdot kgw^{-1}$ Ca-Na-Cl solutions. Preliminary experiments were performed, and determined that adsorption of Se(-II) onto the walls of a polycarbonate reaction

vessel was negligible. The initial concentration of Se(-II) used in all experiments was on average (1.00 ± 0.5) μmol·L^{-1} which is below the expected solubility limit of Se(-II) ensuring that no Se precipitate should form within solution during the experiments. For the duration of the adsorption kinetic experiments, pH_m and Eh measurements were taken at each time interval for each sample to confirm that redox conditions did not change within the polycarbonate reaction vessel which would have allowed Se(-II) to oxidize.

When a measurement was scheduled, a 5.00 mL aliquot was removed from each reaction vessel and placed into a Nalgene Oakridge centrifuge container. These were subsequently centrifuged at 18000.0 RPM or 27579.0 RCF for 30.0 minutes with the Beckman Coulter X-30R centrifuge that was equipped with a F1010 rotor. A previous NWMO technical report confirms that this is adequate centrifugation to separate the liquid and solid components [52]. Finally, a 0.50 mL aliquot of the supernatant Se(-II) solution was removed and mixed with 9.50 mL of deionized water which was measured using the ICP-MS.

2.6.2 - Adsorption Kinetics of Tc(IV) in Ca-Na-Cl Solutions

The Tc(IV) adsorption kinetic steady-state periods with granite and MX-80 bentonite in Ca-Na-Cl solutions were necessary to be determined. There was (20.0 ± 1.0) mg of preconditioned adsorbent, with (10.0 ± 0.5) mL of liquid used, for a resultant liquid/solid ratio of (0.50 ± 0.03) m^3·kg^{-1}. Two experiments were performed with the 0.05 mol·kgw^{-1} and 1.0 mol·kgw^{-1} Ca-Na-Cl solutions. Preliminary experiments were performed, and determined that adsorption of Tc(IV) onto the walls of a polycarbonate reaction vessel was negligible. Initial concentration of Tc(IV) used in experiments was on average (1.37 ± 0.62) nanomol·L^{-1}. This concentration is below the previously reported solubility limit of Tc(IV) thus providing confidence that no Tc(IV) precipitate has formed in solution. For the duration of the adsorption kinetic experiments, pH_m and Eh measurements were taken at each time interval for each sample to confirm that redox conditions did not change within the polycarbonate reaction vessel which would have allowed Tc(IV) to oxidize.

Preparation of a sample to be measured begins with extracting a 4.70 mL aliquot which is transferred into a Beckman Coulter Optima Pro centrifuge tube where it was then centrifuged at $1.00x10^5$ RPM or $5.35x10^5$ RCF for 15.0 minutes at room temperature using a Beckman Coulter Optima MAX-XP Ultracentrifuge equipped with a TLA-110 rotor. To ensure that ultracentrifugation was sufficient to remove the liquid and solid components, the k factor has been compared between the two centrifugation methods. The k-factor of a centrifuge rotor is a measurement of the rotor's pelleting efficiency, and a smaller value is desirable [76]. The reported k value associated with usage of the ultracentrifuge equipped with the TLA-110 rotor is 16.0, whereas it has been calculated to be 1042.5 when using the conventional bench-top centrifuge equipped with the F1010 rotor. Therefore, there is confidence that ultracentrifugation is sufficient to fully separate the liquid and solid components. After centrifugation, a 0.5 mL aliquot was removed and transferred into a polycarbonate reaction vessel that contained 9.5 mL of deionized water and subsequently measured using the ICP-MS.

2.6.3 - Adsorption Kinetics of Tc(IV) in Na-Ca-Cl Solutions

The Tc(IV) adsorption kinetic steady-state periods with shale, limestone, illite, and MX-80 bentonite in Na-Ca-Cl solutions were necessary to be determined. There was (20.0 ± 1.0) mg of preconditioned adsorbent, with (10.0 ± 0.5) mL of liquid used, for a resultant liquid/solid ratio of (0.50 ± 0.03) $m^3 \cdot kg^{-1}$. Two experiments were performed with the 0.1 $mol \cdot kgw^{-1}$ and 6.0 $mol \cdot kgw^{-1}$ Na-Ca-Cl solutions. Initial concentration of Tc(IV) used in experiments was on average (1.37 ± 0.62) $nanomol \cdot L^{-1}$. For the duration of the adsorption kinetic experiments, pH_m and Eh measurements were taken at each time interval for each sample to confirm that redox conditions did not change within the polycarbonate reaction vessel which would have allowed Tc(IV) to oxidize. Preparation of a sample to be measured, and the subsequent measurement is identical to the one described in Section 2.6.2.

2.7 - Batch Adsorption Experiments

2.7.1 - Ca-Na-Cl Solution pH_m and Ionic Strength Influence on Se(-II) Adsorption

After the adsorption kinetic experiments with Se(-II) onto granite and MX-80 bentonite in Ca-Na-Cl solutions were completed, batch adsorption experiments could be carried out. Ionic strength dependency was measured in 0.05, 0.1, 0.24, and 1.0 mol·kgw^{-1} Ca-Na-Cl solutions, whereas pH_m dependency experiments were measured at pH_m values between 4 and 9. Similar to Section 2.6.1, there was (20.0 ± 1.0) mg of preconditioned adsorbent, with (10.0 ± 0.5) mL of liquid used in the experiments. Throughout the duration of all batch adsorption experiments the pH_m and Eh were recorded daily to ensure that reducing conditions were present for the duration of the experiments. If the measured pH_m value differed from the required pH_m value by more than 0.2 units a pH adjustment was performed through addition of either 0.1 N HCl or 0.1 N NaOH. Subsequent sample preparation and measurement is identical to the one described in Section 2.6.1.

2.7.2 - Ca-Na-Cl Solution pH_m and Ionic Strength Influence on Tc(IV) Adsorption

Tc(IV) adsorption with respect to the Ca-Na-Cl solution ionic strength was tested with 0.05, 0.1, 0.24, and 1.0 mol·kgw^{-1} solutions. The pH_m dependency experiments for Tc(IV) adsorption experiments in was measured at pH_m values between 3 and 9. Similar to Section 2.6.2, there was (20.0 ± 1.0) mg of preconditioned adsorbent was used, with (10.0 ± 0.5) mL of liquid in experiments. Throughout the duration the experiments, the pH_m and Eh were recorded daily to ensure that reducing conditions were present. If the measured pH_m value differed from the required pH_m value by more than 0.2 units, a pH adjustment was performed through addition of either 0.1 N HCl or 0.1 N NaOH. Subsequent sample preparation and measurement is identical to the one described in Section 2.6.2.

2.7.3 - Na-Ca-Cl Solution pH_m and Ionic Strength Influence on Tc(IV) Adsorption

Tc(IV) batch adsorption experiments in Na-Ca-Cl solutions had the ionic strength dependency measured in 0.1, 1.0, 3.0, and 6.0 mol·kgw^{-1} solutions. pH_m dependency experiments were measured at pH_m values between 3 and 9. Similar to Section 2.6.3, there was (20.0 ± 1.0) mg of preconditioned adsorbent was used, with (10.0 ± 0.5) mL of liquid in experiments. Throughout the duration the experiments, the pH_m and Eh were recorded daily to ensure that reducing conditions were present. If the measured pH_m value differed from the required pH_m value by more than 0.2 units, a pH adjustment was performed through addition of either 0.1 N HCl or 0.1 N NaOH. Subsequent sample preparation and measurement is identical to the one described in Section 2.6.3.

2.7.4 - Se(-II) Adsorption in CR-10 Solution

An experiment was carried out to determine Se(-II) adsorption onto granite and MX-80 bentonite in CR-10 solution. The length of this adsorption experiment was determined from Se(-II) adsorption kinetic experiments in Ca-Na-Cl solutions with granite and MX-80 bentonite. Solid masses and liquid amounts used are identical to Section 2.6.1. The pH_m of the CR-10 solution was adjusted to pH_m = 7.0. The pH_m and Eh were recorded daily to ensure that reducing conditions were present for the duration of the experiment. If the measured pH_m value differed from the required pH_m value by more than 0.2 units, a pH adjustment was performed through addition of either 0.1 N HCl or 0.1 N NaOH. Subsequent sample preparation and measurement is identical to the one described in Section 2.6.1.

2.7.5 - Tc(IV) Adsorption in CR-10 Solution

Tc(IV) adsorption experiments with granite and MX-80 bentonite in CR-10 solution were also completed. The length of these adsorption experiments was determined from Tc(IV) adsorption kinetic experiments with granite and MX-80 bentonite in Ca-Na-Cl solutions. Solid masses and liquid amounts used are identical to Section 2.6.2. The pH_m of the CR-10 solution was adjusted to pH_m = 7.0. The pH_m

and Eh were recorded daily to ensure that reducing conditions were present for the duration of the experiment. If the measured pH_m value differed from the required pH_m value by more than 0.2 units, a pH adjustment was performed through addition of either 0.1 N HCl or 0.1 N NaOH. Subsequent sample preparation and measurement is identical to the one described in Section 2.6.2.

2.7.6 - Tc(IV) Adsorption in SR-270-PW Solution

Tc(IV) adsorption experiments with shale, limestone, illite, and MX-80 bentonite in SR-270-PW solution were also completed. The length of these adsorption experiments was determined from Tc(IV) adsorption kinetic experiments in Na-Ca-Cl solutions with shale, limestone, illite, and MX-80 bentonite. Solid masses and liquid amounts used are identical to Section 2.6.3. The pH_m of the SR-270-PW solution was adjusted to pH_m = 6.0. The pH_m and Eh were recorded daily to ensure that reducing conditions were present for the duration of the experiment. If the measured pH_m value differed from the required pH_m value by more than 0.2 units, a pH adjustment was performed through addition of either 0.1 N HCl or 0.1 N NaOH. Subsequent sample preparation and measurement is identical to the one described in Section 2.6.3.

Chapter 3 - Surface Complexation Modelling

Completion of the Se(-II) and Tc(IV) adsorption experiments provided data that was then utilized to optimize surface complexation models (SCM's). SCM's have been created to simulate Se(-II) and Tc(IV) adsorption onto granite and MX-80 bentonite in Ca-Na-Cl solutions, and Tc(IV) adsorption onto shale, illite, and MX-80 bentonite in Na-Ca-Cl solutions. Limestone does not have a simulated surface as it is presumed that the mineral assemblage composition is approximately 80.0% calcite, with minor amounts of quartz, dolomite, illite, and chlorite [12]. Given the complexity associated with the surface electrical properties of calcite [77], a non-electrostatic model was not attempted. As such, there is no model presentation that simulates the adsorption of Tc(IV) onto limestone in Na-Ca-Cl solutions. All SCM's were simulated with the geochemical code PHREEQC [78].

3.1 - Specific Ion Interaction Theory

When executing simulations in electrolyte solutions that have substantial ionic strengths, a proper method must be invoked to account for the increased electrostatic interactions between ions of specific interest, and the background electrolyte ions. Specific Ion interaction Theory (SIT) was employed to calculate activity coefficients following Equation (4) [79]. Where: z_j is the charge of ion j, D is the Debye-Hückel term, m_k is the molality of ion k, which is oppositely charged to ion j, and $\varepsilon(j, k)$ is the specific ion interaction parameter. Usage of SIT is acceptable up to an ionic strength of approximately 4.0 mol·kgw^{-1} [79]. This will allow simulations to be completed in all Ca-Na-Cl solutions and up to 3.0 mol·kgw^{-1} in the Na-Ca-Cl solutions. Given this, simulations were not attempted to be optimized with respect to the R_d values obtained from the Tc(IV) batch adsorption experiment in 6.0 mol·kgw^{-1} Na-Ca-Cl solution. Relevant ion interaction coefficients and all Se(-II) and Tc(IV) reactions used throughout the modelling are presented in Table 7 and Table 8, respectively.

$$log(\gamma_j) = -z_j^2 D + \sum^{k} \varepsilon(j,k) m_k \quad (4)$$

Table 7 – Selected ion interaction coefficients specific to Se(-II) and Tc(IV) utilized throughout the surface complexation modelling.

Cation (ion j)	Anion (ion k)	ε(j, k) [kg·mol^{-1}]	Error	Reference
Na^+	OH^-	0.04	0.01	[81]
Na^+	Cl^-	0.03	0.01	[80]
Ca^{2+}	Cl^-	0.15	0.01	[80]
H^+	Cl^-	0.12	0.01	[81]
Na^+	HSe^-	-0.01	0.10	[80]
Ca^{2+}	HSe^-	0.15[a]	0.01	[This study]
$TcO(OH)^+$	Cl^-	0.11	0.01	[22]
Na^+	$TcO(OH)_3^-$	-0.08	0.04	[79]
Ca^{2+}	$TcO(OH)_3^-$	0.15	0.00	[22]
$Tc_2O_2(OH)_2^{2+}$	Cl^-	-0.43	0.11	[79]

[a] The ε(Ca^{2+}, HSe^-) ion interaction coefficient is an estimation based upon corresponding charge type ε(Ca^{2+}, X^-) = 0.15 kg·mol^{-1} [22].

3.2 - Relevant Thermodynamic Data

All solutions being simulated have an identical Na/Ca ratio, ionic strength, and either Ca-Na-Cl concentrations or Na-Ca-Cl concentrations as the solutions used in experiments. All Se(-II) simulations have a Se(-II) concentration of 1.00 μmol·kgw^{-1}, which is on par with the initial Se(-II) concentration used throughout the adsorption experiments. No polyselenide species of the form Se_n^{2-}, where n = 1 – 4, were included in the modelling as it was assumed that these species would form only in more alkaline conditions where $pH_m \geq 10$ [82, 83]. In all Tc(IV) simulations, the Tc(IV) concentration was 1.0 nanomol·kgw^{-1}, which is on par with the initial concentration of Tc(IV) used within all adsorption experiments. Thermodynamic information specific to Se(-II) and Tc(IV) is found in both the Nuclear Energy Agency and Japanese Atomic Energy Agency thermodynamic databases's [64, 79 - 81].

However, ion interaction parameters and a dimer hydrolysis reaction specific to Tc(IV) have been included to improve modelling results.

To establish a surface complexation model that best simulates adsorption of either Se(-II) and Tc(IV), both surface complexation and ion exchange reactions should be considered. In the case of Se(-II), the adsorption of an anion was being simulated while the adsorption of an aqueous species with no charge was simulated in Tc(IV) simulations. Presently, ion exchange reactions are not considered important as they are specific to cations. Therefore, the formation of both Se(-II) and Tc(IV) surface complexes are possible mechanisms which may be able to simulate the adsorption of either Se(-II) and Tc(IV).

Table 8 - Selected reactions specific to Se(-II) and Tc(IV) used throughout the surface complexation modelling.

Reaction	Log K	Error	Reference
$HSe^- + H^+ \leftrightarrow H_2Se(aq)$	3.850	0.050	[81]
$H^+ + SeO_4^{2-} \leftrightarrow HSeO_4^-$	1.750	0.100	[81]
$2\ H^+ + SeO_3^{2-} \leftrightarrow H_2SeO_3(aq)$	11.00	0.269	[81]
$H^+ + SeO_3^{2-} \leftrightarrow HSeO_3^-$	8.360	0.230	[81]
$2\ TcO(OH)_2(aq) + 2\ H^+ \leftrightarrow Tc_2O_2(OH)_2^{2+} + 2\ H_2O(l)$	12.99	0.410	[79]
$TcO(OH)_2(aq) + H^+ \leftrightarrow TcO(OH)^+ + H_2O(l)$	4.563	0.216	[22]
$TcO(OH)_2(aq) + 2\ H^+ \leftrightarrow TcO^{2+} + 2\ H_2O(l)$	4.000	0.000	[22]
$TcO(OH)_2(aq) + H_2O(l) \leftrightarrow TcO(OH)_3^- + H^+$	-10.900	0.400	[22]
$TcO_4^- + 6\ H^+ + 3\ e^- \leftrightarrow TcO^{2+} + 3\ H_2O(l)$	33.414	0.000	[79]
$TcO_2{\cdot}1.6H_2O(s) \leftrightarrow TcO(OH)_2(aq) + 0.6\ H_2O(l)$	-8.415	0.180	[79]

3.3 - Model Definition

Presently, these SCM's assume that the surface of any adsorbent mineral is comprised of amphoteric surface sites at the edges of the mineral sheets. These surface sites are considered to be an analogous representation of the surface functional groups that are typically found at the edge of aluminosilicate minerals. As the amphoteric surface sites are considered to protonate and deprotonate with respect to a varying pH, there will be the formation of an electric double layer and thus a variable surface charge. Typically, protonation and deprotonation behaviour associated with these minerals is described with protolysis reactions and protolysis reaction constants. These SCM's are developed based upon 2-site non-electrostatic surface complexation/cation exchange (2SPNE SC/CE) model, and a component additive (CA) SCM [52, 61, 84 - 91]. Previously, 2SPNE SC/CE models have been shown to be capable of simulating the adsorption of various radionuclides onto different adsorbents with success [52, 61, 84 - 91]. Since this is a 2-site model, there are both strong and weak sites which should be considered within the models. However, with modelling of Se(-II) and Tc(IV) adsorption being performed at trace concentrations, only the strong sites found within the 2SPNE SC/CE model need to be considered [52, 61, 84 - 91].

Component assemblage minerals that are included in these models are feldspar, quartz, biotite, illite, montmorillonite, albite, and chlorite. All assemblage minerals are simulated using a 2SPNE SC/CE SCM. Currently, granite, shale, and MX-80 bentonite are considered to be heterogenous minerals, and as such are each comprised of some of the previously mentioned assemblage minerals. Therefore, the CA SCM approach has further been employed to simulate adsorption of either Se(-II) and Tc(IV) onto granite, shale, and MX-80 bentonite. Table 9 provides the mineral assemblage compositions considered which define the simulated granite, shale, illite, and MX-80 bentonite surfaces. Appendix B contains a petrographic analysis with which the granite surface was defined [92]. Shale and MX-80 bentonite use XRD results obtained from previously published studies to define their assemblage proportions [12, 93, 94]. Illite is assumed to be 100.0% illite.

One reason for pursuing the CA SCM methodology in conjunction with the 2SPNE SC/CE methodology is based upon the assumption that any heterogenous mineral's adsorbent surface will be comprised of multiple adsorbent mineral surfaces, which all have their own unique protolysis characteristics. This should provide more flexibility when modelling adsorption of either Se(-II) or Tc(IV) across a large pH range. A model assumption is that the specific surface area (SSA) associated with a heterogenous adsorbent surface being simulated is distributed proportionately across the assemblage components. Therefore, the SSA's for each mineral assemblage (SSA_i) have been calculated following (5): where, $SSA_{adsorbent}$ is the SSA of the mineral being simulated.

$$SSA_i = SSA_{adsorbent} \cdot (MineralAssemblage\%) \quad (5)$$

For reference: $SSA_{granite}$ = 0.18 $m^2 \cdot g^{-1}$ [95], SSA_{shale} = 10.3 $m^2 \cdot g^{-1}$ [96], SSA_{illite} = 16.4 $m^2 \cdot g^{-1}$ [97], $SSA_{MX\text{-}80}$ = 8.5 $m^2 \cdot g^{-1}$ [98]. The SSA for granite, shale, and illite were determined with N_2 Brunauer-Emmett-Teller (BET) measurements [95 - 97]. The SSA for MX-80 bentonite was determined through Atomic Force Microscopy (AFM), and low-pressure gas adsorption experiments [98]. An important comment is this MX-80 bentonite surface utilizes the lateral edge SSA of 8.5 $m^2 \cdot g^{-1}$, as opposed to larger SSA's of 26.6 $m^2 \cdot g^{-1}$, 753.0 $m^2 \cdot g^{-1}$, or 788.0 $m^2 \cdot g^{-1}$, which have been attributed to the basal plane, interlayer, and total SSA associated with MX-80 bentonite, respectively [98]. This is considered to improve the MX-80 bentonite SCM by restricting the maximum number of possible adsorption sites that exist on the surface. This is believed to assist in preventing either an under- or over-prediction of the concentration of any simulated surface complex. This should provide more appropriate surface complexation constants for any hypothesized surface complexation reactions within this MX-80 bentonite model. Another model assumption is that the site density for any mineral assemblage component that does exist within a heterogenous mineral is equal to the site density of the same mineral assemblage component when found in its homogeneous form.

One discussion will be mentioned specific to the simulated granite surface. In the past, a granite surface was simulated which used an albite component surface within a CA SCM [91]. To simplify the

modelling of both granite and MX-80 bentonite, the protolysis constants and site density that was used to define albite in the previously presented model have been used to define both the feldspar surface within the granite model, as well as the albite surface within the MX-80 bentonite model. A second assumption about the granite model being presented is that the 56.0% feldspar assemblage surface is a summation of the known 37.0% plagioclase feldspar, and 19.0% alkali feldspar mineral amount in granite. These two assumptions are both made on the basis that albite is a known plagioclase feldspar, and that plagioclase is a feldspathic mineral. It should be acknowledged that there may be discrepancies between the surface charge behaviour of albite compared to feldspar as their chemical formulas are $NaAl_3O_8$ and KAl_3O_8, respectively. But, as this is a non-electrostatic SCM, the interactions that may occur between the background electrolyte ions and the amphoteric surface sites are not modelled, and the assumption was presumed justified. Simulated surfaces for granite, shale, illite, and MX-80 bentonite are provided in Tables 10 and 11. Surface speciation curves with respect to pH for granite, shale, illite, and MX-80 bentonite are presented in Figures 1, 2, 3, and 4, respectively.

Table 9 – Average mineralogical composition of granite, shale, illite, and MX-80 bentonite used to define the simulated surfaces. For the readers reference: Appendix B contains a petrographic analysis with which the granite surface was defined [92]. Shale and MX-80 bentonite use XRD results obtained from previously published studies to define their assemblage proportions [12, 93, 94]. Illite is assumed to be 100.0% illite.

Mineral Assemblage	Granite [wt %]	Shale [wt %]	Illite [wt %]	MX-80 bentonite [wt %]
Feldspar	37.0	3.00	0.00	0.00
Alkali Feldspar	19.0	0.00	0.00	0.00
Quartz	34.0	30.0	0.00	3.62
Biotite	3.00	0.00	0.00	0.00
Montmorillonite	0.00	0.00	0.00	85.4
Albite	0.00	0.00	0.00	3.54
Illite	0.00	36.0	100.0	0.00
Chlorite	1.40	24.0	0.00	0.00

Table 10 - Protolysis constants for each constituent mineral assemblage surface utilized within the component additive surface complexation model.

Mineral Assemblage Components		Protonation and Deprotonation Reaction		Reference
		$\equiv SOH + H^+ \leftrightarrow \equiv SOH_2^+$	$\equiv SOH \leftrightarrow \equiv SO^- + H^+$	
Protolysis Constants (log K)	Feldspar / Albite	4.13	-8.46	[91]
	Quartz	-1.26	-7.28	[91]
	Biotite	4.60	-6.40	[91]
	Illite	4.00	-6.20	[97]
	Montmorillonite	4.50	-7.90	[84 - 86]
	Chlorite	5.60	-8.20	[99]

Table 11 - Simulated surfaces and their constituent surfaces with calculated SSA and site densities.

Simulated Surface	Constituent Surface	SSA [$m^2 \cdot g^{-1}$]	Site Density [sites·nm^{-2}]	Reference
Granite	Feldspar_sOH	0.101	4.05	[91]
	Quartz_sOH	0.061	5.67	[91]
	Biotite_sOH	0.005	3.81	[91]
Shale	Illite_sOH	3.71	2.30	[97]
	Quartz_sOH	3.09	5.67	[91]
	Chlorite_sOH	2.47	4.65	[99]
	Feldspar_sOH	0.309	4.05	[91]
Illite	Illite_sOH	16.4	2.30	[97]
MX-80 Bentonite	Montmorillonite_sOH	7.26	5.70	[100]
	Quartz_sOH	0.31	5.67	[91]
	Albite_sOH	0.30	4.05	[91]

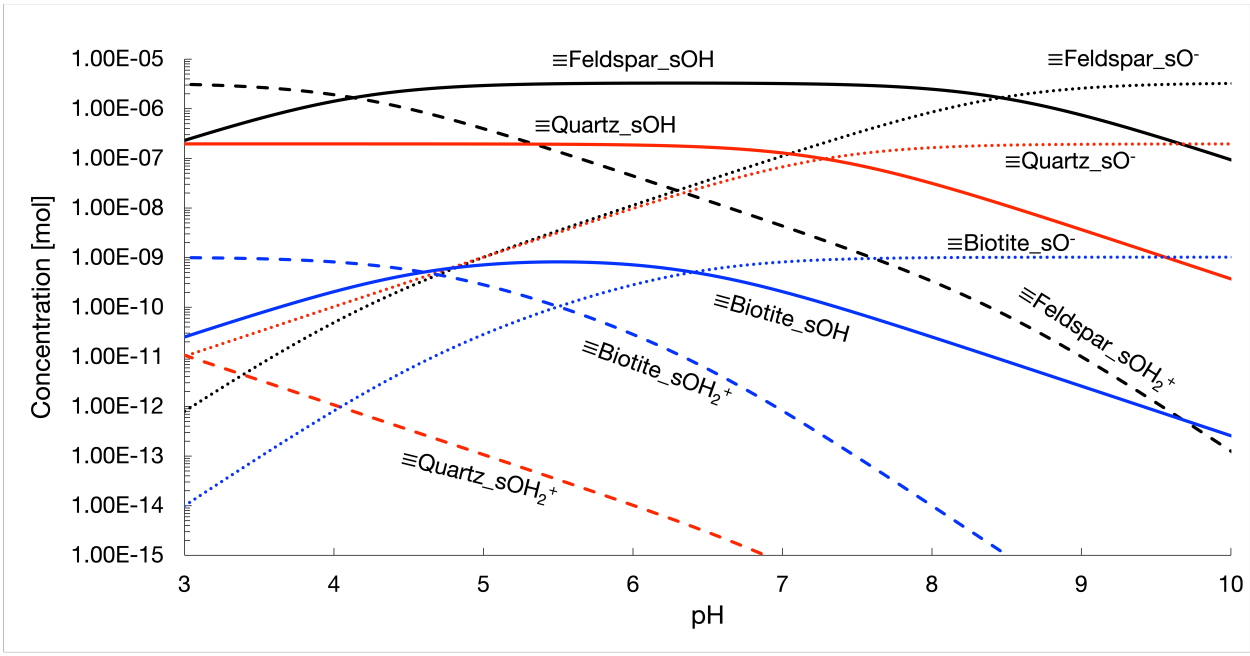

Figure 1 - Surface speciation for the simulated granite surface. Feldspar surfaces are black, quartz surfaces are red, biotite surfaces are blue.

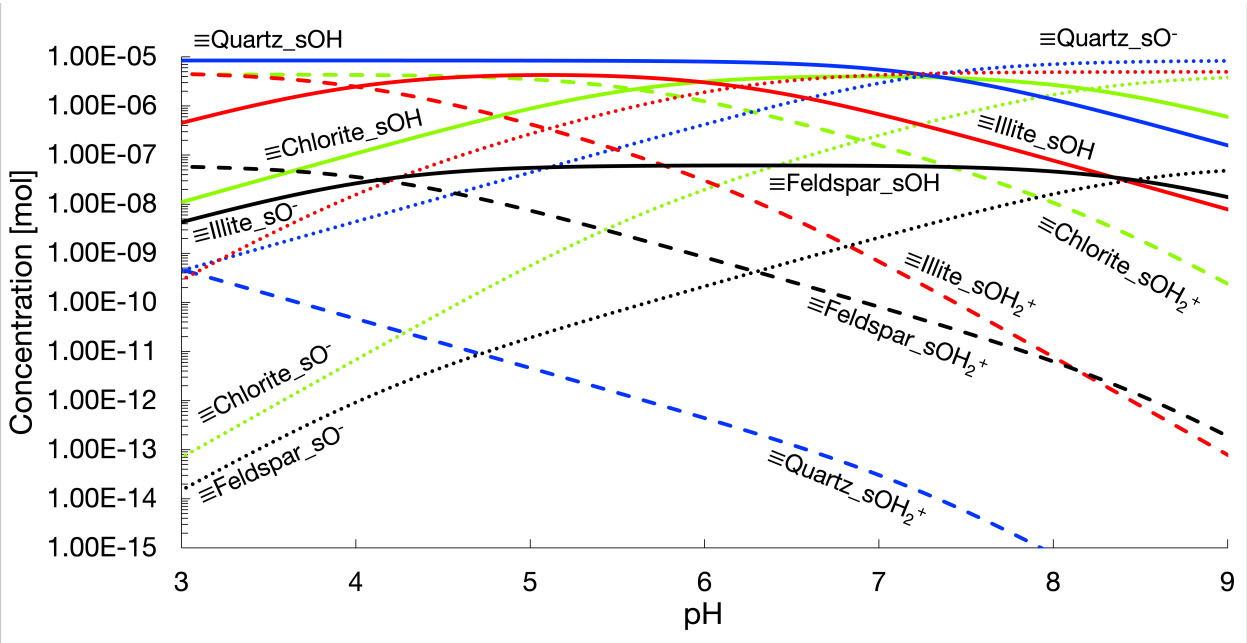

Figure 2 - Surface speciation for the simulated shale surface. Illite surfaces are red, quartz surfaces are blue, feldspar surfaces are black, and chlorite surfaces are green.

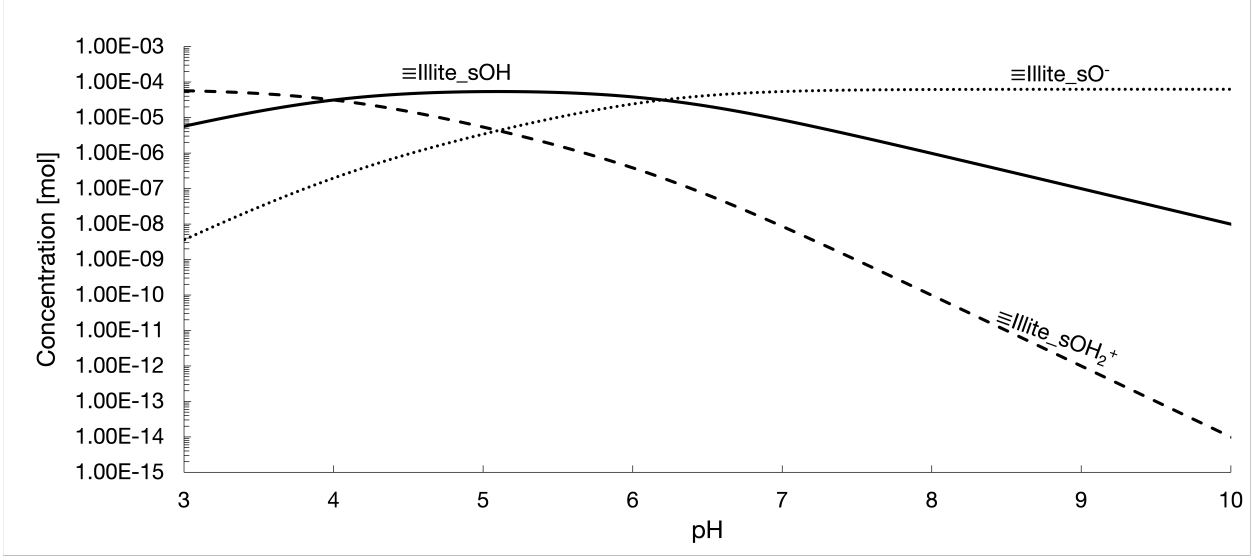

Figure 3 - Surface speciation for the simulated illite surface.

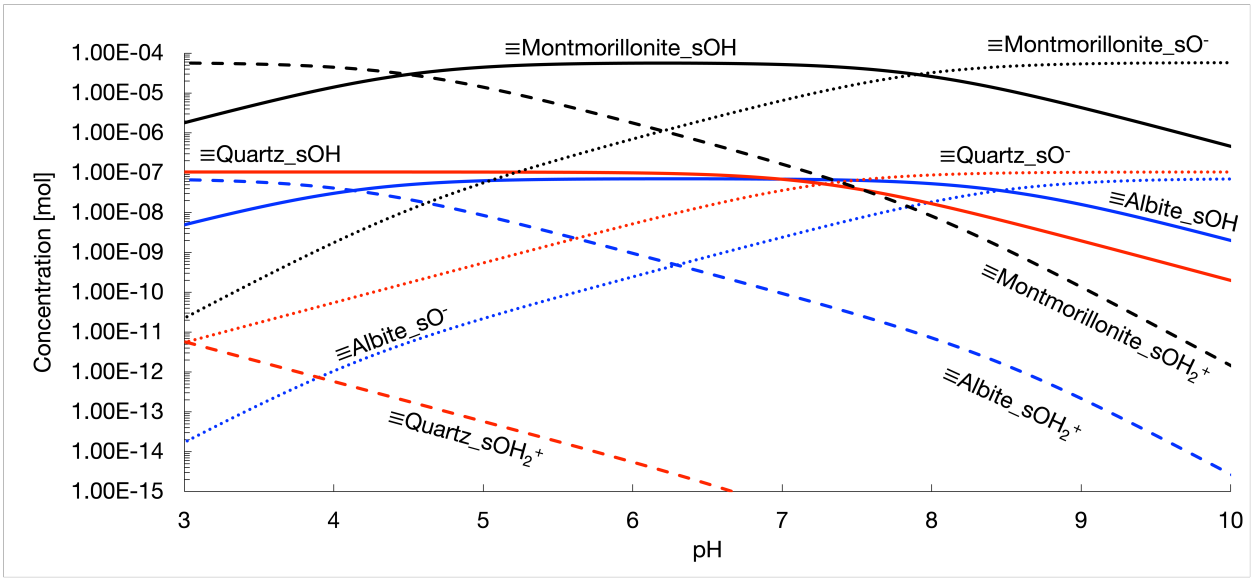

Figure 4 - Surface speciation for the simulated MX-80 bentonite surface. Montmorillonite surfaces are black, quartz surfaces are red, albite surfaces are blue.

3.4 - Surface Complexation

Presently, there are two possible Se(-II) surface complexes with mineral surfaces which have been described with (6) and (7) [55, 61]. The first Se(-II) surface complexation reaction is assumed to be a chemically specific interaction between the HSe^- anion and the surface hydroxyl groups. In contrast, the second Se(-II) surface complexation reaction is assumed to be non-specific, and similar surface complexes would form with background electrolytes and the simulated surface [101]. Furthermore, there are two possible Tc(IV) surface complexes which are described with (8) and (9) [11, 89]. The first Tc(IV) surface complexation reaction is assumed to produce a monodentate surface complex, whereas the second Tc(IV) surface complex is a bidentate surface complex. The denticity associated with a Tc(IV) chelate is dependent upon the number of electrons that the ligands on the adsorbent surface can donate to the central Tc(IV) atom. Optimization of the surface complexation models has been performed through iteratively changing the surface complexation constants associated with (6) and (7) simultaneously, or (8) and (9) simultaneously. Until a best fit has been determined between the surface complexation model and experimental data. Iteratively fitting the surface complexation model was completed through optimizing the hypothesized surface complexation constants which are unable to be constrained prior to the iterative procedure. Error was calculated as the residual sum of squares, and simulations were performed until this error was minimized. Aqueous speciation of Se(-II) and Tc(IV) have been included in Figures A6 and A7, respectively.

$$\equiv SOH + HSe^- \leftrightarrow \equiv SSe^- + H_2O \quad (6)$$

$$\equiv SOH + HSe^- \leftrightarrow \equiv SOH_2HSe \quad (7)$$

$$\equiv SOH + TcO(OH)_2 \leftrightarrow \equiv SOTcO(OH) + H_2O \quad (8)$$

$$2(\equiv SOH) + TcO(OH)_2 \leftrightarrow (\equiv SO)_2TcO(OH)^- + H_2O + H^+ \quad (9)$$

Chapter 4 - Results and Discussion

4.1 - Adsorption Kinetics of Se(-II) onto Granite and MX-80 Bentonite in Ca-Na-Cl Solutions

Adsorption kinetic results for Se(-II) adsorption onto both granite and MX-80 bentonite are presented in Figures 5a and 5b. Granite reached adsorption steady-state conditions within 3 – 5 days, while MX-80 bentonite reaches adsorption steady-state conditions within 7 – 10 days. From these adsorption kinetics results, the adsorption steady-state period for granite and MX-80 bentonite have been set to 7 and 14 days, respectively. Initial pH_m, final pH_m, and the measured R_d values from the adsorption kinetic experiments are presented in Table 12.

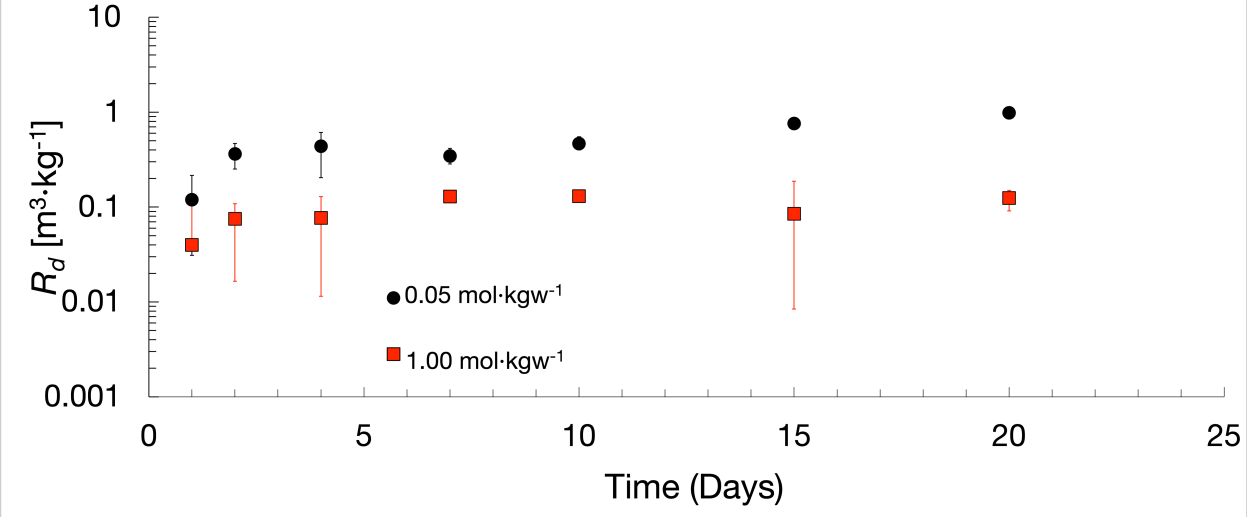

Figure 5a - Adsorption kinetic results for Se(-II) adsorption onto granite in 0.05 and 1.0 mol·kgw^{-1} Ca-Na-Cl solutions. For the readers reference, R_d is defined as the adsorption distribution ratio and was previously defined in Section 2.6, see page 13.

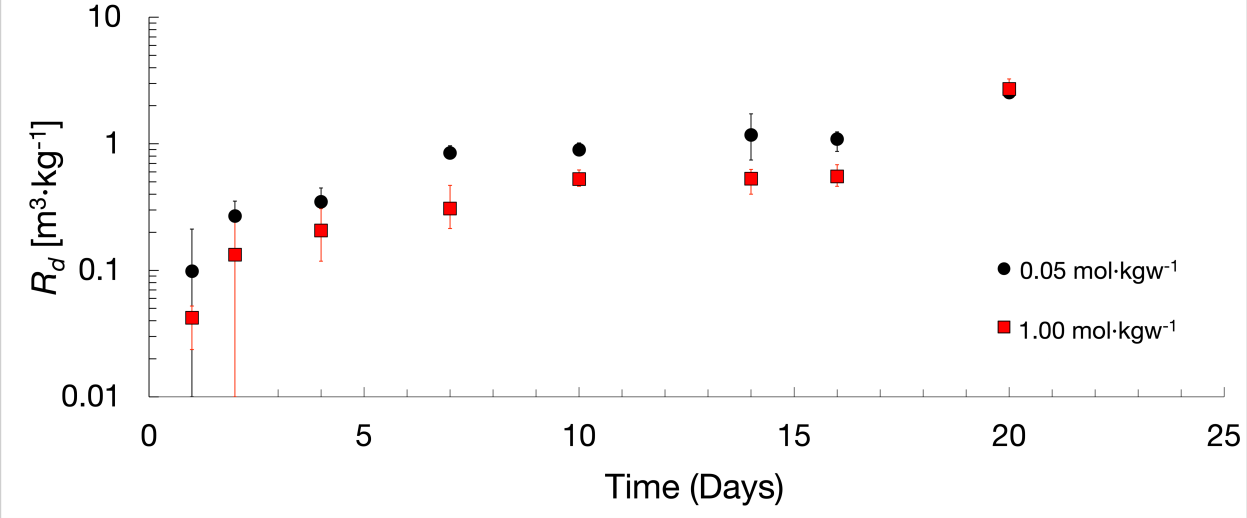

Figure 5b - Adsorption kinetic results for Se(-II) adsorption onto MX-80 bentonite in 0.05 and 1.0 mol·kgw^{-1} Ca-Na-Cl solutions.

Previously, Iida et al., determined that Se(-II) adsorption onto biotite, goethite, and magnetite returned 14-day adsorption steady periods [55]. This contrasts the 7-day adsorption steady state period determined in this study for granite despite the similarity in the minerals containing iron. A reminder is that the granite surface is assumed to be 56.0% feldspar, 34.0% quartz, and 3.0% biotite. Previously, evidence has been shown that quartz does not exhibit an attraction to Se(-II) [55]. Then, with the difference in the iron-containing minerals that are within granite, coupled with the possibility that any possible adsorption reactions involving Se(-II) and iron may require an increased amount of time to reach adsorption steady-state conditions. Presently, a rapid surface adsorption process could dominate Se(-II) adsorption onto granite, and this may explain observed results showing adsorption steady-state conditions are reached in 3 to 5 days. This adsorption process is presumed to be described by the formation of the non-specific surface complex, $\equiv SOH_2HSe$. An assumption is being made however, which is that the adsorption kinetics associated with the formation of the chemically specific, $\equiv SSe^-$ surface complex, are slower compared to the non-specific surface complex. As such, the conservative adsorption steady-state period of 7 days for granite is considered justified.

Recently, Walker et al., presented that Se(-II) adsorption onto MX-80 bentonite in Na-Ca-Cl solutions reached steady-state adsorption conditions in 14 days, which is in agreement with the results

observed in Ca-Na-Cl solutions [61]. Sugiera et al., found an adsorption steady-state period of 7 days associated with the Se(-II) adsorption kinetics onto montmorillonite [57]. Given that MX-80 bentonite is assumed to be approximately 85.0% montmorillonite, the remaining 15.0% may have an increased interaction period, or exhibit no interaction at all with Se(-II). These adsorption kinetic results also provide evidence that MX-80 bentonite adsorbs more Se(-II) than granite, which was shown to occur previously, thus supporting these adsorption kinetic results [57].

Table 12 – Initial pH_m, final pH_m, and measured R_d values for Se(-II) adsorption onto granite and MX-80 bentonite in the 0.05 and 1.0 mol·kgw^{-1} Ca-Na-Cl solutions adsorption kinetics experiments.

Adsorbent	Ionic Strength [mol·kgw^{-1}]	Initial pH_m	Final pH_m	R_d [m^3·kg^{-1}]
Granite	0.05	9.1 ± 0.1	9.1 ± 0.1	0.76 ± 0.08
	1.0	9.3 ± 0.1	9.4 ± 0.1	0.09 ± 0.01
MX-80 Bentonite	0.05	9.1 ± 0.1	9.1 ± 0.1	1.09 ± 0.22
	1.0	9.4 ± 0.1	9.4 ± 0.1	0.55 ± 0.13

4.2 - Adsorption Kinetics of Tc(IV) onto Granite and MX-80 Bentonite in Ca-Na-Cl Solutions

Adsorption kinetic results for Tc(IV) adsorption onto both granite and MX-80 bentonite in Ca-Na-Cl solutions are presented in Figures 6a and 6b. Granite reached adsorption steady-state conditions within 3 – 5 days, while MX-80 bentonite reaches adsorption steady-state conditions within 7 – 10 days. Therefore, the adsorption steady-state period for granite and MX-80 bentonite, have been set to 7 and 14 days, respectively. Initial pH_m, final pH_m, and the measured R_d values from the adsorption kinetic experiments are presented in Table 13.

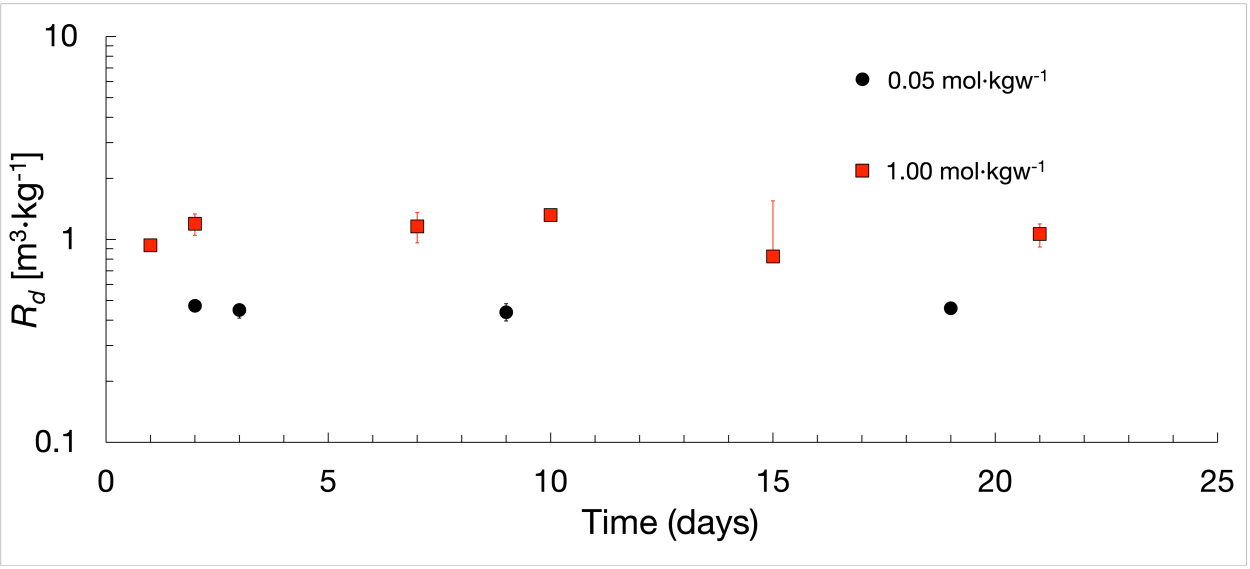

Figure 6a - Adsorption kinetics results for Tc(IV) adsorption onto granite in 0.05 and 1.0 mol·kgw^{-1} Ca-Na-Cl solutions.

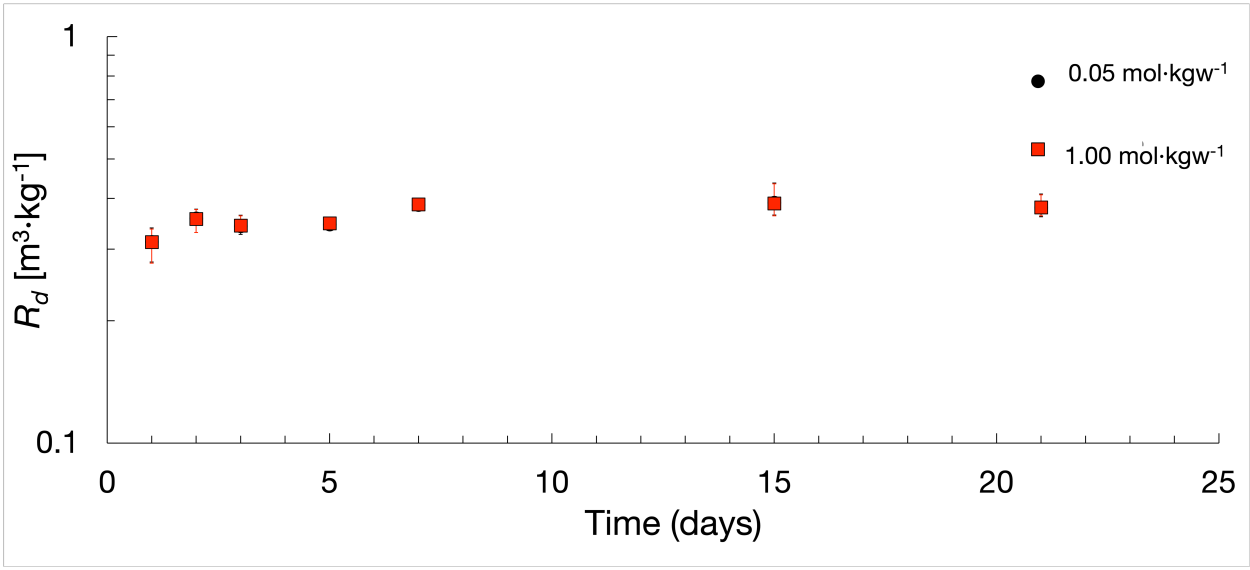

Figure 6b - Adsorption kinetics results for Tc(IV) adsorption onto MX-80 bentonite in 0.05 and 1.0 mol·kgw^{-1} Ca-Na-Cl solutions. R_d values are approximately equal from Tc(IV) adsorption onto MX-80 bentonite in either 0.05 or 1.0 mol·kgw^{-1} Ca-Na-Cl solutions. As such, both data sets are overlayed.

Presently, it is presumed that the adsorption of Tc(IV) onto the predominant minerals which comprise granite could provide an ability for the kinetic Tc(IV) adsorption behaviour observed in this study to be compared. Hallam et al., utilized a 7-day adsorption steady-state period throughout their Tc(IV) batch adsorption experiments onto the adsorbents hematite, geothite, plagioclase feldspar, quartz, and shale [11]. This period is matched by Amaya et al. and Rozov et al., who each use a 7-day periods within their studies [37, 102]. However, Lieser et al., found a need to use an increased period of 10 days [18].

Table 13 – Initial pH_m, final pH_m, and measured R_d values for Tc(IV) adsorption onto granite and MX-80 bentonite in the 0.05 and 1.0 mol·kgw^{-1} Ca-Na-Cl solutions adsorption kinetics experiments.

Adsorbent	Ionic Strength [mol·kgw^{-1}]	Initial pH_m	Final pH_m	R_d [m³·kg^{-1}]
Granite	0.05	8.7 ± 0.1	8.8 ± 0.1	0.46 ± 0.07
	1.0	7.6 ± 0.1	4.8 ± 0.1	1.07 ± 0.15
MX-80 Bentonite	0.05	8.4 ± 0.1	8.4 ± 0.1	0.38 ± 0.03
	1.0	8.1 ± 0.1	8.2 ± 0.1	0.38 ± 0.03

4.3 - Adsorption Kinetics of Tc(IV) onto Shale, Limestone, Illite, and MX-80 Bentonite in Na-Ca-Cl Solutions

The results from the Tc(IV) adsorption kinetic experiments onto shale, limestone, illite, and MX-80 bentonite in Na-Ca-Cl solutions are presented in Figures 7a - 7d. Steady-state adsorption conditions are reached within 5 – 7 days for shale, and within 10 – 14 days for limestone, illite, and MX-80 bentonite, respectively. From these results, the adsorption steady-state period for shale will be 7 days, whereas limestone, illite, and MX-80 bentonite will use 14-day adsorption steady-state periods in the subsequent batch adsorption experiments. Initial pH_m, final pH_m, and the measured R_d values are presented in Table 14.

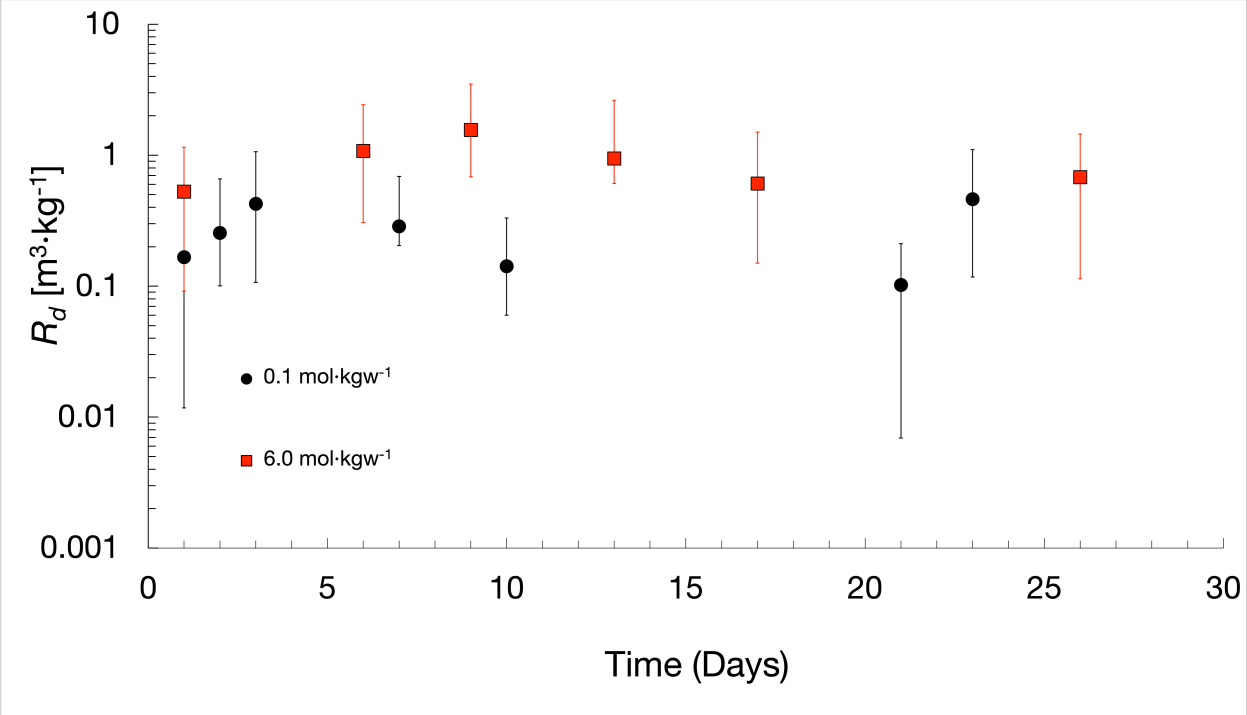

Figure 7a - Adsorption kinetics for Tc(IV) onto shale in 0.1 and 6.0 mol·kgw^{-1} Na-Ca-Cl solutions.

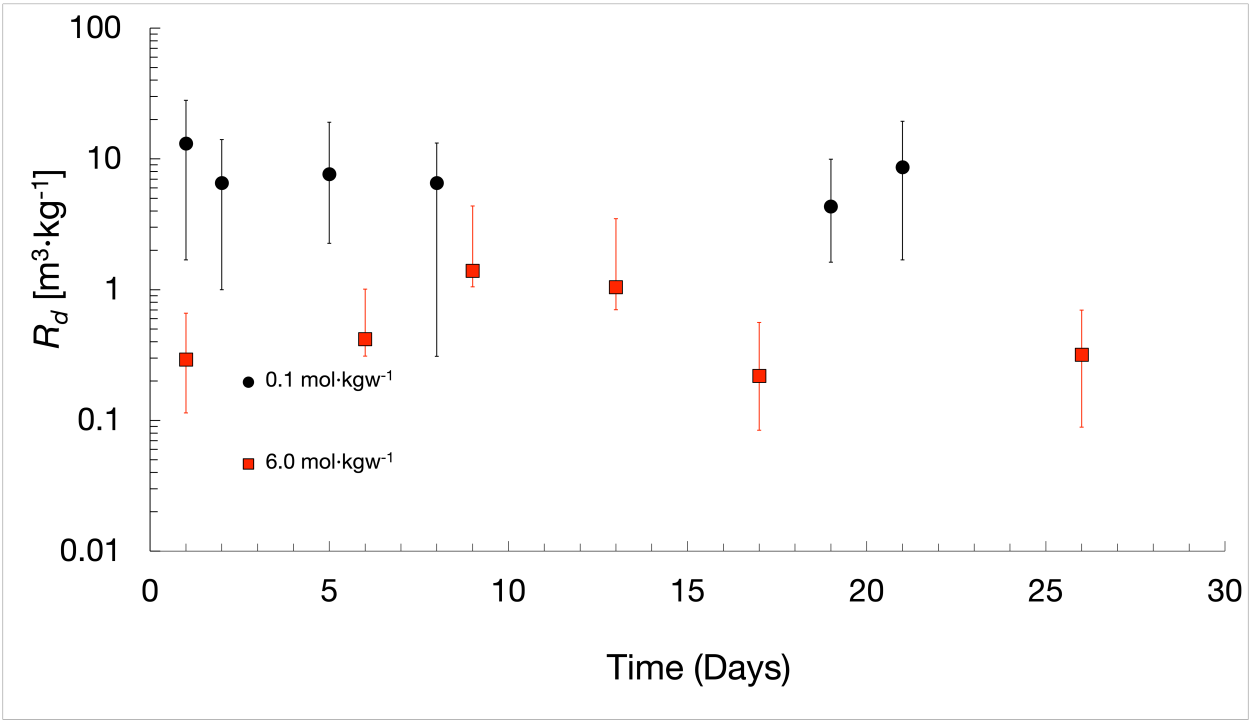

Figure 7b - Adsorption kinetics for Tc(IV) onto limestone in 0.1 and 6.0 mol·kgw^{-1} Na-Ca-Cl solutions.

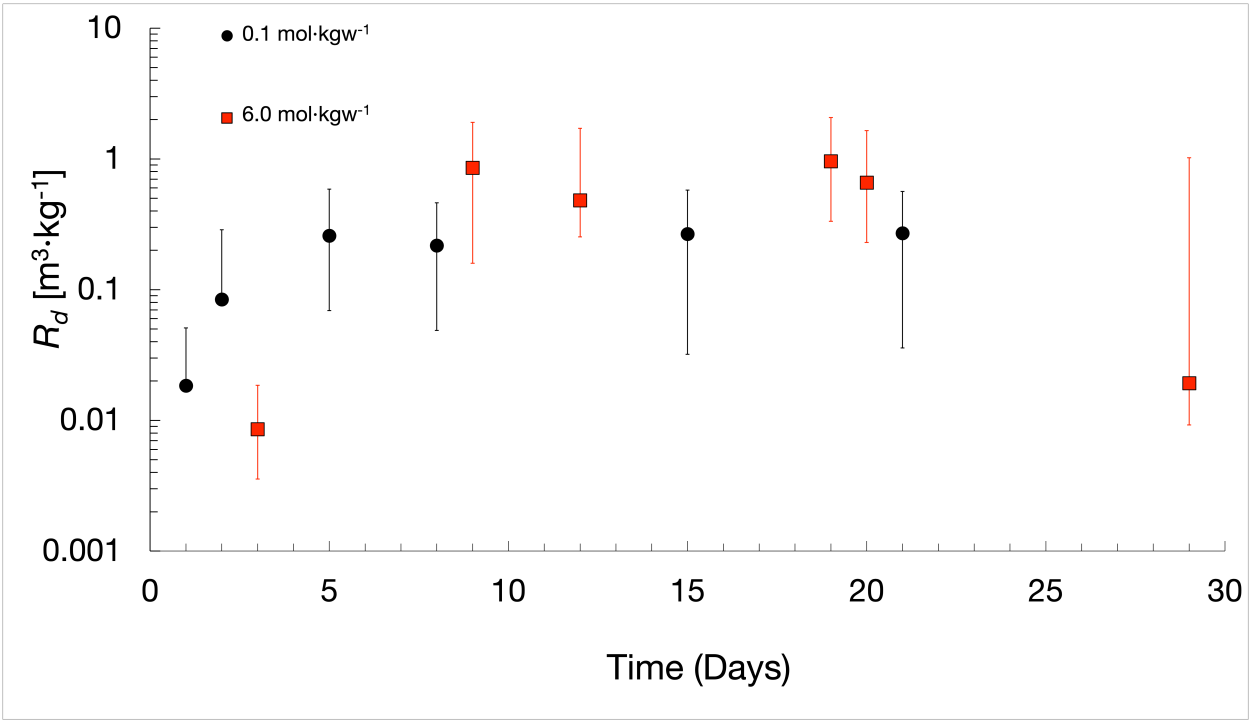

Figure 7c - Adsorption kinetics for Tc(IV) onto illite in 0.1 and 6.0 mol·kgw^{-1} Na-Ca-Cl solutions.

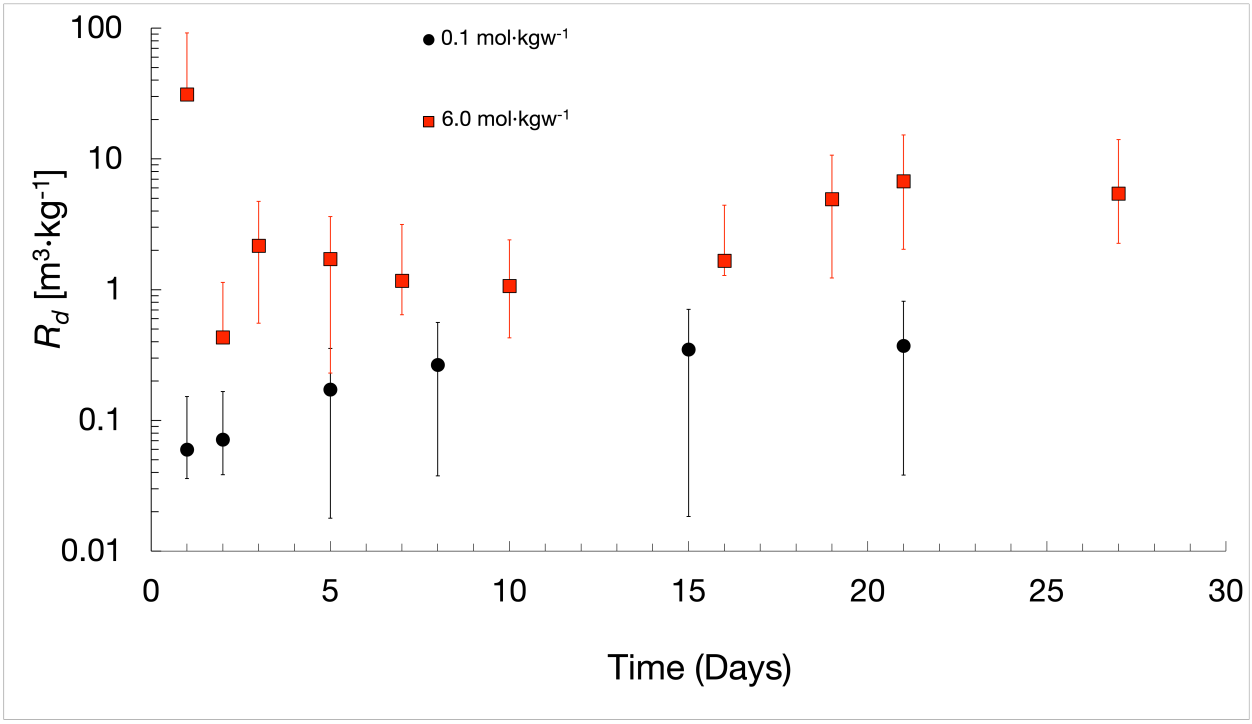

Figure 7d - Adsorption kinetics for Tc(IV) onto MX-80 bentonite in 0.1 and 6.0 mol·kgw^{-1} Na-Ca-Cl solutions.

Tc(IV) adsorption onto illite in Na-Ca-Cl solutions, and Tc(IV) adsorption onto MX-80 bentonite in Ca-Na-Cl and Na-Ca-Cl solutions all have 14-day adsorption steady-state periods. As MX-80 bentonite is assumed to be 85.0% montmorillonite, and montmorillonite and illite are both smectites, the similar periods are to be expected. With the fact that Lieser et al., previously utilized a Tc(IV) adsorption steady-state period of 10-days [18], the longer period of 14-days is considered justified.

Progressing to Tc(IV) adsorption onto shale, Hallam et al., used an identical 7-day adsorption steady-state adsorption period for shale [11]. Therefore, this provides confidence that the 7-day adsorption steady-state period assigned to shale determined from this study, is justified. Further, as the surface of shale is assumed to be 36.0% illite, 30.0% quartz, and 24.0% chlorite, the 7-day adsorption steady-state adsorption period used by Hallam et al., for quartz also coincides with the results from this study [11]. Uniquely, the adsorption steady-state period determined for shale and illite, are 7 and 14 days, respectively. This is despite shale being assumed to be 36.0% illite. The decreased amount of time associated with Tc(IV) adsorption kinetics onto shale could be due to either the quartz or chlorite component exhibiting a rapid adsorption process.

A discussion specific to Tc(IV) adsorption onto limestone is that in the 0.1 mol·kgw^{-1} Na-Ca-Cl solution, Tc(IV) adsorption appears to be a rapid process, with adsorption steady-state conditions being reached within 1-day. However, in 6.0 mol·kgw^{-1} Na-Ca-Cl solution, the adsorption steady-state period is 14-days. Therefore, in all limestone batch adsorption experiments, a period of 14 days was used. At the present, the difference in the kinetics of Tc(IV) adsorption onto limestone is presumed to be associated with an ionic strength effect. Previously, Tc(IV) adsorption behaviour onto sediments was observed to be accelerated in high ionic strength solutions, compared to in low ionic strength conditions [18]. The conservative adsorption steady-state period of 14 days chosen for limestone, was due to the variability in the experimentally determined R_d values, combined with the requirement that Tc(IV) adsorption onto limestone must reach steady-state adsorption conditions. However, it does appear that adsorption of Tc(IV) onto limestone occurred rapidly, with steady-state adsorption conditions reached within 1 - 2 days.

Table 14 – Initial pH_m, final pH_m, and measured R_d values for Tc(IV) adsorption onto shale, illite, and MX-80 bentonite in the 0.1 and 6.0 mol·kgw^{-1} Na-Ca-Cl solution adsorption kinetic experiments.

Adsorbent	Ionic Strength [mol·kgw^{-1}]	Initial pH_m	Final pH_m	R_d [m^3·kg^{-1}]
Shale	0.1	8.3 ± 0.5	7.9 ± 0.5	0.45 ± 0.35
	6.0	7.5 ± 0.5	7.3 ± 0.5	0.67 ± 0.48
Limestone	0.1	8.5 ± 0.1	8.2 ± 0.1	10.1 ± 7.60
	6.0	8.0 ± 0.2	8.0 ± 0.1	0.16 ± 0.14
Illite	0.1	10.8 ± 0.1	11.0 ± 0.1	0.29 ± 0.23
	6.0	8.9 ± 0.1	8.6 ± 0.1	0.02 ± 0.43
MX-80 Bentonite	0.1	10.9 ± 0.1	11.0 ± 0.1	0.35 ± 0.33
	6.0	7.9 ± 0.1	7.6 ± 0.1	4.73 ± 3.20

4.4 - Ca-Na-Cl Solution pH_m and Ionic Strength Influence on Se(-II) Adsorption

Results from the Se(-II) batch adsorption experiments onto granite and MX-80 bentonite with respect to pH and ionic strength in Ca-Na-Cl solutions, are presented in Figures 8 and 9, respectively. SCM's which successfully simulate the determined Se(-II) adsorption data are presented in Figures 8 and 9, respectively.

4.4.1 - Se(-II) Adsorption onto Granite in Ca-Na-Cl Solutions

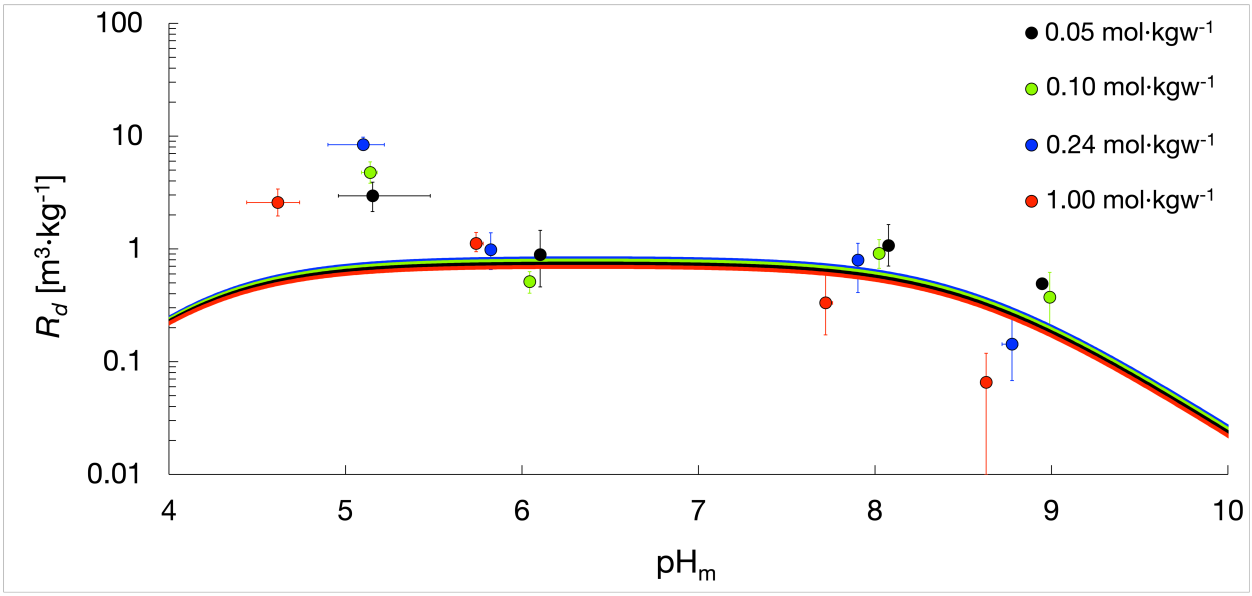

Figure 8 - Se(-II) adsorption onto granite in Ca-Na-Cl solutions and the resultant SCM's.

Se(-II) adsorption onto granite follows the atypical anionic adsorption behaviour, with a decrease in R_d as the solution pH_m increases [55 - 57, 61, 95, 96]. As the solution pH_m increases, the surface charge becomes increasingly negative. Thus, when $pH_m \geq 8.0$, Se(-II) adsorption decreases, which is attributed to the increase in Coulombic repulsive forces between the negatively charged surface and HSe^-. Ionic strength of the Ca-Na-Cl solutions appears to influence the adsorption of Se(-II) onto granite when $pH_m > 6.0$, and ionic strength > 0.1 mol·kgw^{-1}, causing a decrease in R_d, as the solution ionic strength increases. Presently, it is considered that with an increase in the ionic strength, there will be an

increased amount of interactions between background electrolytes, free Se(-II) ions, or the surface itself. Therefore, the increased probability of interaction would lead to an increased amount of Na^{+} - Se(-II) or Ca^{2+}- Se(-II) ion pairs. Yet, with the formation of these ion pairs, the amount of HSe^{-} freely available in the solution that can adsorb onto the granite surface would then decrease. Therefore, the R_d value is expected to decrease with an increase in ionic strength, as observed. Concurrently, the formation of ion pairs will remove available surface sites which could adsorb free Se(-II), in the event it were possible. In the past, evidence of this ionic strength influence was presented specific to the adsorption of Ni(II) onto kaolinite and alluded to a decrease in Ni(II) adsorption when the solution ionic strength increased [103]. A final point is that when $pH_m \leq 5.0$, it is difficult to discern the aforementioned ionic strength effects. It is presumed that in the acidic pH_m regime, the large number of protonated surface sites would lead to such a large degree of electrostatic attraction between HSe^{-}, and the positively charged surface. So much so, that any ionic strength effects may be negligible in comparison.

Previously, R_d values for Se(-II) adsorption onto goethite, magnetite, ferrous oxide, and biotite, were found to range from approximately 0.54 to 38.0 $m^3 \cdot kg^{-1}$, 0.012 to 0.056 $m^3 \cdot kg^{-1}$, 0.33 to 1.1 $m^3 \cdot kg^{-1}$, and 0.028 to 0.13 $m^3 \cdot kg^{-1}$, respectively [55]. These R_d values have been reported within the pH range of approximately $7.0 < pH < 9.0$ to more appropriately coincide with the pH_m range utilized within this thesis, and to support the presented Se(-II) R_d values. There does not appear to be any ionic strength dependant effects present that impacted Se(-II) adsorption onto geothite, magnetite, ferrous oxide, or biotite [55]. But, as granite does display an ionic strength dependency, any one of the mineral assemblage components within granite that does not contain iron may be attributed to that behaviour. Taking into consideration that Se(-II), Se(IV), and Se(VI) all primarily speciate as anions, a similar adsorption behaviour may be expected among them. Ticknor et al. previously found a similar decrease in the adsorption of Se(IV)/Se(VI) onto granite with an increase in ionic strength, and they also determined that R_d values with granite were either negligible, or had values ranging between 0.00018 and 0.0089 $m^3 \cdot kg^{-1}$ [95, 104]. These R_d values, and the adsorption trend coincide with what was observed with Se(-II) and granite, thus further supporting the results presented within this study.

4.4.2 - Se(-II) Adsorption onto MX-80 Bentonite in Ca-Na-Cl Solutions

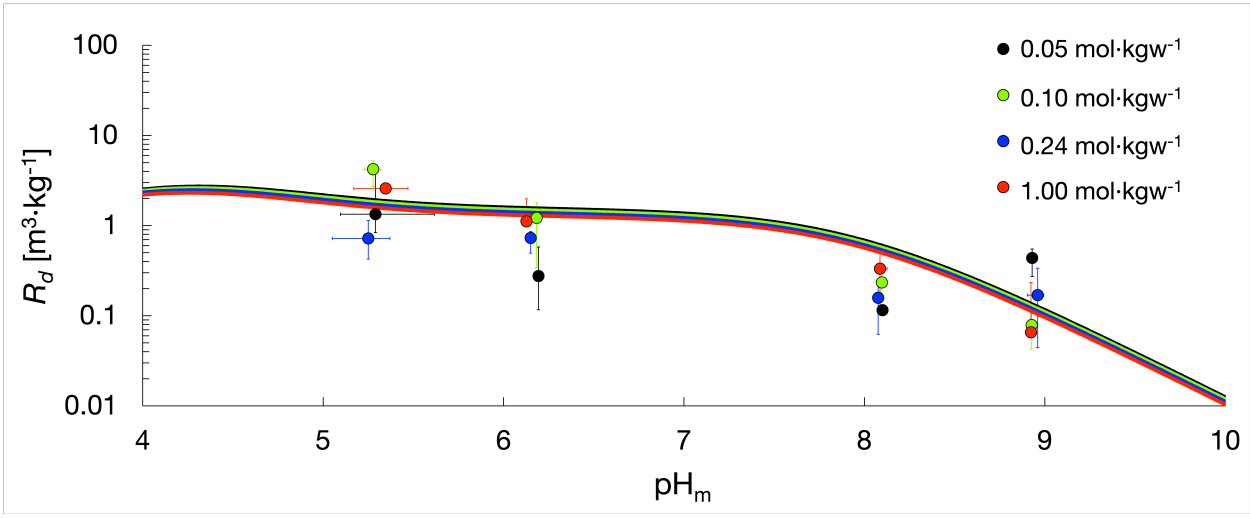

Figure 9 - Se(-II) adsorption onto MX-80 bentonite in Ca-Na-Cl solutions and the resultant SCM's.

Adsorption of Se(-II) onto MX-80 bentonite exhibits a similar trend with respect to solution pH_m as observed from the Se(-II) batch adsorption experiments using granite; which is typical of an anionic adsorption trend [55 - 57, 61, 95, 96]. At the present time, the previous arguments that explained the decrease in Se(-II) adsorption onto granite with an increase in solution pH_m, are presumed suitable to describe the decrease in Se(-II) adsorption onto MX-80 bentonite in 0.1, 0.24, and 1.0 mol·kgw^{-1} Ca-Na-Cl solutions. Regarding Se(-II) adsorption onto MX-80 bentonite in the 0.05 mol·kgw^{-1} Ca-Na-Cl solution, the experimental data presents that R_d at pH_m of 9.0 is within error of the R_d value at pH_m of 6.0. This may allude to a difference in Se(-II) adsorption behaviour with respect to pH_m for only the 0.05 mol·kgw^{-1} Ca-Na-Cl solution. This however does contrast the adsorption behaviour of Se(-II) onto MX-80 bentonite with respect to ionic strength, as there is no substantial trend that can be attributed, given all data points are within error at any given pH_m value. Therefore, it is currently presumed that Se(-II) adsorption onto MX-80 bentonite in the 0.05 mol·kgw^{-1} Ca-Na-Cl solution would coincide with the adsorption behaviour observed with the other ionic strength solutions. Furthermore, the assumption that MX-80 bentonite is approximately 85.0% montmorillonite could allude to the adsorption of Se(-II) onto montmorillonite being

indicative for how MX-80 bentonite interacts with Se(-II). Previously, Se(-II) adsorption onto montmorillonite has shown to be effected by varying solution ionic strength which contrasts the evidence that Se(-II) adsorption onto MX-80 bentonite is independent of ionic strength [57]. It must be acknowledged though, that the remaining 15.0% of MX-80 bentonite, which is considered to be quartz, albite, or amorphous solids, may also interact with Se(-II). If any one of these assemblage components displays an ionic strength dependent effect, then there must be a small proportion of MX-80 bentonite which must present these ionic strength effects. It may be possible though, that the heterogenous mixture of mineral assemblages prevents the ionic strength adsorption effect from being displayed, even though the homogenous montmorillonite component is the predominant mineral assemblage component. With no clear evidence that the solution ionic strength effects R_d values, it is not possible to confirm that the adsorption of Se(-II) onto MX-80 bentonite is independent of the ionic strength. Sugiura et al., determined the adsorption of Se(-II) onto pure montmorillonite returned values that ranged from 0.1 to 1.0 $m^3 \cdot kg^{-1}$ [57]. Walker et al., found that Se(-II) adsorption onto MX-80 bentonite returned R_d values between 1.0 and 5.0 $m^3 \cdot kg^{-1}$ which then decreased to a range of 0.1 to 1.0 $m^3 \cdot kg^{-1}$ as the pH of their Na-Ca-Cl solutions varied [61]. These previous studies support the presented results within this study for Se(-II) adsorption onto MX-80 bentonite in Ca-Na-Cl solutions with similar R_d values.

4.5 - Ca-Na-Cl Solution pH_m and Ionic Strength Influence on Tc(IV) Adsorption

Results from the Tc(IV) batch adsorption experiments onto granite and MX-80 bentonite with respect to pH and ionic strength in Ca-Na-Cl solutions, are presented in Figures 10 and 11, respectively. SCM's which successfully simulate the determined Tc(IV) adsorption data are presented in Figures 10 and 11, respectively.

4.5.1 - Tc(IV) Adsorption onto Granite in Ca-Na-Cl Solutions

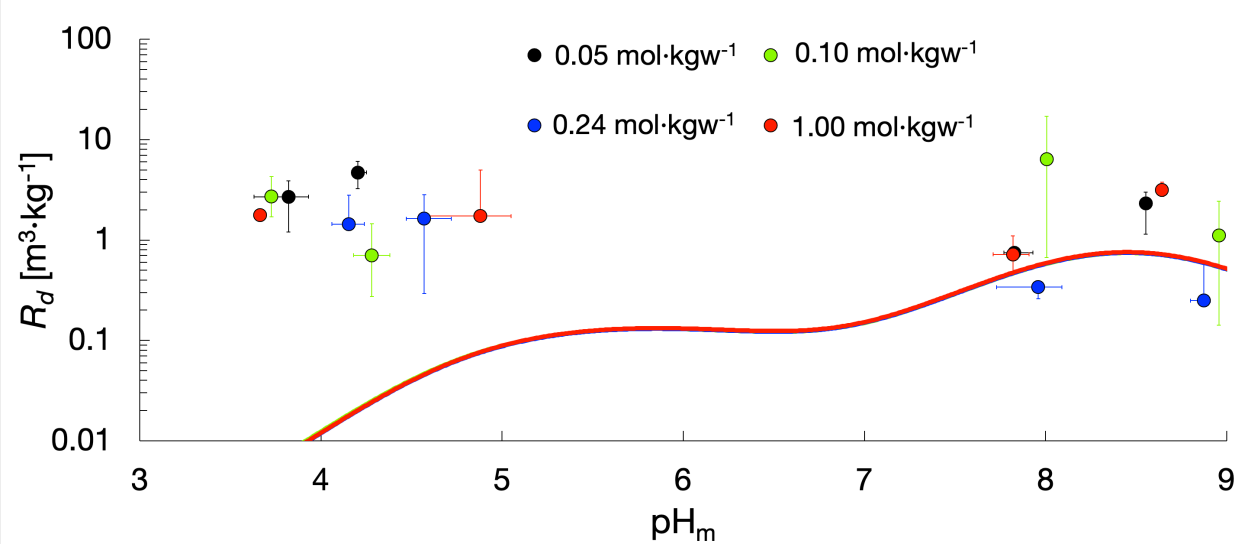

Figure 10 - Tc(IV) adsorption onto granite in Ca-Na-Cl solutions and the resultant surface complexation models.

Transferring from Se(-II) adsorption in Ca-Na-Cl solutions to discussions specific to Tc(IV) adsorption in Ca-Na-Cl solutions begins with observing that the adsorption of Tc(IV) onto granite have R_d values within error of each other with respect to both pH_m and ionic strength. The adsorption behaviour with respect to pH_m is currently attributed to the Coulombic forces that exist between the surface and the Tc(IV) species. Presently, the charge of the Tc(IV) species is thought to be dependant upon the hydrolysis behaviour of Tc(IV) with respect to a varying pH, and is described using the following reaction pathway: $TcO^{2+} \rightarrow TcO(OH)^{+} \rightarrow TcO(OH)_2^{0} \rightarrow TcO(OH)_3^{-}$ [22]. Ligand formation is therefore considered to

be dominant adsorption pathway, as previously postulated [22]. A lack of any noticeable ionic strength effect on Tc(IV) adsorption was previously observed which is considered to support the results presented in Figure 10 [16]. An additional adsorption feature exists within the range, $7.5 < pH_m < 8.5$. This small pH_m regime shows the capacity to allow for an increase in the adsorption of Tc(IV) onto granite. Hallam et al. found that plagioclase feldspar, shale, hematite, geothite, and sand all presented a similar adsorption characteristic near this pH_m regime [11]. At the present, a coupled effect is being considered for the reason in this increase in Tc(IV) adsorption. Near this pH_m regime, the solubility of iron decreases which allows for the surface of granite to change with respect to the amount of free iron surface sites [96]. Then, as Tc(IV) exhibits secondary redox processes with iron [105], there is an additional adsorption pathway which exists only in this narrow pH_m range.

4.5.2 - Tc(IV) Adsorption onto MX-80 Bentonite in Ca-Na-Cl Solutions

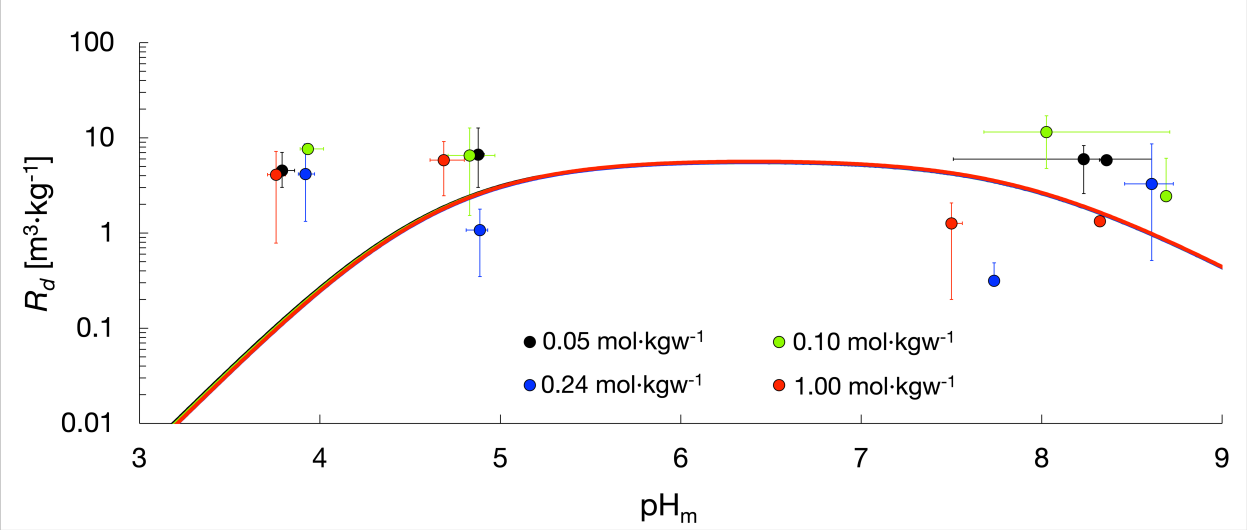

Figure 11 - Tc(IV) adsorption onto MX-80 bentonite in Ca-Na-Cl solutions and the resultant surface complexation models.

A similar adsorption trend with respect to solution pH_m is found when observing Tc(IV) adsorption on MX-80 bentonite to that of granite. This alludes to similar electrostatic interactions governing the adsorption of Tc(IV) in both Ca-Na-Cl solution systems. Furthermore, as R_d values are within error of each other despite the ionic strength varying, it does not appear that Tc(IV) adsorption onto MX-80 bentonite in Ca-Na-Cl solutions is affected by the ionic strength. Similar results were observed in Figure 10, and this evidence coincides with the expectations that the magnitude of Tc(IV) that is able to adsorb is unaffected by variation in the ionic strength [16]. In observation of the similarity in R_d values and adsorption trends found between Figures 11 and 15, R_d values for previous Tc(IV) adsorption onto MX-80 bentonite experiments will be discussed in Section 4.6.4. These values are considered to support the results presented in Figure 11, additionally.

4.6 - Na-Ca-Cl Solution pH_m and Ionic Strength Influence on Tc(IV) Adsorption

Results from the Tc(IV) batch adsorption experiments onto shale, limestone, illite, and MX-80 bentonite with respect to pH and ionic strength in Na-Ca-Cl solutions, are presented in Figures 12, 13, 14, and 15, respectively. SCM's which successfully simulate the Tc(IV) adsorption data onto shale, illite, and MX-80 bentonite are presented in Figures 12, 14, and 15, respectively.

4.6.1 - Tc(IV) Adsorption onto Shale in Na-Ca-Cl Solutions

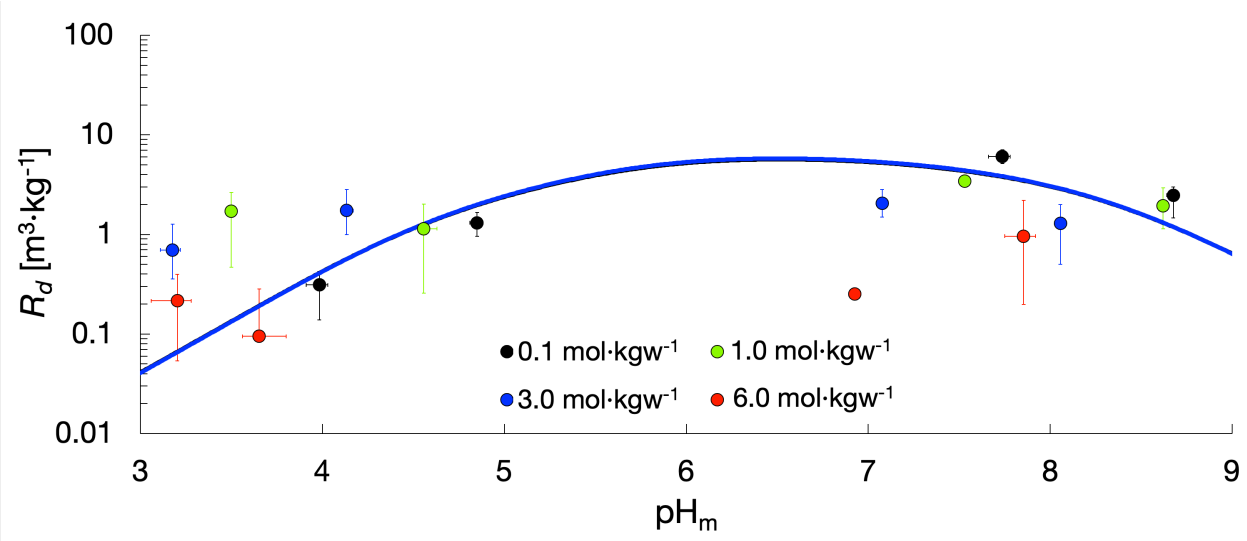

Figure 12 - Tc(IV) adsorption onto shale in Na-Ca-Cl solutions and the resultant surface complexation models. Simulations were not completed with respect to the 6.0 mol·kgw^{-1} Na-Ca-Cl solutions.

Adsorption of Tc(IV) onto shale in Na-Ca-Cl solutions displays the typical Tc(IV) adsorption trend as observed previously with granite and MX-80 bentonite in Ca-Na-Cl solutions. Hallam et al., studied the adsorption of Tc(IV) onto shale, and were able to determine that the adsorption onto shale followed a similar adsorption trend to that found within this study [11]. The largest R_d value determined by Hallam et al., was 4.24 ± 0.58 m^3·kg^{-1} at a pH of 7.14 [11]. This is presumed to coincide with the largest R_d value determined from this study which is 6.07 ± 0.99 m^3·kg^{-1} at a pH_m of 7.74 ± 0.08. A single study carried out by Bertetti was able to produce an R_d value of approximately 0.01 m^3·kg^{-1}, at a pH of 8.5 for Tc(IV)

adsorption onto shale in similar 0.1 mol·kgw^{-1} Na-Ca-Cl solutions [96]. This R_d value is two orders of magnitude smaller than the R_d values determined within this study at similar pH values, and is being attributed to the time-period of the experiment, which was 116 days compared to the 7-day period used within this study [96]. Currently, the assumption is that the long-time associated with the previous experiment would allow for slow kinetic processes to occur which are possibly related to dissolution of the surface. This would then allow for the formation of new solids or colloids, or possible redox reactions to occur between the surface and Tc(IV). Both of these effects would lead to a decrease in R_d as Tc(IV) desorbs from the surface, or is oxidized to Tc(VII). To support this consideration, Lieser et al., found that desorption ratios were greater than adsorption ratios in their Tc(IV) experiment using iron containing minerals [18]. Walton et al., recognized similar desorption behaviour with an increase in time which was attributed to redox reactions [16]. Therefore, with consideration of the similarity exhibited between these results and those of Hallam et al., combined with the difficulty experimentally in ensuring Tc(IV) adsorption is guaranteed at long-time spans is presumed to support the observations presented in Figure 12.

4.6.2 - Tc(IV) Adsorption onto Limestone in Na-Ca-Cl Solutions

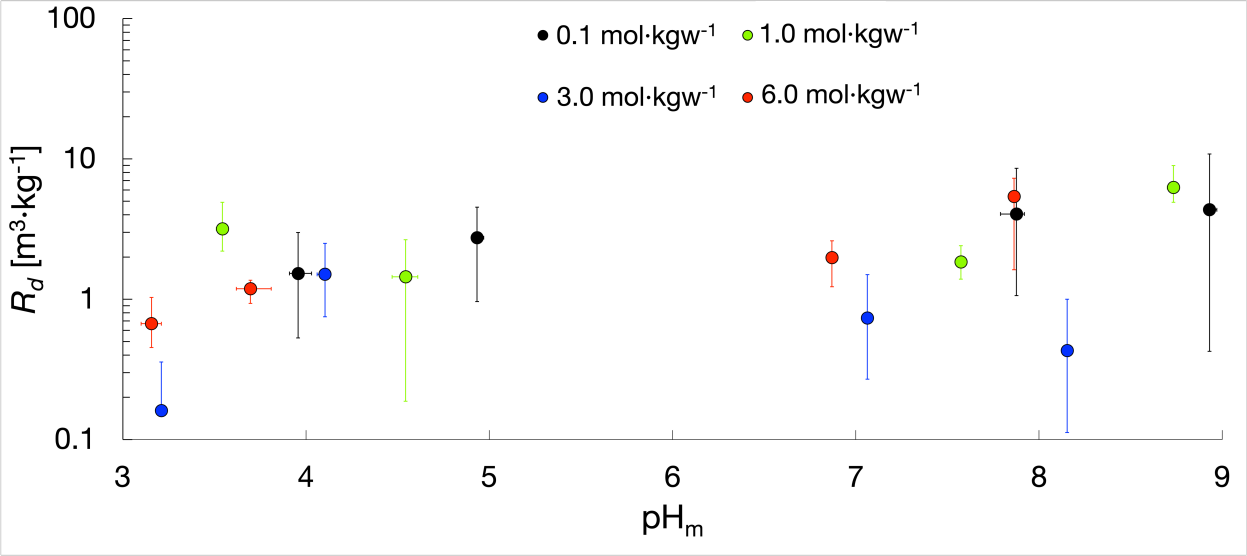

Figure 13 - Tc(IV) adsorption onto limestone in Na-Ca-Cl solutions.

Adsorption of Tc(IV) onto limestone is scattered with large variation. However, it is still possible to ascertain the Tc(IV) adsorption behaviour qualitatively, with the R_d being essentially constant with respect to pH_m. Bertetti investigated Tc(IV) adsorption onto limestone in 0.1 mol·kgw^{-1} Na-Ca-Cl solutions, and found the R_d value to be 100.0 m^3·kg^{-1} at a pH value of 8.5 [96]. Near this pH_m value, the surface properties of limestone are considered to provide an additional adsorption process which would lead to increased R_d values. This effect has been observed with U(IV) adsorption onto calcite within a pH range of 7.95 to 8.21 [106]. This increase in adsorption is attributed to the surface charge of calcite being determined by Ca^{2+} and CO_3^{2-} ions, and not H^+ and OH^- ions [107]. These ions would allow for the formation of either Tc(IV) calcium complexes, or Tc(IV) carbonate complexes, which may then adsorb to the surface. Previously, Tc(IV) calcium carbonate surface complexes were shown to form, and more than one of these carbonate complexes are able to bridge and increase adsorption of Tc(IV) [22]. Subsequently, quantum chemical calculations have been completed and show that the $Ca_3[TcO(OH)_5]^{3+}$ ion could form when Ca^{2+} stabilizes $TcO(OH)_5^{3-}$ [22]. As these are Na-Ca-Cl solutions, the free Ca^{2+} in solution will promote the formation of these ions which is assumed to increase Tc(IV) adsorption onto

limestone. In the past an R_d value equal to 0.00 $m^3 \cdot kg^{-1}$ was recommended for Tc(IV) adsorption onto calcite by Bradbury et al., based upon the ionic radius of Tc(IV) [12, 108]. It must be stated though, that the variation in the reported R_d values for Tc(IV) adsorption onto limestone makes comparisons across literature difficult. However, it could be considered that as Tc(IV) speciates as TcO^{2+}, a comparison to $U(IV)O_2^{2+}$ could be made based on their similar charge, and oxo-cation structure, which may take precedent over the oxidation state in adsorption processes [17]. Previously, R_d values specific to U(VI) adsorption onto calcite returned R_d values within a range of 0.001 $m^3 \cdot kg^{-1}$ to 0.55 $m^3 \cdot kg^{-1}$ [106]. Subsequently, some identified U(VI) carbonate species include $UO_2(CO_3)_2^{2-}$, $UO_2(CO_3)_3^{4-}$, and $UO_2CO_3^0(aq)$, which would coincide with the reported Tc(IV) carbonate species that may form adsorbed bridged complexes [16, 17]. Currently, the similarity in R_d values between U(VI) and Tc(IV) adsorption that have been reported are considered to be a form of justification for the results presented depicting Tc(IV) adsorption onto limestone in Na-Ca-Cl solutions.

4.6.3 - Tc(IV) Adsorption onto Illite in Na-Ca-Cl Solutions

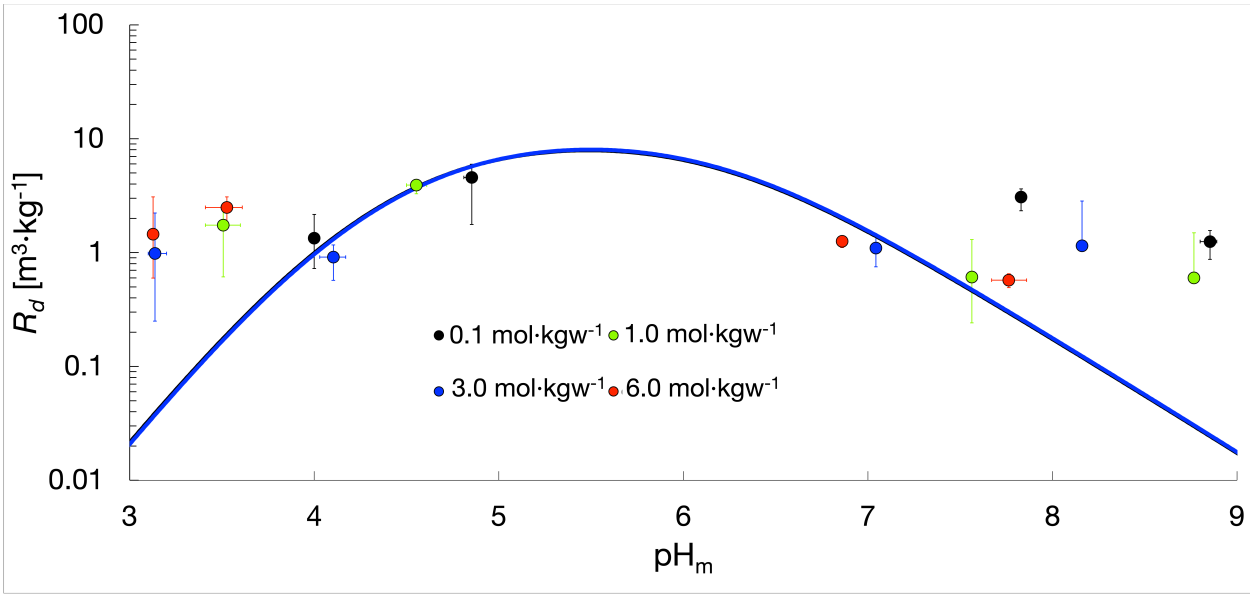

Figure 14 - Tc(IV) adsorption onto illite in Na-Ca-Cl solutions and the resultant surface complexation models. Simulations were not completed with respect to the 6.0 mol·kgw^{-1} Na-Ca-Cl solutions.

The next batch adsorption experiment discussion relates to the adsorption of Tc(IV) onto illite. In similar fashion to results previously presented in this study, there is a constant adsorption trend across both the pH$_m$ regime, and ionic strength regimes experimentally tested with R$_d$ values being within error of each other. In the past, Th(IV) was used as an analogue to represent Tc(IV) in adsorption studies based on their similar oxidation state, and ability to speciate as an aqueous species in the circumneutral pH regime [106]. For the aforementioned reason, there has been a reported R$_d$ value of 4.0 m^3·kg^{-1} obtained from Th(IV) adsorption experiments which was used to represent Tc(IV) adsorption onto illite [106]. However, perspectives have changed and Th(IV) is no longer considered acceptable to act as an analogue for Tc(IV) [109]. This has lead to Tc(IV) adsorption onto illite being attributed with an R$_d$ value of 2.5 m^3·kg^{-1} [109]. This value does coincide with those depicted in Figure 14 which is considered to support the Tc(IV) adsorption onto illite results presented in this study.

4.6.4 - Tc(IV) Adsorption onto MX-80 Bentonite in Na-Ca-Cl Solutions

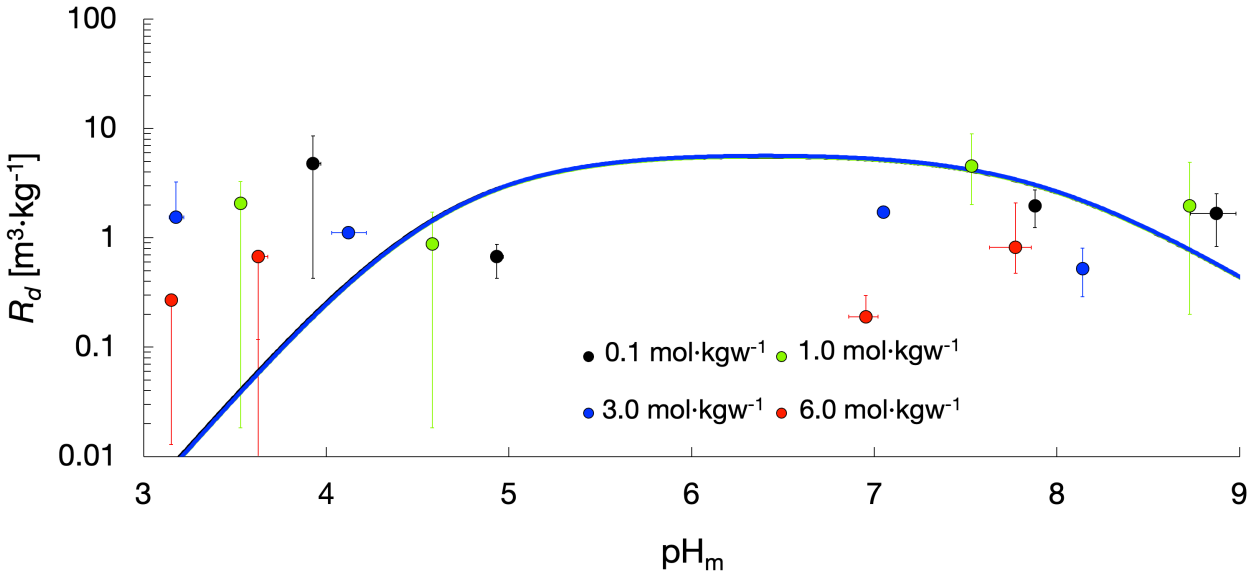

Figure 15 - Tc(IV) adsorption onto MX-80 bentonite in Na-Ca-Cl solutions and the resultant surface complexation models. Simulations were not completed with respect to the 6.0 mol·kgw^{-1} Na-Ca-Cl solutions.

As mentioned, the adsorption of Tc(IV) onto MX-80 bentonite in Na-Ca-Cl solutions is similar to that found in Ca-Na-Cl solutions. Neither the solution pH$_m$, nor the solution ionic strength appear to have an influence on the overall adsorption of Tc(IV) onto MX-80 bentonite in either system as there is constant adsorption across the entire pH$_m$, and ionic strength regimes tested with R_d values all approximately within error. Overtime, there has been an adequate number of studies which have been published specific to Tc(IV) adsorption onto bentonite. Bertetti measured Tc(IV) adsorption onto MX-80 bentonite in Na-Ca-Cl solutions, and reported an R_d value of approximately 10.0 m^3·kg^{-1} [96]. Berry et al. reported R_d values with a range of 4.2 m^3·kg^{-1} to 10.0 m^3·kg^{-1} with seawater, and 0.59 m^3·kg^{-1} to 1.70 m^3·kg^{-1} in deionized water [110]. This range in values is matched by studies from Baston et al. which state that R_d values ranged from 9.8 m^3·kg^{-1} to 10.0 m^3·kg^{-1} in seawater, and 1.4 m^3·kg^{-1} to 21.0 m^3·kg^{-1} in deionized water [111, 112]. Overall, the magnitudes of the reported R_d values attributed to Tc(IV) adsorption onto MX-80 bentonite range from 1.0^{-1} m^3·kg^{-1} to 1.0^1 m^3·kg^{-1}, which coincide with the R_d

values presented in both Figures 11 and 15. This is therefore considered to be evidence that supports the R_d values being presented in this study.

4.7 - Geochemical Simulations of Se(-II) and Tc(IV) Adsorption

After batch adsorption experiments were completed, the data obtained was used to optimize SCM's. Simulations which have been optimized include: Se(-II) adsorption onto granite and MX-80 bentonite in all Ca-Na-Cl solutions, Tc(IV) adsorption onto granite and MX-80 bentonite in all Ca-Na-Cl solutions, and Tc(IV) adsorption onto shale, illite, and MX-80 bentonite in 0.1, 1.0, and 3.0 mol·kgw^{-1} Na-Ca-Cl solutions. In all simulations, R_d is calculated through a summation of the concentrations of either Se(-II) or Tc(IV) that are calculated to be adsorbed onto each mineral assemblage component, which is then divided by the total Se(-II) or Tc(IV) concentration.

$$R_d = \sum_i \frac{[C_{(adsorbed\ onto\ mineral\ assemblage)_i}]}{[C_{total}]} \tag{10}$$

It must be stated that a goal of this modelling approach is to be able to define surface complexation reactions using mineral assemblages which may be used across all surfaces to be modelled, if that mineral assemblage is present. An assumption is that if adsorption of an element is possible on one mineral assemblage within a given heterogenous mineral, then adsorption onto the identical mineral assemblage in a different heterogenous mineral would differ only based on the different proportion considered within each surface, and not the interaction between the element and surface being simulated. This is therefore thought to imply that the surface complexation constant be the same for a given surface complexation reaction with an assemblage mineral that is used in any heterogenous surface model. This model will take into consideration any experimental proof about the adsorption of either Se(-II) or Tc(IV) onto individual mineral surfaces. Or if it is necessary, proof about the adsorption of

either Se(-II) or Tc(IV) onto silanol, aluminol, and ferrol surface sites to propose surface complexation reactions.

Surface complexation reactions, and the associated surface complexation constants for Se(-II) adsorption onto granite and MX-80 bentonite in Ca-Na-Cl solutions are presented in Table 15. Surface complexation reactions, and the associated surface complexation constants for Tc(IV) adsorption onto granite and MX-80 bentonite in Ca-Na-Cl solutions are presented in Table 16. Surface complexation reactions, and the associated surface complexation constants for Tc(IV) adsorption onto shale, illite, and MX-80 bentonite are presented in Table 17. Hypothesized surface complexes specific to Se(-II) adsorption onto granite and MX-80 bentonite are presented in Figures 16 and 17, respectively. Hypothesized surface complexes specific to Tc(IV) adsorption onto granite and MX-80 bentonite in Ca-Na-Cl solutions are presented in Figures 18 and 19, respectively. Tc(IV) surface complexes with shale, illite, and MX-80 bentonite in Na-Ca-Cl solutions are presented in Figures 20, 21 and 22, respectively. Table C1 compiles all surface complexation reactions and surface complexation constants.

4.7.1 - Se(-II) Adsorption Simulations onto Granite and MX-80 Bentonite in Ca-Na-Cl Solutions

Initially, simulations specific to Se(-II) adsorption onto granite and MX-80 bentonite in Ca-Na-Cl solutions did not need to consider a Se(-II) - quartz surface complex. Despite quartz being present in both granite and MX-80 bentonite, an assumption about quartz is that only silanol surface sites are present which have the low Point of Zero Charge (PZC) of 2.2. This is important to consider as the low PZC associated with the silanol sites will effectively repel the anionic HSe^- from the surface as the surface charge becomes more negatively charged in neutral-alkaline systems [55]. This would decrease Se(-II) adsorption onto quartz, if any could occur. Fortunately, there has been evidence that Se(-II) adsorption onto quartz has returned low or undetermined R_d values [55]. Therefore, the low or indeterminate R_d values associated with Se(-II) adsorption onto quartz, a highly crystalline structure, and the low PZC are presumed to justify no inclusion of a Se(-II) - quartz surface complex.

Biotite has been shown to be an effective absorber of Se(-II) in the past, and as such a Se(-II) - biotite surface complex was considered necessary. A previous study was able to simulate the adsorption of Se(-II) onto biotite using only a single outer-sphere surface complex within a triple layer SCM [101]. As these are non-electrostatic SCM's, it is assumed that the outer-sphere surface complex from the triple layer model is equivalent to the non-specific Se(-II) surface complex. Furthermore, R_d values determined from Se(-II) adsorption onto biotite are similar in magnitude to Se(-II) adsorption onto granite R_d values [55]. Given the similarity in R_d values, it is considered that biotite may be dominant absorber of Se(-II) within granite despite biotite only accounting for 3.0% of the granite surface. It must then be stated that biotite may play a more significant role in governing Se(-II) adsorption onto granite than these simulations can depict. In the past, iron oxides have shown to have an important role in the adsorption behaviour of selenites within granite, and these iron oxides would form when biotite is weathered [55, 113, 114]. Despite the possible secondary redox process, the single non specific ≡Biotite_sOH_2HSe surface complex is considered justified.

Of the mineral assemblages within the granite surface, only the feldspar component remains. Feldspar is expected to be a dominant absorber of Se(-II) due to the large proportion within granite which is assumed to be 56.0%. An important consideration regarding feldspar's adsorption capacity is that since it is a tectosilicate, there has been evidence that approximately 10.0% of Se(-II) is able to adsorb at any given pH [55]. This would require the biotite component in the model to be able to simulate the remaining 90.0% of Se(-II) adsorption. Presently, it is considered possible given that biotite is a phyllosilicate mineral, and phyllosilicates have shown pH dependent adsorption trends with Se(-II) adsorption decreasing from approximately 80.0% at pH = 8.5 to approximately 6.0% at pH = 12.0 [55]. Based upon the idea that biotite could account for the remainder of Se(-II) adsorption within granite, a Se(-II) - feldspar surface complex was considered required. However, it was not possible to determine exact Se(-II) adsorption mechanisms onto feldspar from existing literature. Therefore, with knowledge that feldspar is comprised of silanol and aluminol surface sites it may be possible to justify a surface complex. Silanol surface sites are not considered to be able to adsorb Se(-II) for the aforementioned reasons. Fortunately, evidence has been published which depicts that Se(IV) adsorbs onto aluminol

sites, and as Se(-II) and Se(IV) have similar adsorption behaviours, it is considered acceptable to continue with a Se(-II) - feldspar surface complex.

It was then necessary to determine whether a specific or non-specific surface complex would form with the feldspar surface. In the past, Peak et al., were able to characterize the formation of Se(IV) – aluminol inner-sphere surface complexes using XAS measurements [115]. Of the two surface Se(IV) - aluminol complexes, one was determined to be bidentate, while the other was a monodentate surface complex. Based upon the fact Se(IV) forms as an oxyanion which would have a larger molecular size compared to Se(-II), it may not be possible for Se(-II) to form as a bidentate surface complex if the aluminol surface sites are too distant. Therefore, through the process of elimination, the ≡Feldspar_sSe$^-$ surface complex has been included within the models. Previously, an assumption was stated regarding the fact that the feldspar component and albite component within the granite and MX-80 bentonite simulated surfaces, respectively were defined from a single surface. Therefore, these two surfaces utilize identical protolysis constants, and site density in the simulations. The only difference between these two surfaces is their naming convention and calculated SSA. Therefore, it is considered necessary to include an ≡Albite_sSe$^-$ surface complex within the MX-80 bentonite simulations.

Recently, Walker et al., found it possible to simulate the adsorption of Se(-II) onto MX-80 bentonite using a montmorillonite surface and two different surface complexes [61]. Knowing that montmorillonite is a phyllosilicate mineral with an alumina octahedral sheet, and with the previously discussed arguments to support both ≡Feldspar_sSe$^-$ and ≡Albite_sSe$^-$ as surface complexes in the simulations, a ≡Montmorillonite_sSe$^-$ surface complex is included. Finally, since biotite and montmorillonite are both phyllosilicate minerals, it is assumed that Se(-II) adsorption with both surfaces could be similar. Given the inclusion of the ≡Biotite_sOH$_2$HSe surface complex, it was considered justified to also include ≡Montmorillonite_sOH$_2$HSe as a surface complex. In the study published by Walker et al., successful simulation results for Se(-II) adsorption with two surface complexation reactions were presented [61]. These two surface complexes are identical to ≡Montmorillonite_sSe$^-$ and ≡Montmorillonite_sOH$_2$HSe, which are included within the MX-80 bentonite SCM.

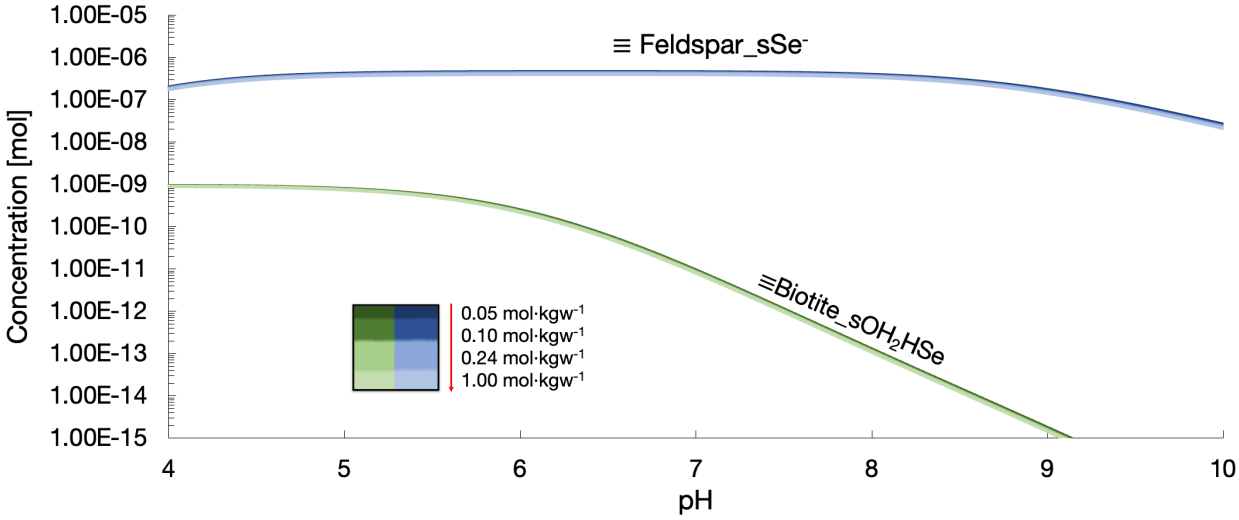

Figure 16 - Simulated Se(-II) surface complexation with the granite surface in Ca-Na-Cl solutions.

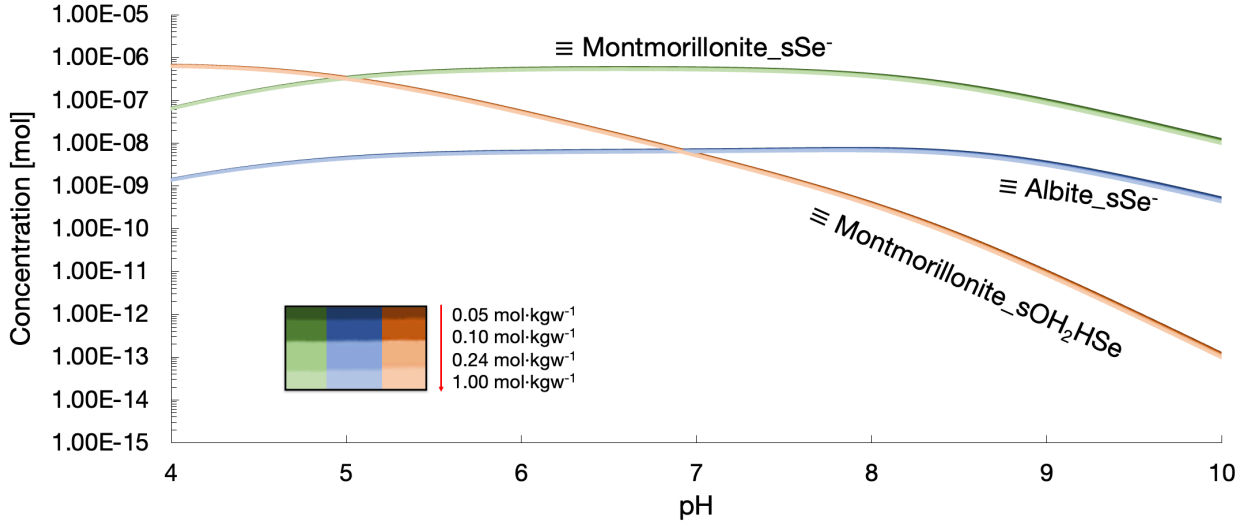

Figure 17 - Simulated Se(-II) surface complexation with the MX-80 bentonite surface in Ca-Na-Cl solutions.

Table 15 - Surface complexation reactions and optimized surface complexation constants for Se(-II) adsorption onto granite and MX-80 bentonite in Ca-Na-Cl solutions.

Simulated Surface	Surface Complexation Reaction	Surface Complexation Constant (LogK)
Granite	≡Feldspar_sOH + HSe^- ↔ ≡Feldspar_sSe^- + H_2O	5.5
	≡Biotite_sOH + HSe^- + H^+ ↔ ≡Biotite_sOH_2HSe	12.0
MX-80 bentonite	≡Albite_sOH + HSe^- ↔ ≡Albite_sSe^- + H_2O	5.5
	≡Montmorillonite_sOH + HSe^- ↔ ≡Montmorillonite_sSe^- + H_2O	4.5
	≡Montmorillonite_sOH + HSe^- + H^+ ↔ ≡Montmorillonite_sOH_2HSe	9.5

4.7.2 - Tc(IV) Adsorption Simulations onto Granite and MX-80 Bentonite in Ca-Na-Cl Solutions

As with the Se(-II) simulations, the first assemblage surface to be discussed will be quartz. If a Tc(IV) - quartz surface complex is considered to exist, it would exist within both the granite and MX-80 bentonite surfaces. Fortunately, there is Tc(IV) adsorption onto quartz R_d values with an optimized Tc(IV) - quartz SCM which can act as supporting evidence for this study. It was possible for Hallam et al., to appropriately fit their Tc(IV) adsorption onto quartz data with use of only a single monodentate surface complex [11]. This has led to the inclusion of the ≡Quartz_sOTcO(OH) surface complex within the subsequent granite, and MX-80 bentonite SCM's. Using the data provided by Hallam et al., a quartz SCM was successful in replicating Tc(IV) adsorption which returns an optimized surface complexation constant of 5.35. The quartz SCM has been included in Table D1 [91]. Figure A8 presents Tc(IV) adsorption onto quartz data and the optimized SCM.

Concurrently with the Tc(IV) - quartz adsorption data, Hallam et al., investigated Tc(IV) adsorption onto plagioclase feldspar [11]. This is beneficial as it assists in presenting a Tc(IV) surface complex with both the feldspar component and the albite component, within the simulated granite and MX-80 bentonite surfaces, respectively. Tc(IV) adsorption onto plagioclase feldspar data exhibited low R_d until a pH of approximately 8.0, where an adsorption peak occurs which disappears before pH 8.5. Adsorption profiles associated with bidentate surface complexes are considered to produce sharp adsorption peaks [11]. In agreement with the aforementioned consideration, Hallam et al., presented a bidentate surface complex which simulated their experimental data successfully [11]. Therefore, it is considered justified to include both the $(\equiv Feldspar\_sO)_2TcO(OH)^-$, and the $(\equiv Albite\_sO)_2TcO(OH)^-$ surface complexes within the granite, and MX-80 bentonite SCM's, respectively. Similarly using the data provided by Hallam et al., a feldspar SCM was fit successfully with the resultant optimized surface complexation constant of -2.25. The feldspar SCM has been included in Table D1 [91]. Figure A9 presents Tc(IV) adsorption onto feldspar data and the optimized SCM.

In contrast to bidentate surface complex adsorption behaviour, monodentate surface complexes exhibit broad and flat adsorption profiles [11]. To the benefit of this study, the adsorption behaviour of

Tc(IV) onto montmorillonite has shown to be uniform throughout pH 3 to 10 [108, 109]. Therefore, in the subsequent MX-80 bentonite SCM's, montmorillonite is expected to form only as the ≡Montmorillonite_sOTcO(OH) surface complex. Initially, it was considered that only the ≡Montmorillonite_sOTcO(OH) surface complexation constant was required to iteratively solve for an within the Tc(IV) - MX-80 bentonite SCM. This is due to the ≡Quartz_sOTcO(OH) and the $(\equiv Albite\_sO)_2TcO(OH)^-$ surface complexation constants being constrained to 5.35 and -2.25, respectively. After optimization, the final surface complexation constant value which best simulated the Tc(IV) adsorption onto MX-80 bentonite data was found to be 5.00. Previously, an R_d value of 5.0 $m^3 \cdot kg^{-1}$, has been utilized to define Tc(IV) adsorption onto montmorillonite [109]. This coincides with the plateauing R_d value of approximately 5.5 $m^3 \cdot kg^{-1}$ which occurs within the pH regime of 5 to 8, see Figure 11.

To fully define the granite SCM, the biotite component needs to consider the formation of either a monodentate or bidentate surface complex. Given the expectation that Se(-II) could adsorb onto phyllosilicates similarly, it is considered that the adsorption of Tc(IV) adsorption onto both adsorbents could be similar too. Given this consideration, the ≡Biotite_sOTcO(OH) surface complex has been included in the Tc(IV) - granite SCM. With the already constrained surface complexation constants specific to quartz and feldspar, only the biotite surface complexation constant was iteratively optimized to return a final value of 8.10. An effort was made to ensure that adsorption of Tc(IV) onto granite was essentially constant within the pH regime of 5 through 8. This was done to ensure that the final Tc(IV) - granite SCM would coincide with the abundance of experimental data which alludes to a constant adsorption behaviour throughout the circumneutral pH regime. Given the difference exhibited in Figure 10 between the simulation results and the experimental data within the pH regime of 4 - 5, future work will attempt to improve this Tc(IV) - granite SCM. As it has been previously stated that the charge associated with the Tc(IV) species is expected to vary with the hydrolysis behaviour of Tc(IV), the surface complexation of Tc(IV) may also follow this hydrolysis behaviour. Figure A7 does allude to the $TcO(OH)^+$ species being dominant at the low pH range, which if adsorption of a $TcO(OH)^+$ species could occur would improve the low pH regime SCM results.

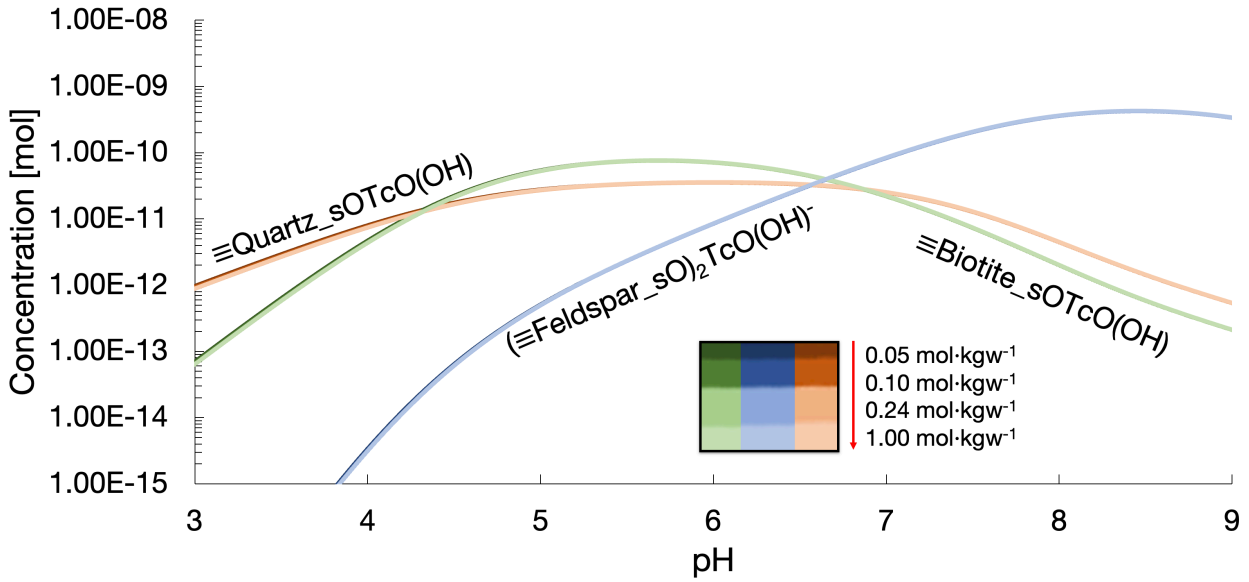

Figure 18 - Simulated Tc(IV) surface complexation with the granite surface in Ca-Na-Cl solutions.

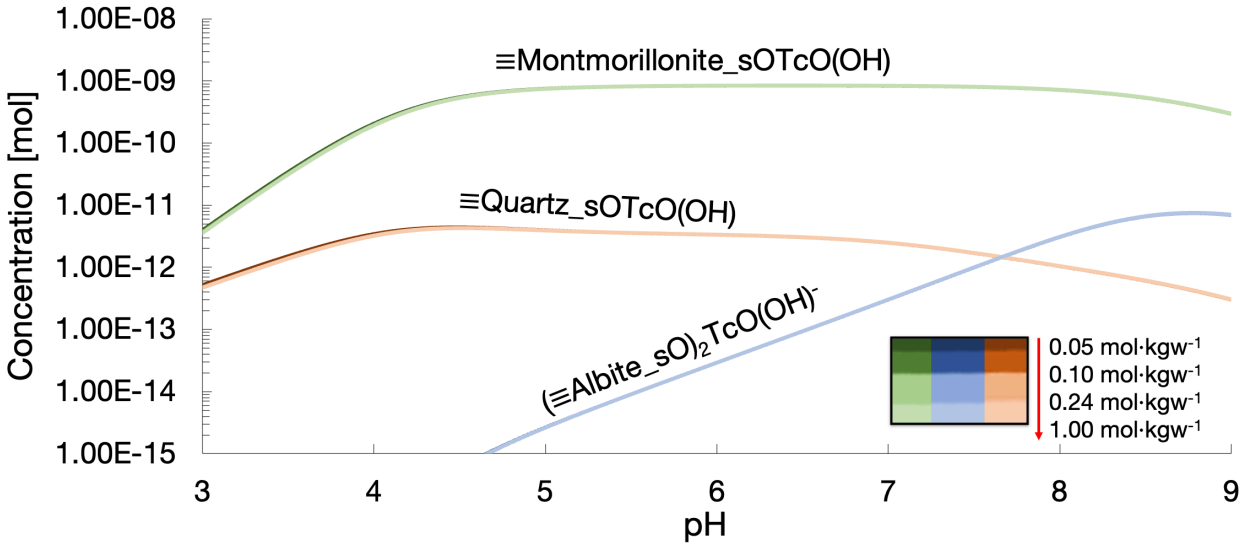

Figure 19 - Simulated Tc(IV) surface complexation with the MX-80 bentonite surface in Ca-Na-Cl solutions.

Table 16 - Surface complexation reactions and optimized surface complexation constants for Tc(IV) adsorption onto granite and MX-80 bentonite in Ca-Na-Cl solutions.

Simulated Surface	Surface Complexation Reaction	Surface Complexation Constant (LogK)
Granite	≡Biotite_sOH + $TcO(OH)_2$ ↔ ≡Biotite_sOTcO(OH) + H_2O	8.10
	≡Quartz_sOH + $TcO(OH)_2$ ↔ ≡Quartz_sOTcO(OH) + H_2O	5.35
	2 (≡Feldspar_sOH) + $TcO(OH)_2$ ↔ $(≡Feldspar\_sO)_2TcO(OH)^-$ + H_2O + H^+	-2.25
MX-80 bentonite	≡Quartz_sOH + $TcO(OH)_2$ ↔ ≡Quartz_sOTcO(OH) + H_2O	5.35
	≡Montmorillonite_sOH + $TcO(OH)_2$ ↔ ≡Montmorillonite_sOTcO(OH) + H_2O	5.00
	2 (≡Albite_sOH) + $TcO(OH)_2$ ↔ $(≡Albite\_sO)_2TcO(OH)^-$ + H_2O + H^+	-2.25

4.7.3 - Tc(IV) Adsorption Simulations onto Shale, Illite, and MX-80 Bentonite in Na-Ca-Cl Solutions

A benefit of the model approach as stated previously is that surface complexes defined for mineral assemblages are applicable to every SCM if that mineral assemblage exists in a given SCM. Furthermore, given the model being non-electrostatic in nature, there is the presumption that surface complexes defined in Ca-Na-Cl solution systems should be applicable in Na-Ca-Cl solution systems. Based upon the assemblages considered in shale, illite, and MX-80 bentonite, multiple surface complexes can be immediately defined based upon arguments presented in Section 4.7.2. These surface complexes include: ≡Quartz_sOTcO(OH), $(\equiv Feldspar\_sO)_2TcO(OH)^-$, $(\equiv Albite\_sO)_2TcO(OH)^-$, and ≡Montmorillonite_sOTcO(OH). Instantly, the MX-80 bentonite SCM in Na-Ca-Cl solutions is identical to the MX-80 bentonite SCM in Ca-Na-Cl solutions.

Based upon the assumed composition of shale, only the illite and chlorite mineral assemblages need to have a Tc(IV) surface complex defined, if one is possible. From the results presented in Figure 14, it was necessary to include a Tc(IV) - illite surface complex. It is presently considered that this surface complex should be the monodentate one of the form, ≡Illite_sOTcO(OH), based upon the broad and flat adsorption profile exhibited from the experimental data. Additionally, as montmorillonite and illite are both smectites, similar Tc(IV) monodentate surface complexes are hypothesized to form, and as such both surface complexes are considered to have an another form of justification for inclusion within these SCM's. From the aforementioned benefit of this modelling method, the ≡Illite_sOTcO(OH) surface complex will be assumed to describe the entire illite SCM. After optimization of the Tc(IV) - illite SCM, the final surface complexation constant determined is 5.25.

In the past, Hallam et al., investigated the adsorption of Tc(IV) onto shale, and found an adsorption trend which coincides with the one presented in Figure 12. A successful SCM was subsequently presented which required both monodentate and bidentate surface complexes to simulate Tc(IV) adsorption onto shale [11]. Previously in the granite SCM, biotite was accredited with the formation of a Tc(IV) monodentate surface complex. Currently, as it is known that chlorite can form when biotite is weathered [113]. Tc(IV) could adsorb onto the biotite and chlorite surfaces in a similar manner.

For this reason, the monodentate chlorite surface complex, ≡Chlorite_sOTcO(OH) has been considered. Based upon the previous SCM's, the ≡Quartz_sOTcO(OH), ≡Illite_sOTcO(OH), and the $(\equiv Feldspar\_sO)_2TcO(OH)^-$ surface complexation constants are already constrained leaving only the chlorite surface complexation constant able to be iteratively improved during the optimization process which results in a final value of 6.00.

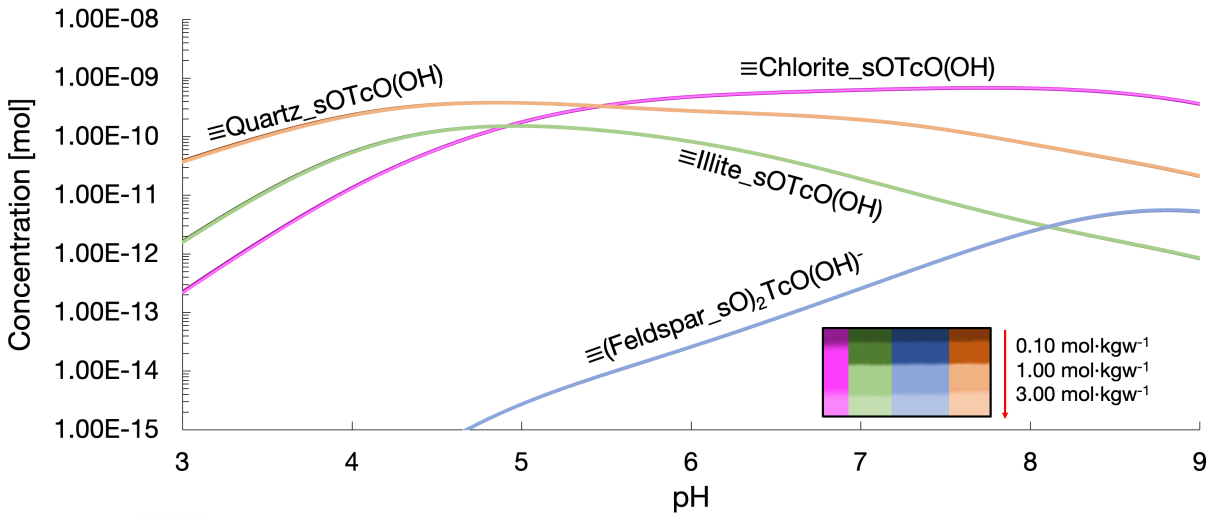

Figure 20 - Simulated Tc(IV) surface complexation with the shale surface in Na-Ca-Cl solutions.

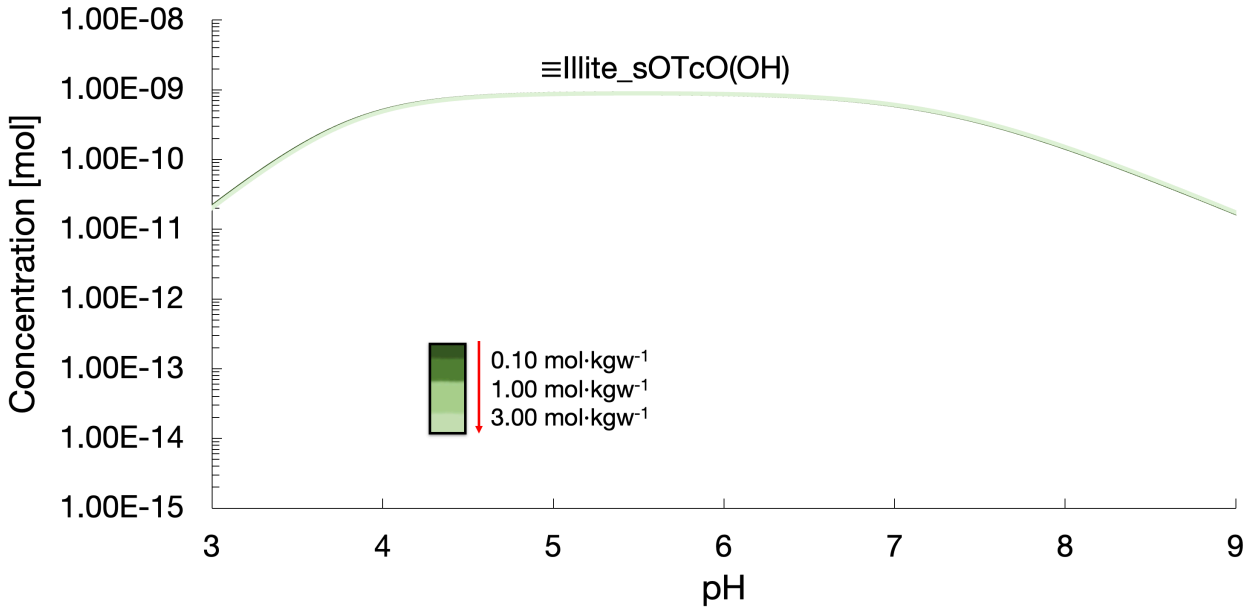

Figure 21 - Simulated Tc(IV) surface complexation with the illite surface in Na-Ca-Cl solutions.

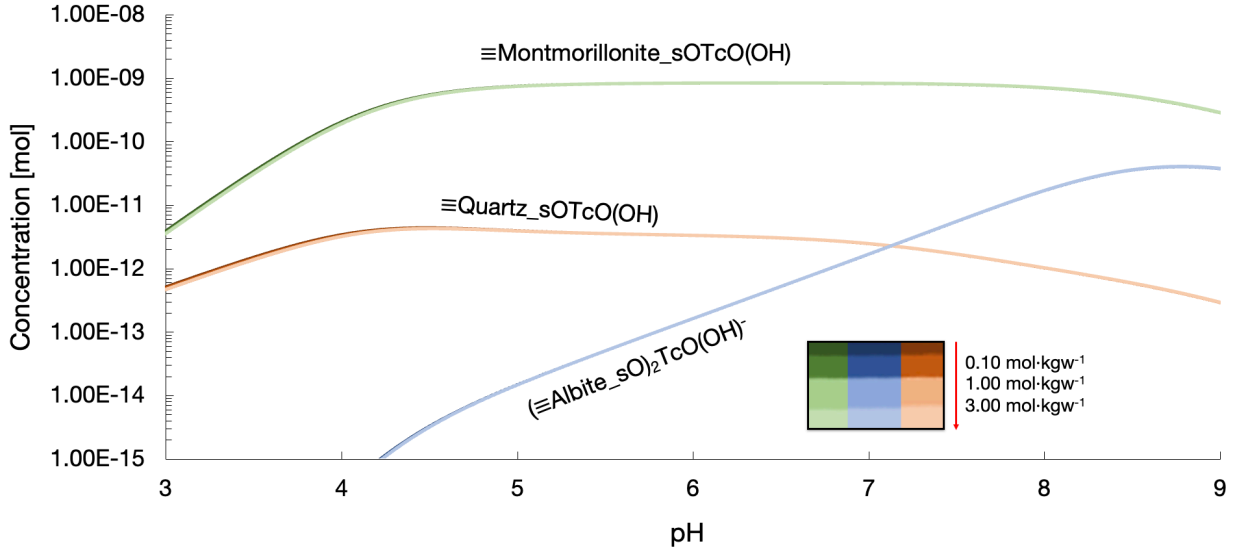

Figure 22 - Simulated Tc(IV) surface complexation with the MX-80 bentonite surface in Na-Ca-Cl solutions.

Table 17 - Surface complexation reactions and optimized surface complexation constants for Tc(IV) adsorption onto shale, illite, and MX-80 bentonite in Na-Ca-Cl solutions.

Simulated Surface	Surface Complexation Reaction	Surface Complexation Constant (LogK)
Shale	≡Illite_sOH + $TcO(OH)_2$ ↔ ≡Illite_sOTcO(OH) + H_2O	5.25
	≡Quartz_sOH + $TcO(OH)_2$ ↔ ≡Quartz_sOTcO(OH) + H_2O	5.35
	≡Chlorite_sOH + $TcO(OH)_2$ ↔ ≡Chlorite_sOTcO(OH) + H_2O	6.00
	2 (≡Feldspar_sOH) + $TcO(OH)_2$ ↔ (≡Feldspar_sO)$_2$TcO(OH)$^-$ + H_2O + H^+	-2.25
Illite	≡Illite_sOH + $TcO(OH)_2$ ↔ ≡Illite_sOTcO(OH) + H_2O	5.25
MX-80 bentonite	≡Quartz_sOH + $TcO(OH)_2$ ↔ ≡Quartz_sOTcO(OH) + H_2O	5.35
	≡Montmorillonite_sOH + $TcO(OH)_2$ ↔ ≡Montmorillonite_sOTcO(OH) + H_2O	5.00
	2 (≡Albite_sOH) + $TcO(OH)_2$ ↔ (≡Albite_sO)$_2$TcO(OH)$^-$ + H_2O + H^+	-2.25

4.7.4 - Linear Energy Free Relationships

There is a Linear Free Energy Relationship (LFER) concept which compares surface complexation constants with hydrolysis constants of metals which undergo adsorption. This LFER allows for either a prediction of surface complexation constants or a way to gauge the accuracy of the final optimized values. The LFER follows the form presented in (8), where *logK* is the surface complexation constant, $log^{OH}K$ is the hydrolysis constant associated with the adsorbing metal species.

$$logK = a log^{OH}K + b \tag{11}$$

As there is a good correlation between hydrolysis constants and surface complexation constants, the LFER alludes to the complexation of metals with hydroxyl groups on mineral surfaces [116, 117]. A collection of LFER's have been presented in Table 18, and have been included in Figure 23. All surface complexation constants which can be found compiled in Table C1 have been plotted in Figure 23 to compare with the LFER's. For reference the values of $log^{OH}K$ associated with Se(-II) and Tc(IV) are 3.85 and 4.00, respectively.

Table 18 - Linear Free Energy Relationships for various minerals and oxides.

Adsorbent Surface	Linear Free Energy Relationship	Reference
Montmorillonite[a]	$log^{S}K = (0.90 \pm 0.02) log^{OH}K + 8.1 \pm 0.3$	[118, 119]
Illite	$log^{S}K = (0.83 \pm 0.02) log^{OH}K + 7.9 \pm 0.4$	[120]
Hematite (α-Fe_2O_3)	$logK = 1.7 log^{OH}K + 14.6$	[121]
SiO_2	$logK = 0.62 log^{OH}K - 0.09$	[122]
α-FeOOH	$logK = 0.75 log^{OH}K + 3.75$	[123]
α-Al_2O_3	$logK = 0.98 log^{OH}K + 6.02$	[124]
γ-Al_2O_3	$logK = 0.57 log^{OH}K - 0.29$	[125, 126]
$Fe_2O_3 \cdot H_2O$ (am)	$logK = 0.56 log^{OH}K + 0.66$	[125, 126]

a) - Surface complexation constants ($log^{S}K$) associated with montmorillonite and illite are associated with the strong sites which are considered in the SCMs

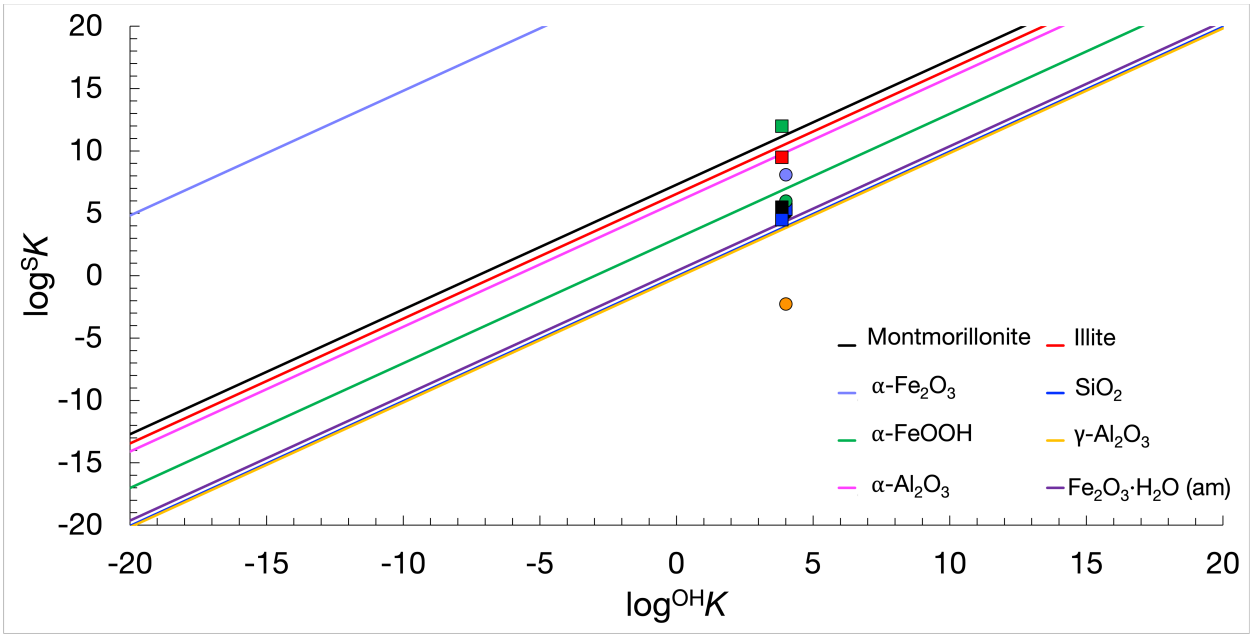

Figure 23a - Linear Free Energy Relationships for minerals and oxides compared with all surface complexation constants. Se(-II) values are represented with squares while Tc(IV) values are represented with circles.

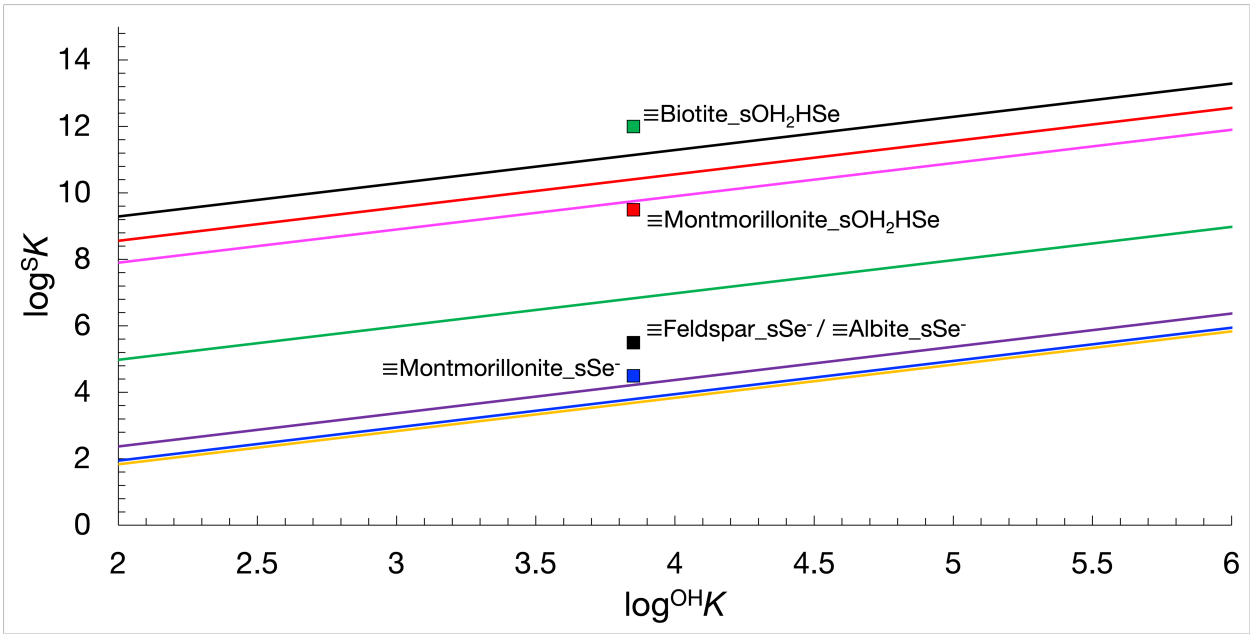

Figure 23b - Linear Free Energy Relationships for minerals and oxides compared with Se(-II) surface complexation constants. Zoomed in for visibility.

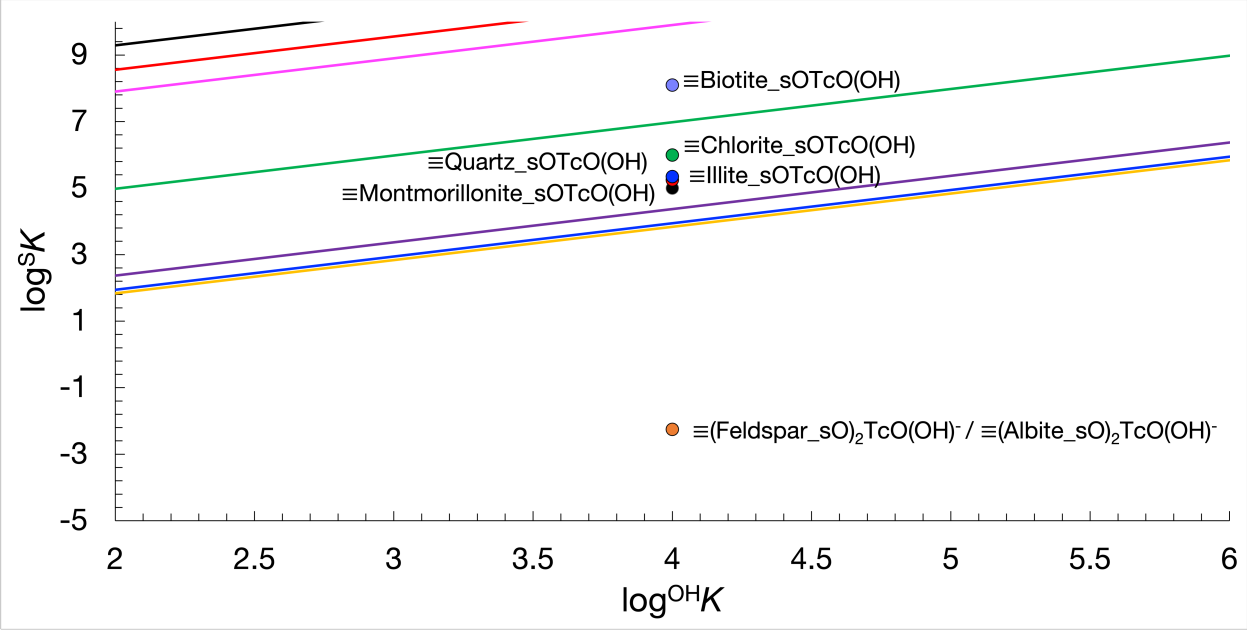

Figure 23c - Linear Free Energy Relationships for minerals and oxides compared with Tc(IV) surface complexation constants. Zoomed in for visibility.

Initially it is considered important to acknowledge the variety exhibited among LFER's depending upon the adsorbents composition. This is considered to imply that these relationships could vary among any single mineral, which is in itself composed of pure oxide assemblage components. Given this distinction, all surface complexes which form with the montmorillonite and illite surfaces are under-estimations compared with their expected value from the LFER. Observing the Tc(IV) surface complexation constants, Grambow et al., did also find that the monodentate surface complexation constant was an under-estimation of the expected value using the same montmorillonite LFER [89], they did not compare with their bidentate surface complexation constant value. However, if these surface complexes are considered to form with silanol, aluminol, or ferrol surface sites, then the final optimized surface complexation constants do appear to coincide more appropriately with the pure oxide LFERs. In Figure 23c, the surface complexation constant associated with $(\equiv Feldspar\_sO)_2TcO(OH)^-$ and $(\equiv Albite\_sO)_2TcO(OH)^-$ has been included for completeness and comparison. With recognition that their may be between 0.5 and 2.0 log units of error associated with the expected surface complexation constants [118 - 120]. The final values as such, which were determined through constraining with

previous adsorption data or optimization of SCM's with respect to the experimental data presented in this study, are presently considered acceptable with respect to the modelling methodology employed.

4.8 - Adsorption of Se(-II) onto Granite and MX-80 Bentonite in CR-10 Solution

Final R_d values which were determined from Se(-II) batch adsorption experiments with granite and MX-80 bentonite in CR-10 solution are presented in Table 19. These results will provide valuable information regarding how Se(-II) is expected to adsorb in the geosphere with the multitude of ions found in the groundwater. A reminder is that The Revell Site is characterized by a crystalline bedrock with a groundwater that the CR-10 solution is based upon.

Se(-II) adsorption onto granite in CR-10 solution is greater than the R_d value determined from Se(-II) adsorption onto MX-80 bentonite in CR-10 solution. This does contrast the previous adsorption behaviour in Ca-Na-Cl solutions, where Se(-II) R_d values with MX-80 bentonite were greater than those specific to granite. Currently, to explain this, the formation of an unknown ion pair between Se(-II) and any one of the multitude of ions that exist within CR-10 solution could then adsorb onto the granite surface and lead to an increase in R_d. Granite is considered to have a large abundance of minerals with widely varying proportions. It may then be possible that one of the mineral assemblage components which was not included in the simulated surface may be a strong adsorber of this unknown ion pair. Also it has been determined that Se(-II) adsorption onto granite is dependant upon the ionic strength, with R_d decreasing as ionic strength increases. The returned R_d value for Se(-II) adsorption onto granite in CR-10 solution is greater than any R_d value in Ca-Na-Cl solutions, except at pH_m = 5.0. When considering the ionic strength of CR-10 is approximately 0.24 mol·kgw^{-1}, the large R_d value suggests that the ionic strength dependency effects may be dominated by the adsorption of the unknown aqueous Se(-II) species, secondary redox processes, or possible precipitation of a crystalline Se compound. Some possible examples of alkali metal selenides to consider based upon the ions present in CR-10 solution include Li_2Se(cr), Na_2Se(cr), NaHSe(aq), K_2Se(cr), CaSe(cr), and SrSe(cr) [64]. It must be briefly mentioned that the increased R_d determined from Se(-II) adsorption onto granite in CR-10 solution compared to that obtained in Ca-Na-Cl solutions is a benefit in any post-closure safety assessment. An example is if there is an alkali metal selenide forming in the groundwater representation used within

these experiments, it is presumed that the same alkali metal selenide will form in the groundwater present within the DGR. This would then decrease the aqueous concentration of Se(-II) present within the geosphere, if Se(-II) were to exist in the geosphere in a mobile form, thus decreasing the mobility associated with Se(-II).

In the past there have been reports associated with the adsorption of Se(-II) for usage in the both the Swiss and Finnish nuclear waste disposal programs. Despite the differences in the bedrock, and groundwater chemistry observed between different international DGR projects, the adsorption of Se(-II) is consistently characterized with low adsorption, as R_d values range from undetermined values to approximately 0.03 $m^3 \cdot kg^{-1}$ [127, 128]. The low amount of Se(-II) adsorption is observed within this study despite the adsorbent materials being granite and MX-80 bentonite. It further has been reported that Se(-II) adsorption onto sedimentary rocks in Na-Ca-Cl solution does not exceed 5.00 $m^3 \cdot kg^{-1}$ [12, 61]. The increased adsorption within the Canadian geological environment is possibly attributed to the increased solution ionic strength. This comparison is still considered to provide confidence in the presented R_d values for Se(-II) adsorption onto both granite and MX-80 bentonite, as the R_d values are within the expected range of approximately 1.00×10^{-2} $m^3 \cdot kg^{-1}$ to 1.00×10^{1} $m^3 \cdot kg^{-1}$ at the similar neutral to basic pH regimes previously studied.

Table 19 - Final R_d values for Se(-II) adsorption onto granite and MX-80 bentonite in CR-10 solution.

Adsorbent	Final pH_m	R_d [$m^3 \cdot kg^{-1}$]
Granite	6.89 ± 0.20	1.80 ± 0.10
MX-80 Bentonite	6.81 ± 0.20	0.47 ± 0.38

4.9 - Adsorption of Tc(IV) onto Granite and MX-80 Bentonite in CR-10 Solution

Final R_d values which were determined from Tc(IV) batch adsorption experiments with granite and MX-80 bentonite in CR-10 solution are presented in Table 20. Tc(IV) adsorption onto granite and MX-80 bentonite in Ca-Na-Cl solutions can currently be considered to produce R_d values within the range of 0.1 $m^3 \cdot kg^{-1}$ to 10.0 $m^3 \cdot kg^{-1}$, based upon the results presented in Figures 10 and 11. Given that the R_d values for Tc(IV) adsorption onto granite and MX-80 bentonite in CR-10 solution are within this range, these results are considered justified. Additionally, Tc(IV) may exhibit interactions with solute ions in the CR-10 solution which would not occur in the Ca-Na-Cl solutions. There have been studies conducted which state that in addition to the $Ca_3[TcO(OH)_5]^{3+}$ ion, there could also exist an $Mg_3[TcO(OH)_5]^{3+}$ ion [22]. Further, $TcO(HSO_4)^+$ and $TcOSO_4$ have been shown to exist [79, 129, 130]. This could imply their formation in CR-10 solutions based upon the minor sulphate amount present. Given the formation of these Tc(IV) species, if any were able to be adsorbed would allow for the existence of an additional Tc(IV) adsorption pathways which exist only in the CR-10 solution.

Table 20 - Final R_d values for Tc(IV) adsorption onto granite and MX-80 bentonite in CR-10 solution.

Adsorbent	Final pH_m	R_d [$m^3 \cdot kg^{-1}$]
Granite	7.59 ± 0.20	1.47 ± 0.25
MX-80 Bentonite	7.46 ± 0.09	2.19 ± 0.33

4.10 - Adsorption of Tc(IV) onto Shale, Limestone, Illite, and MX-80 Bentonite in SR-270-PW Solution

Final R_d values which were determined from Tc(IV) batch adsorption experiments with shale, limestone, illite, and MX-80 bentonite in SR-270-PW solution are presented in Table 21. Similar to the argument presented in Section 4.9, Tc(IV) adsorption in Na-Ca-Cl solutions is considered to produce R_d values with a range of 0.1 $m^3 \cdot kg^{-1}$ to 10.0 $m^3 \cdot kg^{-1}$. Therefore, the R_d values specific to Tc(IV) adsorption in SR-270-PW solution are considered on par and are presently thought to be justified. In the past, Bertetti studied the adsorption of Tc(IV) onto shale, limestone, and MX-80 bentonite in SR-270-PW brine solution, and measured R_d values of 0.02 $m^3 \cdot kg^{-1}$, 10.0 $m^3 \cdot kg^{-1}$, and 5.0 $m^3 \cdot kg^{-1}$, respectively [96]. Walton et al., determined R_d values for Tc(IV) adsorption onto sediments with groundwaters as being: (0.89 ± 0.18) $m^3 \cdot kg^{-1}$, (0.77 ± 0.13) $m^3 \cdot kg^{-1}$, and (0.99 ± 0.18) $m^3 \cdot kg^{-1}$, respectively under both low and high salinity conditions [16]. These similar R_d values from previous studies are considered to further support those which have been presented in this study.

Additional Tc(IV) adsorption pathways may exist in SR-270-PW solution also due to possible Tc(IV) interactions with solute ions. One minor solute ion within SR-270-PW solution is bicarbonate, and as discussed previously in Section 4.6.2, there may be Tc(IV) calcium carbonate complexes which may form and adsorb with the surface [22]. At the present, it is known that TcS_2 and Tc_2S_7 exist in addition to the previously mentioned $TcO(HSO_4)^+$ and $TcOSO_4$ species [79, 129, 130]. Previously, Vinsova et al., determined that sulphide containing minerals were able to adsorb Tc(VII) through a reduction process that produces either an adsorbable Tc(IV) species, or the sparingly soluble $TcO_2 \cdot 1.6H_2O$(am) precipitate [31]. As the concentration of Tc(IV) used in this study is below the solubility limit of Tc(IV), it is presumed that only the Tc-S species which form, would be capable of adsorption. In observation of the results that Vinsova et al., reported from their Tc(IV) adsorption onto bentonite adsorption experiments, one additive is useful to discuss. Bentonite with iron sulphide was shown to be capable of retaining Tc(IV) with R_d values that approach a value of 1.68 $m^3 \cdot kg^{-1}$, at a pH value of 8.0 after 7-days [31]. This value is larger than the one reported for Tc(IV) adsorption onto MX-80 bentonite in SR-270-PW solution. However, it is

believed that the increased concentration of the Fe(III)/Fe(II) redox pair from the iron sulphide added to the MX-80 bentonite contributes to the increased Tc(IV) adsorption.

Table 21 - Final R_d values for Tc(IV) adsorption onto shale, limestone, illite, and MX-80 bentonite in SR-270-PW solution.

Adsorbent	Final pH_m	R_d [$m^3 \cdot kg^{-1}$]
Shale	5.84 ± 0.12	0.16 ± 0.10
Limestone	5.76 ± 0.11	0.44 ± 0.21
Illite	5.24 ± 0.10	1.86 ± 0.44
MX-80 Bentonite	5.19 ± 0.49	0.23 ± 0.10

Chapter 5 - Conclusion

The adsorption behaviour of: Se(-II) onto granite and MX-80 bentonite in Ca-Na-Cl solutions, Tc(IV) onto granite and MX-80 bentonite in Ca-Na-Cl solutions, and Tc(IV) onto shale, limestone, illite, and MX-80 bentonite in Na-Ca-Cl solutions has been elucidated. Surface complexation models have also been defined which have successfully simulated the adsorption of both Se(-II) and Tc(IV). No simulations were attempted to be optimized with the Tc(IV) adsorption onto limestone data. Finally, R_d values have been determined specific to: Se(-II) adsorption onto granite and MX-80 bentonite in CR-10 solution, Tc(IV) adsorption onto granite and MX-80 bentonite in CR-10 solution, and Tc(IV) adsorption onto shale, limestone, illite, and MX-80 bentonite in SR-270-PW solution.

Adsorption kinetic experiments show that Se(-II) and Tc(IV) adsorption onto granite and MX-80 bentonite in Ca-Na-Cl solutions both reach adsorption steady-state conditions in 7- and 14-days, respectively. Tc(IV) adsorption onto shale reaches adsorption steady-state conditions in 7-days, whereas steady-state conditions are reached in 14-days for limestone, illite, and MX-80 bentonite when Na-Ca-Cl solutions were used. Se(-II) adsorption onto granite and MX-80 bentonite are both effected by the solution pH, with R_d decreasing as pH increases. Tc(IV) adsorption onto all adsorbents tends to follow an atypical trend, with there being constant R_d with respect to pH. Adsorption of Se(-II) onto granite is influenced by a variation in solution ionic strength which causes R_d to decrease with an increase in the ionic strength. This effect is not found when observing Se(-II) adsorption onto MX-80 bentonite as R_d values are within error for all ionic strengths. Tc(IV) adsorption onto all adsorbents does not allude to any ionic strength dependancy effects with regards to the total amount of Tc(IV) able to be adsorbed, as R_d values are within error.

New simulated surfaces have been developed for granite, shale, and MX-80 bentonite based on their mineral assemblage components. Granite has been assumed to be feldspar, quartz, and biotite. Shale has been assumed to be illite, quartz, and chlorite. MX-80 bentonite has been assumed to be montmorillonite, quartz, and albite. Illite has been assumed to be 100.0% illite for simplicity. Se(-II) adsorption onto granite is best simulated with the $\equiv$Feldspar_sSe^- and $\equiv$Biotite_sOH_2HSe surface

complexes. Se(-II) adsorption onto MX-80 bentonite is best simulated with the ≡Albite_sSe$^-$, ≡Montmorillonite_sSe$^-$, and ≡Montmorillonite_sOH$_2$HSe surface complexes. Tc(IV) adsorption onto granite is best simulated with the ≡Biotite_sOTcO(OH), ≡Quartz_sOTcO(OH), and (≡Feldspar_sOH)$_2$TcO(OH)$^-$ surface complexes. Tc(IV) adsorption onto MX-80 bentonite is best simulated with the ≡Quartz_sOTcO(OH), ≡Montmorillonite_sOTcO(OH), and (≡Albite_sOH)$_2$TcO(OH)$^-$ surface complexes. Tc(IV) adsorption onto shale is best simulated with the ≡Quartz_sOTcO(OH), ≡Illite_sOTcO(OH), ≡Chlorite_sOTcO(OH), and (≡Feldspar_sOH)$_2$TcO(OH)$^-$ surface complexes. Tc(IV) adsorption onto illite is best simulated with only the ≡Illite_sOTcO(OH) surface complex.

Lastly, batch adsorption experiments present evidence that Se(-II) adsorption onto granite and MX-80 bentonite in CR-10 solution returns R_d values of (1.80 ± 0.10) $m^3 \cdot kg^{-1}$, and (0.47 ± 0.38) $m^3 \cdot kg^{-1}$, respectively. Tc(IV) adsorption onto granite and MX-80 bentonite in CR-10 solution returns R_d values of (1.80 ± 0.10) $m^3 \cdot kg^{-1}$, and (2.19 ± 0.33) $m^3 \cdot kg^{-1}$, respectively. Tc(IV) adsorption onto shale, limestone, illite, and MX-80 bentonite in SR-270-PW solution returned R_d values of (0.16 ± 0.10) $m^3 \cdot kg^{-1}$, (0.44 ± 0.21) $m^3 \cdot kg^{-1}$, (1.86 ± 0.44) $m^3 \cdot kg^{-1}$, and (0.23 ± 0.10) $m^3 \cdot kg^{-1}$, respectively. All adsorption experiment data that has been presented within this thesis, in conjunction with the surface complexation models, are considered to be beneficial to developing the scientific understanding associated with both Se(-II) and Tc(IV) adsorption processes. Regardless of the final repository location site being either The Revell Site or The South Bruce Site. This work may support the implementation of a used nuclear fuel repository within Canada.

Progressing forwards, there is hope that work will be completed with regards to elucidating the migration behaviours of Se(-II) and Tc(IV) in terms of both adsorption and transport processes. Utilization of Density Functional Theory (DFT) and Molecular Dynamics (MD) allows for microscopic simulations to be completed, which allow for the diffusivity of a radionuclide to be determined. These results will be compared to both diffusion and adsorption studies to attempt and understand Se(-II) and Tc(IV) adsorbed surface complexes more completely.

Chapter 6 - References

[1] – Gierszewski, P., Parmenter, A., *Confidence in Safety – South Bruce Site*, Nuclear Waste Management Organization, NWMO-TR-2022-15, 2022

[2] - Gierszewski, P., Parmenter, A., *Confidence in Safety – Revell Site,* Nuclear Waste Management Organization, NWMO-TR-2022-14, 2022

[3] - *Postclosure Safety Assessment of a Used Fuel Repository in Crystalline Rock*, Nuclear Waste Management Organization, NWMO-TR-2017-02, 2017

[4] – Naserifard, N., Lee, A., Birch, K., Chiu, A., Zhang, X., *Deep Geological Repository Conceptual Design Report Crystalline / Sedimentary Rock*, Nuclear Waste Management Organization, APM-REP-00440-0211-R000, 2017

[5] – Jörg, G., R. Bühnemann., Hollas, S., Kivel, N., Kossert, K., Van Winckel, S., Lierse v Gostomski, G., *Preparation of radiochemically pure ^{79}Se and highly precise determination of its half-life*, Appl. Radiation and Isotopes, Vol. 63, 2339 - 2351, 2017

[6] – Jordan, N., Franzen, C., Lutzenkirchen, J., Foerstendorf, H., Hering, D., Weiss, S., Heim, K., Brendler, V., *Adsorption of selenium(VI) onto nano transition alumina*, Environ. Sci. Nanotech., 2018

[7] – Jordan, N., Ritter, A., Foerstendorf, H., Scheinost, A. C., Weiss, S., Heim, K., Grenzer, J., Mucklich A., Reuther, H., *Adsorption mechanism of selenium(VI) onto maghemite*, Geochimica et Cosmochimica Acta, Vol. 103, 63 - 75, 2013

[8] – Li, X., Puhakka, E., Ikonen, J., Soderland, M., Lindberg, A., Holgersson, S., Martin, A., Siitari-Kauppi M., *Sorption of Se species on mineral surfaces, part 1: batch sorption and multi-site modelling*, Appl. Geochem., Vol. 95, 147 - 157, 2018

[9] – Hardy, W. A., Silvey, G., Townes, C. H., Burke, B. F., Strandberg, M. W. P., Parker, G. W., Cohen, V. W., *The Nuclear Moments of ^{79}Se*, Phys. Review, Vol. 6, 1532 – 1537, 1953

[10] – Videnska, K., Palagyi, S., Stamberg, K., Vodickova, H., Havlova, V., *Effect of grain size on the sorption and desorption of SeO_4^{2-} and SeO_3^{2-} in columns of crushed granite and fracture infill from granitic water under dynamic conditions,* J. Radioanal. Nucl. Chem., Vol. 298, 547-554, 2013

[11] – Hallam, R. J., Evans, N. D. M., Jain, S. L., *Sorption of Tc(IV) to some geologic materials with reference to radioactive waste disposal*, Mineralogical Magazine, Vol. 75(4), 2439 – 2448, 2011

[12] – Vilks, P., Yang, T., *Sorption of Selected Radionuclides on Sedimentary Rocks in Saline Conditions – Reported Values, Nuclear Waste Management Organization*, NWMO-TR-2018-03, 2018

[13] – Hess, N. J., Qafoku, O., Xia, Y., Moore, D. A., Felmy, A, R., *Thermodynamic Model for the Solubility of TcO2·xH2O in Aqueous Oxalate Systems*, J. Solution Chem, Vol. 37, 1471 – 1487, 2008

[14] – Skomurski, F. N., Rosso, K. M., Krupka, M. K., McGrail, B. P., *Technetium Incorporation into Hematite (α-Fe_2O_3)*, Environ. Sci. Technol., Vol 44, 5855-5861, 2010

[15] – German, K. E., Peretrukhin, V. F., Belyaeva, L. I., Kuzina, O. V., *Sorption of Long-Lived Technetium from Radioactive Wastes and Ground Water by Sulfides and Sulfide Rocks*, Technetium and Rhenium Chemistry and Nuclear Medicine 4, (Bressanone-Bolzano-Italy, 12-14 September, Nicolini, M., Bandoli, G., Mazzi, U. eds), SGEditoriali, 93 – 97, Padova, 1994

[16] – Walton, F. B., Paquette, J., Ross, J. P. M., Lawrence, W. E., *Tc(IV) and Tc(VII) Interactions with Iron Oxyhydroxides*, Nucl. And Chem. Waste Management, Vol. 6, 121-126, 1986

[17] - Boggs, M. A., Dong, W., Gu, B., Wall, N. A., *Complexation of Tc(IV) with acetate at varying ionic strengths*, Radiochim Acta. Vol. 98, 583-587, 2010

[18] – Lieser, K. H., Bauscher, Ch., *Technetium in the Hydrosphere and Geosphere I. Chemistry of Technetium and Iron in Natural Waters and Influence of the Redox Potential on the Sorption of Technetium*, Radiochimica Acta. Vol. 42, 205-213, 1987

[19] – Lukens Jr., W. W., Bucher, J. J., Edelstein, N. M., Shuh, D. K., *Products of Pertechnetate Radiolysis in Highly Alkaline Solution: Structure of $TcO{\cdot}xH_2O$*, Environ. Sci. Technol., Vol. 36, 1124-1129, 2002

[20] – Yalcintas, E., Scheinost, A. C., Gaona, X., Altmaier, M., *Systematic XAS Study on the Reduction and Uptake of Tc by Magnetite and Mackinawite*, Dalton Trans., Vol. 45. 17874-17885, 2016

[21] – Vinsova, H., Koniova, R., Koudelkova, M., Jedinakova-Krizova, V., *Sorption of Technetium and Rhenium on Natural Sorbents Under Anaerobic Conditions*, J. of. Radioanal. Chem., Vol. 261 (2), 407-413, 2004

[22] – Yalcintas, E., Gaona, X., Altmaier, M., Dardenna, K., Polly, R., Geckeis, H., *Thermodynamic description of Tc(IV) Solubility and Hydrolysis in dilute to concentrated NaCl, $MgCl_2$ and $CaCl_2$ Solutions*, Dalton, Trans. Vol. 45, 8916-8936, 2016

[23] – Liu, D. J., Yao, J., Wang, B., Bruggeman, C., Maes, N., *Solubility Study of Tc(IV) in a granitic water*, Radiochim. Acta., Vol. 95, 523-528, 2007

[24] – Bondietti, E. A., Francis, C. W., *Geologic Migration Potentials of Technetium-99 and Neptunium-237*, Science, New Series, Vol. 203 (4387), 1337-1350, 1979

[25] – Pearce, C. I., Moore, R. C., Morad, J. W., Asmussen, R. M., Chatterjee, S., Lawter, A. R., Levitskaia, T. G., Neeway, J. J., Qafoku, N. P., Rigali, M. J., Saslow, S. A., Szecsody, J. E., Thallapally, P. K., Wang, G., Freedman, V., *Technetium immobilization by materials through sorption and redox-driven processes: A literature review*, Sci. of the Total Environ., Vol. 716, 132849, 12 pages, 2020

[26] – Smith, F. N., Um, U., Taylor, C. D., Kin, D.-S., Schewiger, M. J., Kruger, A. A., *Computational Investigation of Technetium(IV) Incorporation into Inverse Spinels: Magnetite (Fe_3O_4) and Trevorite ($NiFe_2O_4$)*, Environ. Sci. Technol., Vol. 50, 5216-5224, 2016

[27] – Yalcintas, E., Gaona, X., Scheinost, A. C., Kobayashi, T., Altmaier, M., Geckeis, H., *Redox Chemistry of Tc(VII)/Tc(IV) in dilute to concentrated NaCl and $MgCl_2$ solutions*, Radiochim Acta., Vol 103 (1), 57-72, 2015

[28] – Westsik, Jr., J. H., Cantrell, K. J., Serne, R. J., Qafoku, N. P., *Technetium Immobilization Forms Literature Survey,* Pacific Northwest National Laboratory, PNNL-23329, EMSP-RPT-023

[29] – Parker, T. G., Omoto, T., Dickens, S. M., Wall, D. E., Wall, N. A., *Complexation of SO_4^{2-} in NaCl Medium*, J. of Sol. Chem., Vol. 47, 1192-1201, 2018

[30] – Warwick, P., Aldridge, S., Evans, N., Vines, S., *The solubility of technetium(IV) at high pH*, Radiochim Acta., Vol. 95, 709-716, 2007

[31] – Vinsova, H., Vecernik, P., Jedinakova-Krizova, V., *Sorption Characteristics of ^{99}Tc onto Bentonite Material with different additives under anaerobic conditions*, Radiochim Acta., Vol. 94, 435-440, 2006,

[32] – Meena, A. H., Arai, Y., *Environmental Geochemistry of Technetium*, Environ. Chem. Lett., Vol. 15, 241-263, 2017

[33] – Huber, F. M., Totskiy, Y., Marsac, R., Schild, D., Pidchenko, I., Vitova, T., Kalmykov, S., Geckeis, H., Schager, T., *Tc interaction with crystalline rock from Aspo (Sweden): Effect of in-situ rock capacity*, Applied Geochem., Vol. 80, 90-101, 2017

[34] – Zachara, J. M., Heals, S. M., Jeon, B., Kukkadapu, R. K., Liu, C., *Reduction of pertechnetate [Tc(VII)] by aqueous Fe(II) and the nature of solid phase redox products*, US Department of Energy Publications, 161

[35] – Eriksen, T. E., Ndalamba, P., Bruno, J., Caceci, M., *The Solubility of $TcO{\cdot}nH_2O$ in Neutral to Alkaline Solutions under Constant pCO_2*, Radiochimica Acta., Vol. 58/59, 67-70, 1992

[36] – Boglaienko, D., Levitskaia, T. G., *Abiotic Reductive Removal and Subsequent Incorporation of Tc(IV) into Iron Oxides: A Frontier Review*, Environmental Science: Nano, 19 pages, 2019

[37] – Amaya, T., Kobayashi, W., Suzuki, K., *Adsorption Study of the Tc(IV) on Rocks and Minerals Under Simulated Geological Conditions*, Mat. Res. Soc. Symp. Proc., Vol. 353, 1005-1012, 1995

[38] – Farrell, J., Bostick, W. D., Jarabek, R. J., Fiedor, J. N., *Electrosorption and Reduction of Pertechnetate by Anodically Polarized Magnetite*, Environ. Sci. Technol., Vol. 33, 1244-1249, 1999

[39] – Peretyazhko. T., Zachara, J. M., Heald, S. M., Jeon, B.-H., Kukkadapu, R. K., *Heterogenous reduction of Tc(VII) by Fe(II) at the solid-water interface*, US Department of Energy Publications, 163

[40] – Peretyazhko, T., Zachara, J. M., Heald, S. M., Kukkadapu, R. K., Liu, C., Plymale, A. E., Resch, C. T., *Reduction of Tc(VII) by Fe(II) Sorbed on Al (hydr)oxides*, Environ. Sci. Technol. Vol. 42, 5499 – 5506, 2008

[41] – Said, K. B., Fattahi, M., Musikas, Cl., Abbe, J. Ch., *The speciation of Tc(IV) in chloride solutions*, Radiochim Acta., Vol. 88, 567-571, 2000

[42] – Begg, J. D. C., Burke, I. T., Charnock, J. M., Morris, K., T*echnetium reduction and oxidation behaviour in Dounreay soils*, Radiochim Acta, Vol. 96, 631-636, 2008

[43] – Krupka, K. M., Serne, R. J., *Geochemical Factors Affecting the Behaviour of Antimony, Cobalt, Europium, Technetium, and Uranium in Vadose Sediments*, Pacific Northwest National Laboratory, PNNL-14126, 2002

[44] – Bar-Yosef, B., Meek, D., *Selenium Sorption by Kaolinite and Montmorillonite*, Soil Sci. Vol. 144 11-19, 1987

[45] – Gupta, M., Gupta, S., *An Overview of Selenium Uptake, Metabolism, and Toxicity in Plants,* Frontiers in Plant Sci., Vol. 7, 2074, 2017

[46] – Zhang, Y., Moore, J. N., *Selenium Fractionation and Speciation in a Wetland System*, Environ. Sci. Technol. 30 (2020) 2613-2619

[47] – Koch-Steindl, H., Prohl, G., *Consideration on the behaviour of long-lived radionuclides in the soil*, Radiation Environ. Biophys. Vol. 40, 93-104, 2001

[48] – Medri, C., Bird, G., *Non-Human Biota Dose Assessment Equations and Data*, Nuclear Waste Management Organization, NWMO-TR-2014-02 R001, 2015

[49] – Greger, N., *Uptake of nuclides on plants*, Svensk Karnbranslehantering AB (SKB), 20014, TR-04-14

[50] – Ho, M., *The Long-Term Biogeochemistry of ^{79}Se, ^{99}Tc, and ^{90}Sr in Complex Environmental Systems*, PhD Thesis, Department of Chemistry – Radiochemistry, University of Helsinki, 2022

[51] – Racette, J., Nagasaki, S., *Pursuing Long-Term Nuclear Waste Safety in Canada for Seven Generations and Beyond: A Radio-Ethnobotany Case Study,* 41st Annual Conference of the Canadian Nuclear Society and 46th Annual CNS/CNA Student Conference, June 5 – 8, 2022

[52] – Nagasaki, S., Saito, T., Yang, T. T., *Sorption Behaviour of Np(V) on illite, shale, and MX-80 in high ionic strength solutions*, J. of Radioanal. and Nucl. Chem. Vol. 308, 143-153, 2016

[53] – Altmaier, M., Neck, V., Fanghanel, T., *Solubility of Zr(IV), Th(IV), and Pu(IV) hydrous oxides in $CaCl_2$ solutions and the formation of ternary Ca-M(IV)-OH complexes*, Radiochimica Acta, Vol. 96, 541-550, 2008

[54] – Altmaier, M., Metz, V., Neck, V., Muller, R., Fanghanel, T., *Solid-Liquid equilibria of $Mg(OH)_2$(cr) and $Mg_2(OH)_3Cl{\cdot}4H_2O$(cr) in the system Mg-Na-H-OH-Cl-H_2O at 25^oC*, Geochimica et Cosmochimica Acta, Vol. 67, 3595-3601, 2003

[55] - Iida, Y., Yamaguchi, T., Tanaka, T., *Sorption Behaviour of hydroselenide (HSe^-) onto iron containing minerals*, J. of Nucl. Sci. and Technol., Vol. 51, 305-322, 2014

[56] – Iida, Y., Tanaka, T., Yamaguchi, T., Nakayama, S., *Sorption Behaviour of Selenium(-II) on Rocks under Reducing Conditions*, J. of Nucl. Sci. and Technol., Vol. 48, 279-291, 2011

[57] – Sugiura, Y., Tomura, T., Ishidera, T., Doi, R., Clarence P., Franciso, M., Shiwaku, H., Kobayashi, T., Matsumura, D., Takahashi, Y., Tachi, Y., *Sorption Behaviour of Selenide on Montmorillonite*, J. of Radioanal. and Nucl. Chem., Vol. 324, 615-622, 2020

[58] – Iida, Y., Yamaguchi, T., Nakayama, S., Nakajima, T., Sakamoto, Y., *The Solubility of Metallic Selenium under Anoxic Conditions*, Mat. Res. Soc. Symp. Proc., Vol. 663, 2001

[59] – Iida, Y., Tanaka, T., Yamaguchi, T., Nakayama, S., *Solubility of Selenium at High Ionic Strength Under Anoxic Conditions*, J. of Nucl. Sci. and Technol., Vol. 47, 431-438, 2010

[60] – Iida, Y., Yamaguchi, T., Tanaka, T., Kitamura, A., Nakayama, S., *Determination of the Solubility Limiting Solid of Selenium in the Presence of Iron Under Anoxic Conditions*, Japanese Atomic Energy Research Institute, 2010

[61] – Walker, A., Racette, J., Saito, T., Yang, T. T., Nagasaki, S., *Sorption of Se(-II) on illite, MX-80 bentonite, shale, and limestone in Na-Ca-Cl Solutions*, Nucl. Eng. And Technol., Vol. 54, 1616-1622, 2022

[62] – Zhao, J., Matsune, H., Takanaka, S., Kishida, N., *Reduction of selenate with hydrazine monohydrate over Pt crystals in aqueous solution*, Chem. Eng. J., Vol. 308, 963-973, 2017

[63] – Chen, J. P., Lim, L. L., *Key factors in chemical reduction by hydrazine for recovery of precious metals*, Chemosphere, Vol. 49, 363-370, 2002

[64] - Olin, A., Nolang, B., Osadchii, E. G., Ohman, L-O., Rosen, E., *Chemical Thermodynamics of Selenium*, Nuclear Energy Agency, 2004

[65] – *Postclosure Safety Assessment of a Used Fuel Repository in Sedimentary Rock*, Nuclear Waste Management Organization, NWMO-TR-2018-08, 2018

[66] – Bard. A. J., Faulkner, L. R., *Electrochemical Methods Fundamental Applications,* John Wiley & Sons, ISBN 0-471-05542-5, 1980

[67] – Meyer, R. E., Arnold, W. D., *The Electrode Potential of the Tc(IV)-Tc(VII) Couple**, Radiochimica Acta., Vol. 55, 19-22, 1991

[68] – Fredrickson, J. K., Zachara, J. M., Kennedy, D. W., Kukkadapu, R. K., McKinley, J. P., Heald, S. M., Liu, C., Plymale, A. E., *Reduction of TcO4- by sediment-associated biogenic Fe(II)*, Geochimica et Cosmochimica Acta., Vol. 68, No. 15, 3171-3187, 2004

[69] – Cobble, J. W., Smith Jr, Wm. T., Boyd, G. E., *Thermodynamic Properties of Technetium and Rhenium Compounds. II. Heats of Formation of Technetium Heptoxide and Pertechnic Acid, Potential of the Technetium(IV)-Technetium(VII) Couple, and a Potential Diagram for Technetium*, Division of Physical and Inorganic Chemistry, 121st Meeting, American Chemical Society, March 23-26, 5777-5782, 1953

[70] – Maslennikov, A., Masson, M., Peretroukhine, V., Lecomte, M., *Technetium Electrodeposition from Aqueous Formate Solutions at Graphite Electrode: Electrochemical Study*, Radiochim. Acta., Vol. 84, 53-58, 1999

[71] – Mazzocchin, G. A., Magno, F., Mazzi, U., Portanova, R., *Voltammetric Behaviour of Aqueous Technetate(VII) Ion*, Inorganica Chimica Acta, Vol. 9, 263-268, 1974

[72] – Maslennikov, A., Masson, M., Peretroukhine, V., Lecomte, M., *Technetium Electrodeposition from Aqueous Formate Solutions: Electrolysis Kinetics and Material Balance Study*, Radiochim Acta., Vol. 83, 31-37, 1998

[73] – Mazzocchin, G-A., Mazzi, U., Portanova, R., Traverso, O., *Quantitative Determinations of Technetate(VII) and Technetium(IV)*, J. Inorg. Nucl. Chem., Vol. 36, 3783-3788, 1974

[74] - Goguen, J., Walker, A., Racette, J., Riddoch, J., Nagasaki, S., *Sorption of Pd on illite, MX-80 bentonite, shale in Na-Ca-Cl solutions*, Nucl. Eng. and Tech., Vol. 53, 894-900, 2021

[75] - Yang, T. T., *Personal Correspondence*, Nuclear Waste Management Organization, 2018

[76] - Beckman Coulter, Inc., *Instructions for Use – TLA-110 Fixed Angle Rotor*, PN TL-TB-019AK, 2022

[77] – Thompson, D. W., Pownall, P. G., S*urface Electrical Properties of Calcite*, J. Colloid and Interference Sci., Vol. 131, No. 1, 1989

[78] - Parkhurst, D. L., Appelo, C. A. J., *Description of Input and Examples for PHREEQC Version 3 – A Computer Program for Speciation, Batch-Reaction, One-Dimensional Transport, and Inverse Geochemical Calculations*, U.S. Geological Survey Techniques and Methods, 2013

[79] – Grenthe. I., Gaona. X., Plyasunov, A. V., Rao, L., Runde, W. H., Grambow, B., Konings, R. J. M., Smith, A. L., Moore, E. E., *Second Update on the Chemical Thermodynamics of Uranium, Neptunium, Plutonium, Americium, and Technetium*, Nuclear Atomic Agency, OECD Publishing, Paris, 2020

[80] - Doi, R., Kitamura, A., Yui, M., J*AEA Thermodynamic Database for Performance Assessment of Geological Disposal of High-level and TRU Wasters: Selection of Thermodynamic Data of Selenium*, Japanese Atomic Energy Agency, JAEA-Review 2009-051, 2009

[81] – Kitamura, A., Fujiwara, K., Doi, R., Yoshida, Y., *Update of JAEA-TDB: Additional Selection of Thermodynamic Data for Solid and Gaseous Phases on Nickel, Selenium, Zirconium, Technetium, Thorium, Uranium, Neptunium, Plutonium, and Americium, Update of Thermodynamic Data on Iodine, and Some Modifications*, Japanese Atomic Energy Agency, Geological Research Isolation Unit, JAEA-Data/Code 2012-006, 2012

[82] – Licht, S., Forouzan, F., *Speciation Analysis of Aqueous Polyselenide Solutions*, J. Electrochem. Soc., Vol. 142, 1546-1551, 1995

[83] – Lyons, L. E., Young, T. L., *Alkaline Selenide, Polyselenide Electrolytes: Concentrations, Absorption Spectra, and Formal Potentials*, Aust. J. Chem., Vol. 39, 511-527, 1986

[84] – Bradbury, M. H., Baeyens, B., *A mechanistic description of Ni and Zn sorption on Na-montmorillonite Part I: Titration and Sorption Measurements*, J. of Contam. Hydrol., Vol 27, 199-222, 1997

[85] – Bradbury, M. H., Baeyens, B., *A mechanistic description of Ni and Zn sorption on Na-montmorillonite Part II: modelling*, J. of Contam. Hydrol., Vol. 27, 223-248, 1997

[86] – Bradbury, M. H., Baeyens, B., *A Quantitative Mechanistic Description of Ni, Xn, and Ca Sorption on Na-Montmorillonite*, Paul Schreer Institute, PSI Bericht Nr. 95-12, 1995

[87] - Bradbury, M. H., Baeyens, B., *Sorption modelling on Illite Part 1: Titration Measurements and Sorption of Ni(II), Co(II), Eu(III), and Sn(IV)*, Geochim. Cosmochim. Acta., Vol. 73, 990-1003, 2009

[88] - Bradbury, M. H., Baeyens, B., *Sorption modelling on Illite Part 2: Actinide sorption and linear free-energy relationships*, Geochim. Cosmochim. Acta., Vol. 73, 1004-1013, 2009

[89] – Grambow, B., Fattahi, M., Montavon, G., Moisan, C., Giffaut, E., *Sorption of Cs, Ni, Pb, Eu(III), Am(III), Cm, Ac(III), Tc(IV), Th, Zr, and U(IV) on MX-80 bentonite: An experimental approach to assess model uncertainty*, Radiochim. Acta., Vol. 94, 627-636, 2006

[90] – Li, X., Puhakka, A., Liu, L., Zhang, W., Ikonen, J., Lindberg, A., Slitari-Kauppi, M., *Multi-Site Surface Complexation Modelling of Se(IV) sorption on biotite*, Chem. Geo., Vol. 533, 119433, 2020

[91] – Iida, Y., Yamaguchi, T., Tanaka, T., Hemmi, K., *Sorption Behaviour of thorium onto granite and its constituent minerals*, J. Nucl. Sci. Technol., Vol. 53, 1573-1584, 2016

[92] – Yang, T. T., *Personal Correspondence*, Nuclear Waste Management Organization, 2023

[93] – Bradbury, M. H., Baeyens, B., *Physico-Chemical Characterisation Data and Sorption Measurements of Cs, Ni, Eu, Th, U, Cl, I, and Se on MX-80 Bentonite*, Paul Schrerrer Institut, PSI Bericht Nr. 11-05, 2011

[94] – Dixon, D., Mam, A., Rimal, S., Stone, J., Siemens, G., *Bentonite Seal Properties in Saline Water*, Nuclear Waste Management Organization, NWMO-TR-2018-20, 2018

[95] – Ticknor, K. V., McMurray, J., *A Study of Selenium and Tin Sorption on Granite and Geothite*, Radiochimica Acta., Vol. 73, 149-156, 1996

[96] – Bertetti, F. P., *Determination of Sorption Properties for Sedimentary Rocks Under Saline, Reducing Conditions – Key Radionuclides*, Nuclear Waste Management Organization, NWMO-TR-2016-08, 2016

[97] – Wang, L., Maes, A., De Canniere, P., van der Lee, J., *Sorption of Europium on Illite (Silver Hill Montana)*, Radiochim Acta., Vol. 82, 233-237, 1998

[98] – Tournassat, C., Neaman, A., Villieras, F., Bosbach, D., Charlet, L., *Nanomorphology of montmorillonite particles: Estimation of the clay edge sorption site density by low-pressure gas adsorption and AFM observations*, American Mineralogist, Vol. 88, 1989-1995, 2003

[99] – Zazzi, A., Jakobsson, A-M., Wold, S., *Ni(II) Sorption onto Chlorite*, Appl. Geochem., Vol. 27, 1189-1193, 2012

[100] – Wanner, H., Albinsson, Y., Karnland, O., Wieland, E., Wersin, P., Charlet, L., *The Acid/Base Chemistry of Montmorillonite*, Radiochimica Acta., Vol. 66/67, 157-162, 1994

[101] - Wu, C. H., Lo, S. L., Lin, C. F., Kuo, C. Y., *Modelling Competitive Adsorption of Molybdate, Sulfate, and Selenate on γ-Al_2O_3 by the Triple Layer Model,* J. of Colloid and Interface Sci., Vol. 233, 259-264, 2001

[102] – Rozov, K. B., Rumynin, V. G., Nikulenkov, A. M., Leskova, P. G., Sorption of ^{137}Cs, ^{90}Sr, Se, ^{99}Tc, $^{152(154)}$Eu, $^{239(240)}$Pu on fractured rocks of the Yeniswysky site (Nizhne-Kansky massif, Krasnoyarsk region, Russia), J. Environmental Radioactivity, Vol 192, 513-523, 2018

[103] - Mattigod, S. V., Gibali, A. S., Page, A. L., *Effect of Ionic Strength and Ion Pair Formation on the Adsorption of Nickel onto Kaolinite*, Clays and Clay Minerals, Vol. 27, 411-416, 1976

[104] – Ticknor, K. V., Vandergraaf, T. T., McMurray, J., Biosvenue, L., Wilkin, D. L., *Parametric Studies of Factors Affecting Se and Sn Sorption*, Atomic Energy of Canada Ltd., AECL TR-723, COG-95-554, 1996

[105] - Skomurski, F. N., Rosso, K. M., Krupka, M. K., McGrail, B. P., *Technetium Incorporation into Hematite (α-Fe_2O_3),* Environ. Sci. Technol., Vol 44, 5855-5861, 2010

[106] - Kaplan, D. I., Gervais, T. L., Krupka., *Uranium(VI) Sorption to Sediments Under High pH and Ionic Strength Conditions*, Radiochimica Acta., Vol. 80, 201-211, 1998

[107] - Savenko, A. V., *Sorption of UO_2^{2+} on Calcium Carbonate*, Radiochemistry, Vol. 43, No. 2, 174-177, 2001

[108] - Bradbury, M. H., Baeyens, B., Thoenen, T., *Sorption Data Bases for Generic Swiss Argillaceous Rock Systems*, NAGRA-TR-09-03, 2010

[109] - Bradbury, M. H., Baeyens, B., *Comparison of the reference Opalinus Clay and MX-80 bentonite sorption data bases used in the Entsorgungsnachweis with sorption data bases predicted from sorption measurements on illite and montmorillonite*, NAGRA-TR-09-07, 2010

[110] – Berry, J. A., Yui, M., Kitamura, A., *Sorption Studies of Radioelements on Geological Materials*, Japanese Atomic Energy Agency, JAEA-2007-074, 2007

[111] - Baston, G. M. N., Berry, J. A., Brownsword, M., Cowper, M. M., Heath, T. G., Tweed, C. J., *The Sorption of Uranium and Technetium on Bentonite, Tuff, and Granodiorite*, Mat. Res. Soc. Symp. Proc., Vol. 353, 989-996, 1995

[112] - Baston, G. M., Berry, J. A., Brownsword, M., Heath, T. G., Ilett, D. J., Tweed, C. J., Yui, M., *The Effect of Temperature on the Sorption of Technetium, Uranium, Neptunium, and Curium on Bentonite, Tuff, and Granodiorite*, Mat. Res. Soc. Symp. Proc., Vol. 465, 805-812, 1997

[113] - Twidale, C. R., Bourne, J. A., Vidal Romani, J. R., *Origin of Miniature Mogotes in Granite, King Rocks, Southern Yilgarn Block, Western Australia*, Cuaternario y Geomorfologia, Vol. 13, 33-34, 1999

[114] - Baik, M-H., Lee, S-Y., Jeong, J., *Sorption and reduction of selenite on chlorite surfaces in the presence of Fe(II) ions*, J. of Environ. Radioactivity, Vol. 126, 209-215, 2013

[115] - Peak, D., *Adsorption mechanisms of selenium oxyanions at the aluminum oxide/water interface*, J. Colloid and Interface Sci., Vol. 303, 337-345, 2006

[116] - Wells, P. R., *Linear Free Energy Relationships*, Chem. Rev., Vol. 63, No. 2, 171-219, 1963

[117] - Xie, Y., Powell, B. A., *Linear Free Energy Relationship for Actinide Sorption to Graphene Oxide*, Apple. Mater. Interfaces, Vol. 10, 32086-32092, 2018

[118] - Bradbury, M. H., Baeyens, B., *Modelling the Sorption of Mn(II), Co(II), Ni(II), Zn(II), Cd(II), Eu(III), Am(III), Sn(IV), Th(IV), Np(V), and U(VI) on montmorillonite: Linear free energy relationships and estimates of surface binding constants for some selected heavy metals and actinides*, Geochimica et Cosmochimica Acta., Vol. 69, No. 4, 875-892, 2005

[119] - Bradbury, M. H., Baeyens, B., *Modelling sorption data for the actinides Am(III), Np(IV), and Pu(V) on montmorillonite*, Radiochim. Acta., Vol. 94, 619-625, 2006

[120] - Bradbury, M. H., Baeyens, B., *Sorption modelling on illite. Part II: Actinide sorption and linear free energy relationships*, Geochimica et Cosmochimica Acta, Vol. 73, 1004-1013, 2009

[121] - Romanchuk, A. Y., Kalmykov, S. N., *Actinide sorption onto hematite: experimental data, surface complexation modelling and linear free energy relationship*, Radiochim. Acta, Vol. 102, No. 4, 303-310, 2014

[122] - Schindler, P. W., Dick, F. R., Wolf, P. R., *Ligand Properties of Surface Silanol Groups I. Surface Complex Formation with Fe^{2+}, Cu^{2+}, Cd^{2+}, and Pb^{2+}*, J. Of Colloid and Interface Sci., Vol. 55, No. 2, 469-475, 1976

[123] - Balistrieri, L., Brewer, P. G., Murray, J. W., *Scavenging residence times of trace metals and surface chemistry of sinking particles in the deep ocean*, Deep-Sea Research, Vol. 28A, 101-121, 1981

[124] - Hachiya, K., Sasaki, M., Spruta, Y., Mikami, N., Yasunaga, T., *Static and Kinetics Studies of Adsorption-Desorption of Metal Ions on a γ-Al_2O_3 Surface. 1. Static Study of Adsorption-Desorption*, J. Phys. Chem., Vol. 88, 23-27, 1984

[125] - Davis, J. A., Beckie, J. O., *Effect of Adsorbed Complexing Ligands on Trace Metals Uptake by Hydrous Oxides*, Environ. Sci. And Technol., Vol. 12, 1309-1315, 1978

[126] - Davis, J. A., Beckie, J. O., *Surface Ionization and Complexation at the Oxide/Water Interface II. Surface Properties of Amorphous Iron Oxyhydroxide and Adsorption of Metal Ions*, J. Colloid and Interface Sci., Vol. 67, No. 1, 90-107, 1978

[127] – Baeyens, B., Thoenen, T., Bradbury, B. H., Marques-Fernandes, M., S*orption Data Bases for Argillaceous Rocks and Bentonite for the Provisional Safety Analyses for SGT-E2*, Nat. Coop. for the Dispos. Of Radioactive Waste, NAGRA TR 12-04, 2014

[128] – Soderlund, M., Lusa, M., Virtanen, S., Valimaa, I., Hakanen, M., Lehto, J., *Distribution Coefficients of Caesium, Chlorine, Iodine, Niobium, Selenium, and Technetium on Olkiluoto Soils*, Posiva, Working Report 2013-068, 2014

[129] - Parker, T. G., Omoto, T., Dickens, S. M., Wall, D. E., Wall, N. A., *Complexation of SO_4^{2-} in NaCl Medium*, J. of Sol. Chem., Vol. 47, 1192-1201, 2018

[130] - German, K. E., Shiryaev, A. A., Safonov, A. V., Obruchnikova, Y. A., Ilin, V. A., Tregubova, V. E., *Technetium sulphide – formation kinetics, structure, and particle speciation*, Radiochim. Acta., Vol. 103, No. 3, 199-203, 2015

Appendix A - Supporting Figures

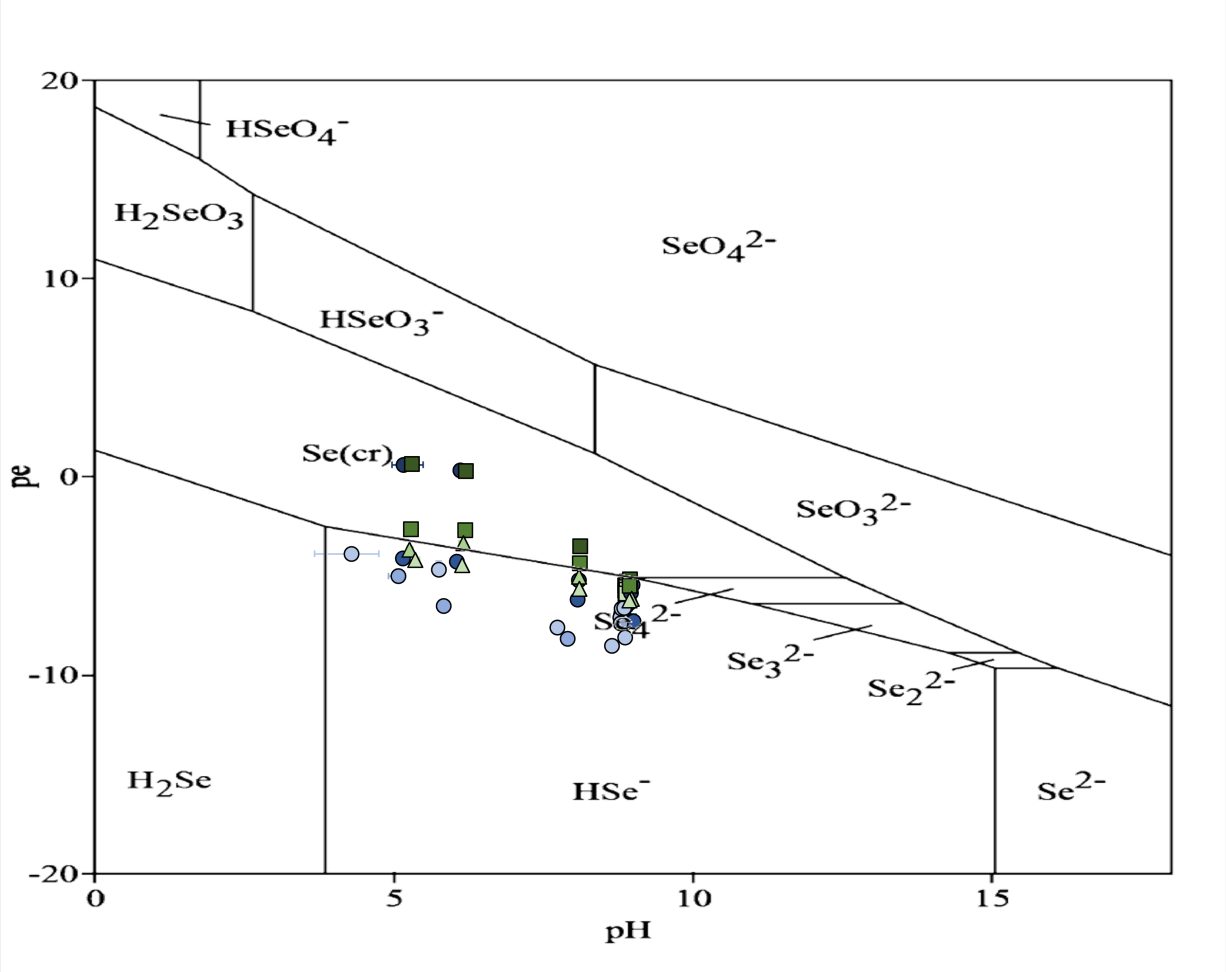

Figure A1 - Pourbaix diagram for Se - O - H system with $[Se]_{tot}$ = 1.00x10^{-6} mol·L^{-1}. Eh vs. pH measurements were taken for Se(-II) adsorption in Ca-Na-Cl solutions. Eh was converted to pe to coincide with units of the Pourbaix diagram. Blue circles coincide with granite, green squares coincide with MX-80 bentonite.

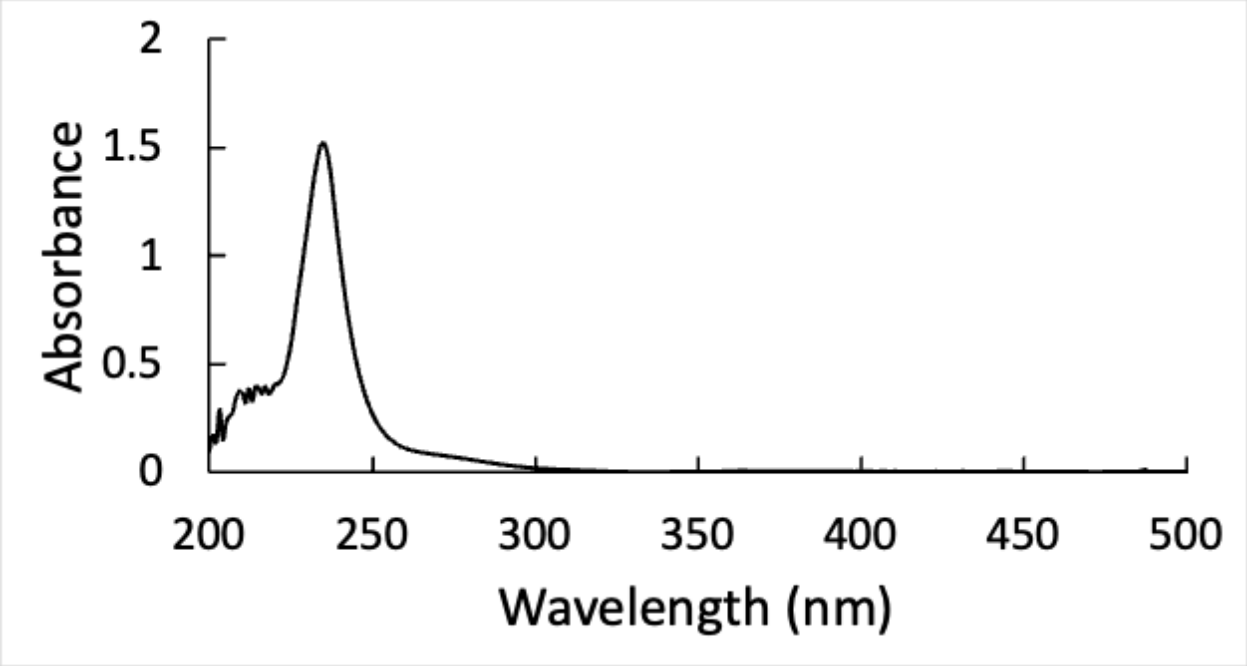

Figure A2- UV-Vis spectrum of prepared Se(-II) solution used to confirm the reduction methodology was successful.

Figure A3 - Electrolytic Cell used to reduce Tc(VII) to Tc(IV). The RE is to the left with the green alligator clip. The Pt WE is in the middle with the two black alligator clips. The CE is in the front with the red alligator clip.

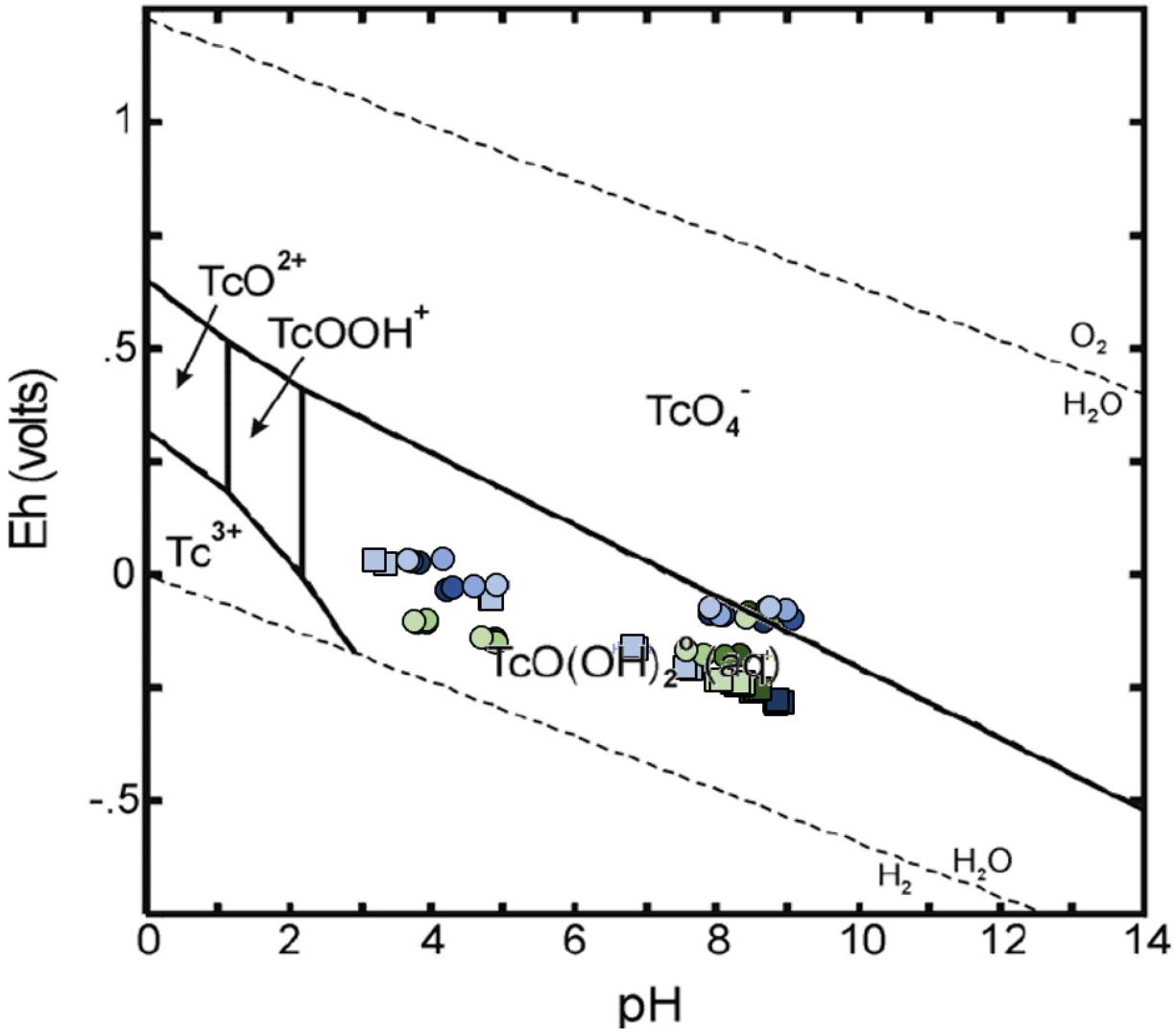

Figure A4 - Pourbaix diagram for Tc-O-H system with $[Tc]_{tot}$ = 1.00x10^{-9} mol·L^{-1}. Eh vs. pH measurements were taken for Tc(IV) adsorption in Ca-Na-Cl solutions. Blue circles coincide with granite, green squares coincide with MX-80 bentonite.

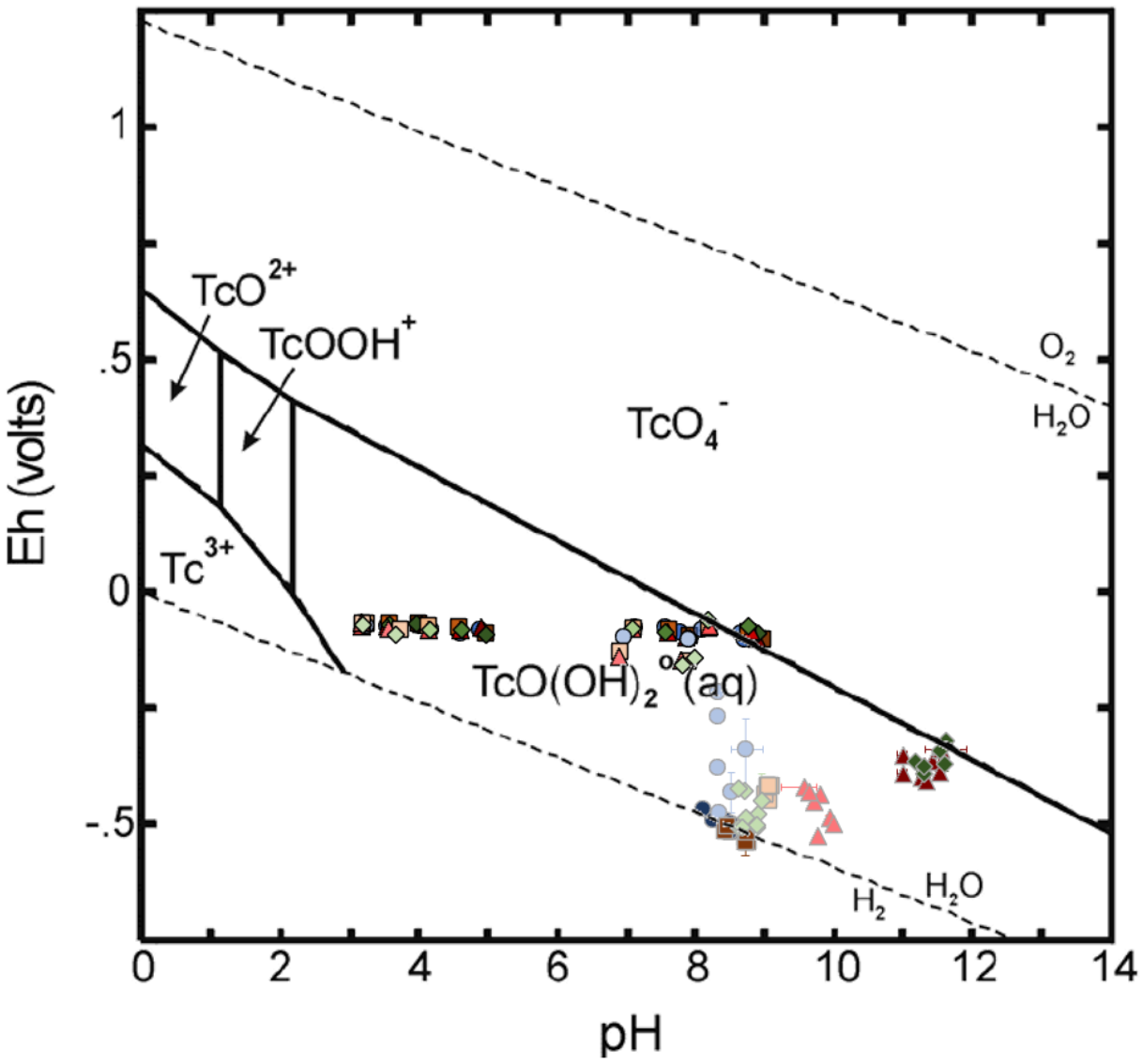

Figure A5 - Pourbaix diagram for Tc-O-H system with $[Tc]_{tot}$ = 1.00x10^{-9} mol·L^{-1}. Eh vs. pH measurements were taken for Tc(IV) adsorption in Na-Ca-Cl solutions. Blue circles coincide with shale, orange squares coincide with limestone, red triangles coincide with illite, and green diamonds coincide with MX-80 bentonite.

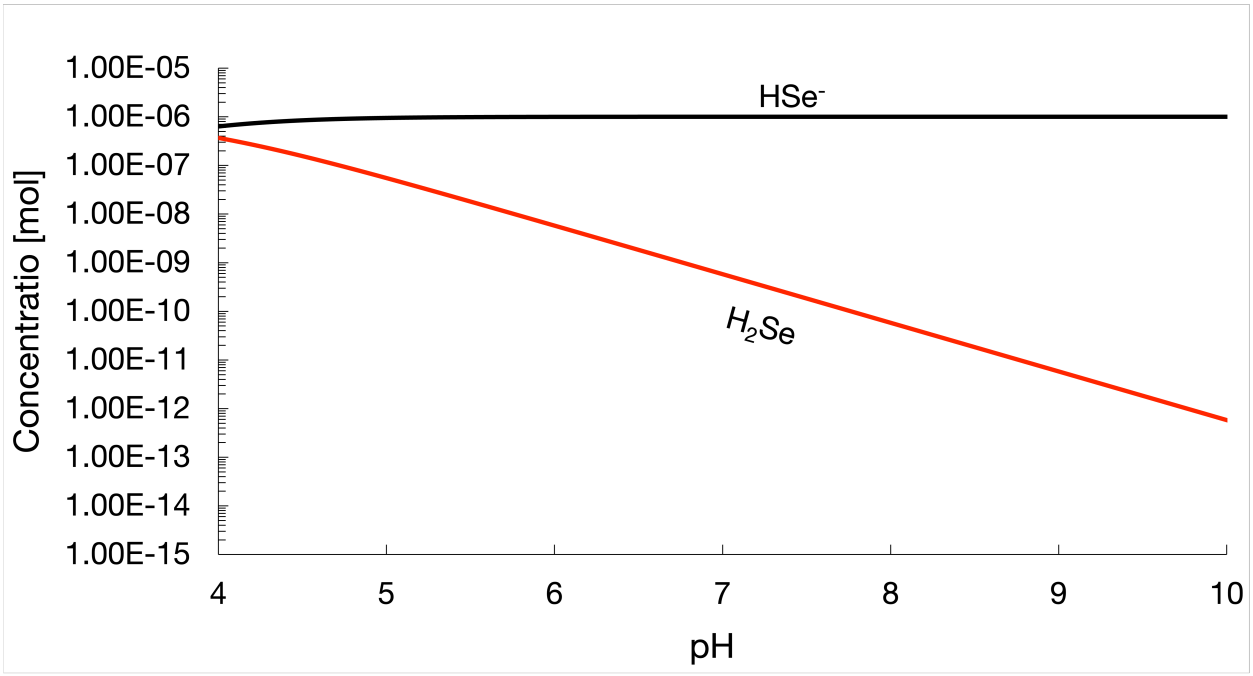

Figure A6 - Aqueous speciation associated with Se(-II).

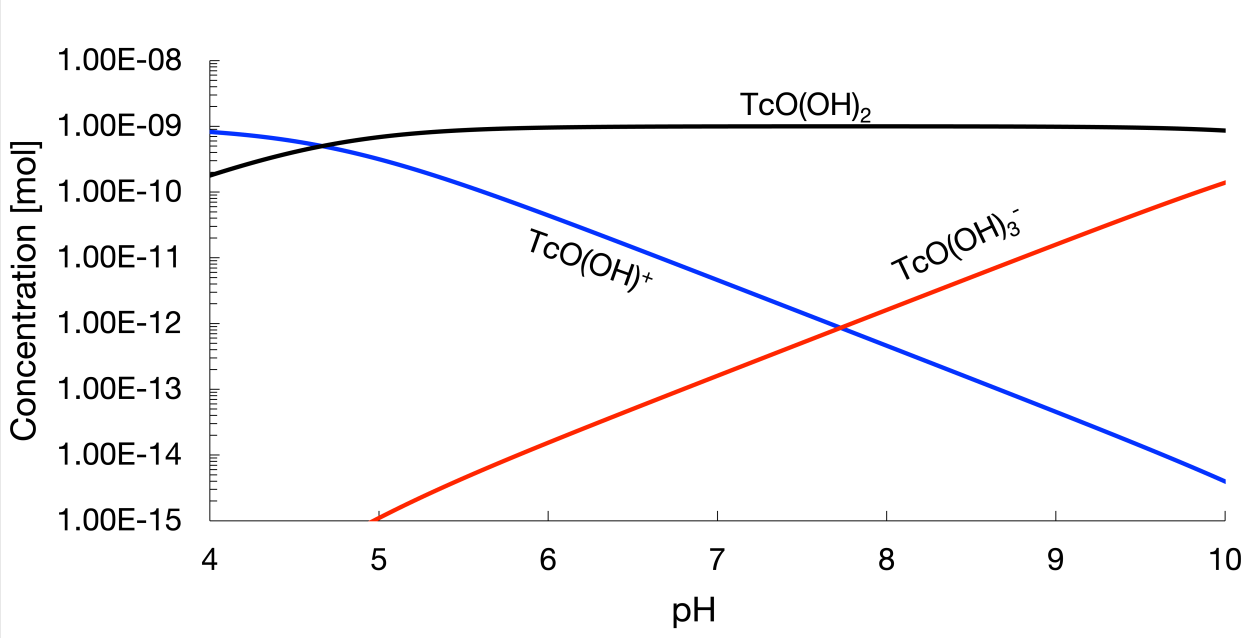

Figure A7 - Aqueous speciation associated with Tc(IV).

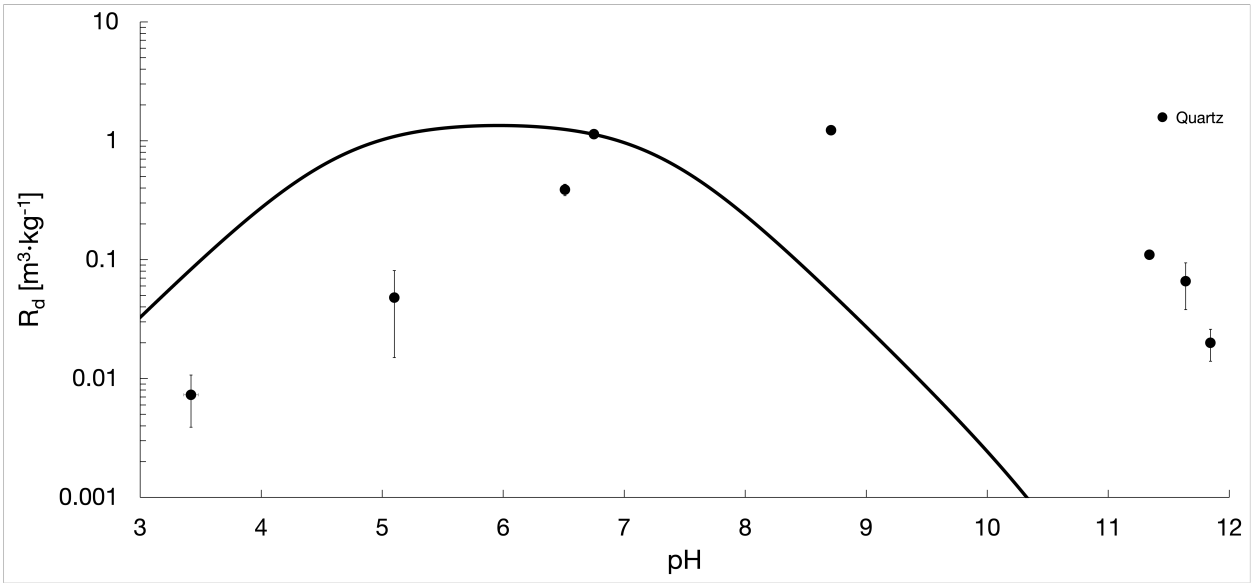

Figure A8 - Adsorption of Tc(IV) onto quartz data [11]. Black curve is the optimized Quartz SCM with a ≡Quartz_sOTcO(OH) surface complexation constant of 5.50.

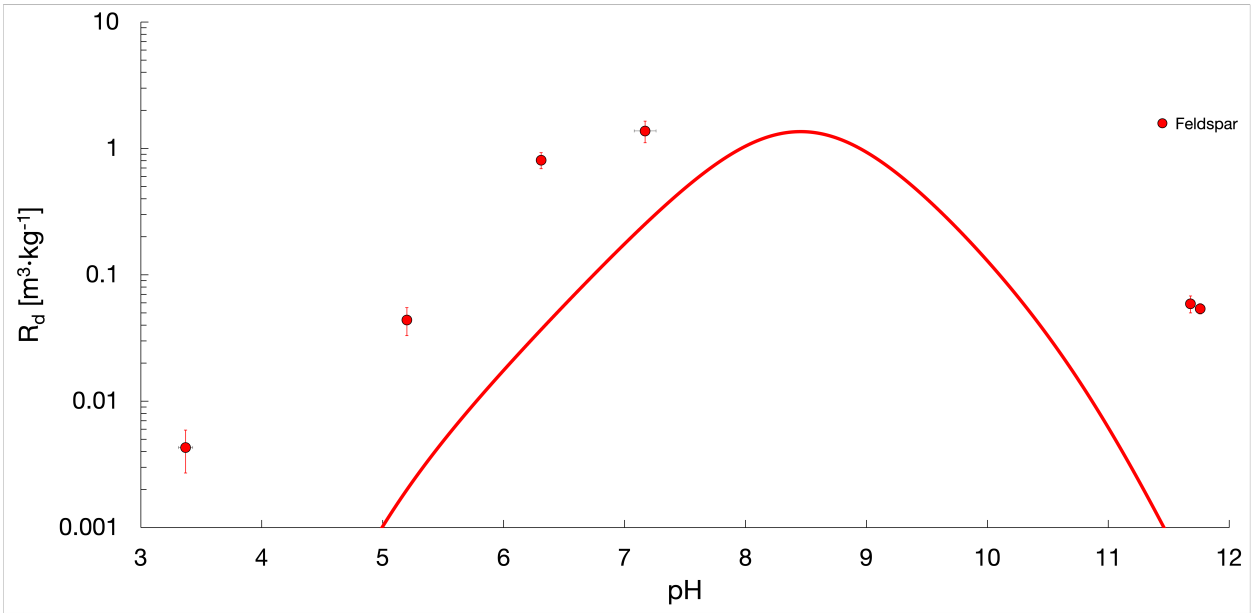

Figure A9 - Adsorption of Tc(IV) onto plagioclase feldspar data [11]. Red curve is the optimized Feldspar SCM with a $(\equiv Feldspar\_sO)_2TcO(OH)^-$ surface complexation constant of -2.25.

Appendix B - Petrographic Analysis of Granite

Petrographic Examination of Dimension Stone
ASTM C 295

Customer: **Cold Spring Granite** **Date:** **February 17, 2004**

Sample ID: **Performed by:** **Mark Lukkarila**

Sample Description: **Pink, phaneritic, porphyritic granite. With the exception of the phenocrysts, the texture was granular. The phenocrysts were comprised of pink alkali-feldspar. Darker minerals included biotite, magnetite, and hornblende.**

Mineralogical Composition	%	Chemical Formula	Description
Plagioclase Feldspar	37	$NaAlSi_3O_8$	Colorless,low relief, anhedral, biaxial negative, with weak interference colors. Typical polysynthetic twinning was common. Some crystals exhibited strain and fracturing (see photo # 1)
Quartz	34	SiO_2	Colorless, low relief, uniaxial positive. anhedral. Strained quartz was common. Quartz was commonly rutilated and exhibited consertal texture
Alkali-Feldspar (microcline, perthite, microperthite)	19	$(K,Na)AlSi_3O_8$	Colorless, low relief, anhedral, biaxial positive, weak interference colors with one imperfect cleavage. Simple Carlsbad and crosshatch twinning common
Biotite	3	$K2(Mg,Fe)_{6-4}(Fe,Al,Ti)_{0-2}[Si_{6-5},Al_{2-3}O_{20}](OH,F)_4$	Pleochroic from brown to green, typical platy cleavage and birds-eye maple structure.
Myrmekite	2	$NaAlSi_3O_8$ - SiO_2	Intergrowth of plagioclase and quartz
Chlorite	1.4	$(Mg,Al,Fe)_6(Si, Al)_4O_{20}(OH)_8$	Pleochroic from green to pale green with anomalous blue interference colors under crossed nichols. Typical platy cleavage
Muscovite (including sericite)	1	$K_2Al_4[Si_6Al_2O_{20}](OH, F)_4$	Colorless, moderate relief, biaxial negative with strong third order interference colors. Typical platy cleavage
Opaques (Magnetite)	0.9	Fe_3O_4	Black, blocky, anhedral, metallic luster in reflected light. Strongly magnetic
Hornblende	0.9	$Ca_2(Mg, Fe)_4(Al, Fe)(Si_7Al)O_{22}(OH)_2$	Pleochroic form colorless, pale green, to dark green. Anhedral to subhedral prismatic and columnar habit were observed
Epidote (Clinozoisite, Zoisite)	0.2	$Ca_2Al_3O[Si_2O_7][SiO_4](OH)$	Colorless, subhedral, high relief, prismatic, biaxial negative, first order orange interference colors. Often associated with cholorite.
Sphene	0.2	$CaTiSiO_5$	Yellowish-brown, high relief, anhedral to Subhedral, strong birefringence, one good cleavage
Zircon	trace	$ZrSiO_4$	Colorless, high relief, anhedral, uniaxial positive, weak birefringence

Alterations: **Some sericitization was observed, especially in the plagioclase feldspar.**

Rock Name: **Porphyritic Granite**

Figure B1 - Petrographic Analysis of the granite sample.

Appendix C - Compiled Se(-II) and Tc(IV) Surface Complexation Constants

Table C1 - Surface complexation reactions and optimized surface complexation constants for both Se(-II) and Tc(IV) adsorption compiled from all simulations

Simulated Surface	Surface Complexation Reaction	(LogK)
Granite	≡Feldspar_sOH + HSe^- ↔ ≡Feldspar_sSe^- + H_2O	5.50
	≡Biotite_sOH + HSe^- + H^+ ↔ ≡Biotite_sOH_2HSe	12.00
MX-80 Bentonite	≡Albite_sOH + HSe^- ↔ ≡Albite_sSe^- + H_2O	5.50
	≡Montmorillonite_sOH + HSe^- ↔ ≡Montmorillonite_sSe^- + H_2O	4.50
	≡Montmorillonite_sOH + HSe^- + H^+ ↔ ≡Montmorillonite_sOH_2HSe	9.50
Granite	≡Biotite_sOH + $TcO(OH)_2$ ↔ ≡Biotite_sOTcO(OH) + H_2O	8.10
	≡Quartz_sOH + $TcO(OH)_2$ ↔ ≡Quartz_sOTcO(OH) + H_2O	5.35
	2 (≡Feldspar_sOH) + $TcO(OH)_2$ ↔ ≡(Feldspar_s$O)_2$TcO$(OH)^-$ + H_2O + H^+	-2.25
MX-80 Bentonite (Ca-Na-Cl)	≡Quartz_sOH + $TcO(OH)_2$ ↔ ≡Quartz_sOTcO(OH) + H_2O	5.35
	≡Montmorillonite_sOH + $TcO(OH)_2$ ↔ ≡Montmorillonite_sOTcO(OH) + H_2O	5.00
	2 (≡Albite_sOH) + $TcO(OH)_2$ ↔ ≡(Albite_s$O)_2$TcO$(OH)^-$ + H_2O + H^+	-2.25
Shale	≡Illite_sOH + $TcO(OH)_2$ ↔ ≡Illite_sOTcO(OH) + H_2O	5.25
	≡Quartz_sOH + $TcO(OH)_2$ ↔ ≡Quartz_sOTcO(OH) + H_2O	5.35
	≡Chlorite_sOH + $TcO(OH)_2$ ↔ ≡Chlorite_sOTcO(OH) + H_2O	6.00
	2 (≡Feldspar_sOH) + $TcO(OH)_2$ ↔ ≡(Feldspar_s$O)_2$TcO$(OH)^-$ + H_2O + H^+	-2.25
Illite	≡Illite_sOH + $TcO(OH)_2$ ↔ ≡Illite_sOTcO(OH) + H_2O	5.25
MX-80 Bentonite (Na-Ca-Cl)	≡Quartz_sOH + $TcO(OH)_2$ ↔ ≡Quartz_sOTcO(OH) + H_2O	5.35
	≡Montmorillonite_sOH + $TcO(OH)_2$ ↔ ≡Montmorillonite_sOTcO(OH) + H_2O	5.00
	2 (≡Albite_sOH) + $TcO(OH)_2$ ↔ ≡(Albite_s$O)_2$TcO$(OH)^-$ + H_2O + H^+	-2.25

Appendix D - Component Assemblage Mineral Surface Complexation Models

Table D1 - Simulated component assemblage mineral surfaces and their with SSA and site densities.

Simulated Surface	SSA [$m^2 \cdot g^{-1}$]	Site Density [$sites \cdot nm^{-2}$]	Reference
Quartz	0.7	5.67	[91]
Feldspar	1.0	4.05	[91]